RESIDUE NUMBER SYSTEM CODED DIFFERENTIAL SPACE-TIME-FREQUENCY CODING

By

Roseline Nyongarwizi Akol

Submitted in fulfilment of the academic requirement for the degree of doctor of philosophy in the School of Electrical, Electronic and Computer Engineering, University of KwaZulu-Natal

January 2007

Abstract

The rapidly growing need for fast and reliable transmission over a wireless channel motivates the development of communication systems that can support high data rates at low complexity. Achieving reliable communication over a wireless channel is a challenging task largely due to the possibility of multipaths which may lead to inter-symbol interference (ISI). Diversity techniques such as time, frequency and space are commonly used to combat multipath fading. Classical diversity techniques use repetition codes such that the information is replicated and transmitted over several channels that are sufficiently spaced. In fading channels, the performance across some diversity branches may be excessively attenuated, making throughput unacceptably small. In principle, more powerful coding techniques can be used to maximize the diversity order. This leads to bandwidth expansion or increased transmission power to accommodate the redundant bits. Hence there is need for coding and modulation schemes that provide low error rate performance in a bandwidth efficient manner. If diversity schemes are combined, more independent dimensions become available for information transfer.

The first part of the thesis addresses achieving temporal diversity through employing error correcting coding schemes combined with interleaving. Noncoherent differential modulation does not require explicit knowledge or estimate of the channel, instead the information is encoded in the transitions. This lends itself to the possibility of turbo-like serial concatenation of a standard outer channel encoder with an inner modulation code amenable to noncoherent detection through an interleaver. An iterative approach to joint decoding and demodulation can be realized by exchanging soft information between the decoder and the demodulator. This has been shown to be effective and hold hope for approaching capacity over fast fading channels. However most of these schemes employ low rate convolutional codes as their channel encoders. In this thesis we propose the use of redundant residue number system codes. It is shown that these codes can achieve comparable performance at minimal complexity and high data rates.

The second part deals with the possibility of combining several diversity dimensions into a reliable bandwidth efficient communication scheme. Orthogonal frequency division multiplexing (OFDM) has been used to combat multipaths. Combining OFDM with multiple-input multiple-output (MIMO) systems to form MIMO-OFDM not only reduces the complexity by eliminating the need for equalization but also provides large channel capacity and a high diversity potential. Space-time coded OFDM was proposed and shown to be an effective transmission technique for MIMO systems. Space-frequency coding and space-time-frequency coding were developed out of the need to exploit the frequency diversity due to multipaths. Most of the proposed schemes in the literature maximize frequency diversity predominantly from the frequency-selective nature of the fading channel. In this thesis we propose the use of residue number system as the frequency encoder. It is shown that the proposed space-time-frequency coding scheme can maximize the diversity gains over space, time and frequency domains.

The gain of MIMO-OFDM comes at the expense of increased receiver complexity. Furthermore, most of the proposed space-time-frequency coding schemes assume frequency selective block fading channels which is not an ideal assumption for broadband wireless communications. Relatively high mobility in broadband wireless communications systems may result in high Doppler frequency, hence time-selective (rapid) fading. Rapidly changing channel characteristics impedes the channel estimation process and may result in incorrect estimates of the channel coefficients. The last part of the thesis deals with the performance of differential space-time-frequency coding in fast fading channels.

Dedication

I would like to dedicate this thesis to all working mothers especially those that have excelled in their careers. Well, I do not know how you cope but it has been tough on my side.

Preface

The research work discussed in this thesis was performed by Mrs. Roseline Nyongarwizi Akol, under the supervision of Professor. Fambirai Takawira, at the University of KwaZulu-Natal's school of Electrical, Electronic and Computer Engineering, in the Centre of Radio Access Technologies which is sponsored by Alcatel and Telkom South Africa through the Centre of Excellence programme.

Part of this thesis has been presented by the author at the South African Telecommunications Networks and Applications Conference (SATNAC) in 2003 and 2004, the International Conference on Telecommunications (ICT), Cape Town, South Africa, in 2005, IEEE Wireless Communications and Networking Conference (WCNC), Las Vegas, Nevada, USA in 2006. Part of this thesis has also been submitted to the IEEE International Conference on Communications (ICC), to be held in Glasgow, Scotland, United Kingdom, 2007 and to the IEEE Transactions on Vehicular Technology journal.

The whole thesis, unless otherwise stated, is the author's original work and has not been submitted in part, or whole to any other University.

Acknowledgements

I wish to thank my supervisor Professor Fambirai Takawira for his insight and guidance that has been invaluable both to the substance and spirit of my research. Your unique approach to research, professionalism and patience has been crucial to the completion of this thesis. I will be forever grateful for having worked under your supervision.

I would like to express my heartfelt gratitude to my husband Dr. George Yepusa Akol and my daughter Charlotte Nyongarwizi Akol for allowing me to pursue my PhD. It has been difficult staying apart and I know that time lost can never be replaced. I am however relived that finally my studies are coming to an end and we will be reunited, leaving happily thereafter.

Thanks are owed to Alcatel and Telkom South Africa for their valued financial support and providing the equipment necessary for the completion of my PhD.

I would like to thank the Third World Organization for Women in Science (TWOWS) for taking the risk and financially investing towards my PhD. I would like TWOWS to know that its financial assistance kept me focused towards completing my PhD.

Special thanks go to Dr. Hongju Xu, for his invaluable suggestions, comments and criticism. His door was always open whenever I needed any help or was stuck during the course of my research. I would also like to thank Mr. Bruce Harrison our System administrator, and all our administrative staff for their help in issues not directly related to my research.

Last but not least, I would like express my appreciation to my postgraduate colleagues for their help and friendship and for making the place habitable. Special thanks to Dr. Telex Magloire Ngatched Nkouatchah for proof reading my thesis.

Contents

List of Figures

List of Acronyms

ADSL	Asymmetric digital subscriber line
AWGN	Additive white Gaussian noise
BCH	Bose-Chaudhuri-Houcquenghem (code)
BER	Bit error rate
BEX	Base extension
BPSK	Binary phase shift keying
CRT	Chinese remainder theorem
DFDM	Decision feedback differential modulation
DM	Differential modulation
IFFT	Inverse fast Fourier transform
ISI	Inter-symbol interference
FEC	Forward error correction
FFT	Fast Fourier transform
LLR	Log-likelihood ratio
MAP	Maximum a posteriori (decoding)
MIMO	Multiple-input multiple-output
ML	Maximum likelihood (decoding)

MPSK	M-ary phase shift keying
MRC	Mixed radix conversion
MSDM	Multi-symbol differential modulation
OFDM	Orthogonal frequency division multiplexing
pdf	probability density function
PEP	Pairwise error probability
QPSK	Quadrature phase shift keying
RNS	Residue number system
RRNS	Redundant residue number system
RS	Reed Solomon
SISO	Soft-input soft-output
SNR	Signal-to-noise ratio
SFBC	Space-frequency block code
STBC	Space-time block code
STFC	Space-time-frequency code
STTC	Space-time trellis code
TCM	Trellis coded modulation
Wi-Fi	Wireless fidelity
WiMAX	Worldwide interoperability for microwave access

List of Notations

d_{free}	Minimum free distance
$d_{\min}$	Minimum Hamming distance
E_b / N_o	Signal-to-noise ratio per information bit
f_D	Maximum Doppler frequency
$(\cdot)^{\mathcal{H}}$	Conjugate transpose
$\mathbf{I}_n$	$n \times n$ identity matrix
$J_o(\cdot)$	Bessel function of the first kind
L	Channel order or number of multipaths
M_b	Temporal diversity component
M_r	Number of receive antennas
M_t	Number of transmit antennas
N_c	Number of OFDM tones
N	Number of symbol observation periods
$N_o / 2$	Double sided power spectral density of AWGN
$\mathrm{Re}\{\mathrm{a}\}$	Real part of a

$\Re$	Transmission or code rate
$(\cdot)^T$	Transpose
T	Symbol duration
$tr(\cdot)$	Trace of a matrix
$(\cdot)^*$	Complex conjugate

CHAPTER 1

INTRODUCTION

1.1 Broadband Wireless Communications

Due to the enormous growth in the wireless communication industry in the last decade, there is need for techniques to reliably communicate at high data rates and efficiently use the available bandwidth. Several technologies have been developed to efficiently utilize the available bandwidth. One such technology that has shown promising results is the use of multiple transmit and receive antennas known as multiple-input multiple-output (MIMO) communications system. In MIMO systems, the information signal at both sides of the communication link i.e. the transmitter and the receiver, is combined in such a way that the quality (average bit error rate or BER) or data rates (bits per second) is improved. The prospect of improved reliability or high data rates at no extra bandwidth has revolutionized the communications industry, with the only hardship being the practical implementation especially at the mobile terminal. As the subscriber units are gradually evolving from just being pocket telephones to sophisticated wireless internet access points and video machines, the stringent size and complexity constraints are being relaxed. This makes application of multiple antennas a possibility at both sides of the link.

The channel capacity is the maximum possible transmission rate such that the error probability of the received information signal is arbitrarily small. Although the channel capacity for additive white Gaussian noise (AWGN) channels was first derived by Shannon [1] in 1948, a breakthrough that increases the channel capacity was only realized by the use of multiple transmit and receiver antennas [2], [3], [4]. By transmitting and receiving information from several antennas that are adequately

separated to ensure independent propagation, it was shown that the channel capacity increases with increasing number of antennas without increasing the bandwidth [2]. Several studies devoted to MIMO channel modelling, information theory and antenna design show that the channel capacity substantially increases in particular through the principle of spatial multiplexing.

MIMO systems also possess a potential spatial diversity gain that can be used to combat channel fading. By transmitting and receiving information from several antennas, multiple independent fade replicas of the data symbols can be obtained at the receiver. The probability that all the signal replicas will vanish during a single fade is reduced, hence achieving more reliable reception.

A core idea in MIMO systems is space-time signal processing. In order to protect transmission against errors caused by channel fading and AWGN, joint coding across transmit antennas and time, known as space-time (ST) coding was introduced [86], [87]. In space-time coding, a space-time encoder generates code symbols, equal to the number of transmit antennas, that are transmitted simultaneously, one symbol from each antenna. A lot of research has been devoted to the design and construction of space-time codes. Several space-time architectures have been generalized in terms of diversity gains or coding gains or both. Although space-time codes were revisited in form of trellis codes (STTC) [86], [95], [96], [97], their popularity took off with the discovery of space-time block codes (STBC) [88], [89], [90], [6], [7]. This is mainly due to their simple construction and linear signal processing at the receiver of space-time block codes compared to a multidimensional Viterbi algorithm required for space-time trellis codes. Although space-time block codes achieve the same spatial diversity gains as space-time trellis codes, they possess marginal or no coding gains.

1.2 Wireless Channels

The major impairments of wireless communication systems are fading caused by destructive addition of multipaths in the propagation channel and co-channel interference from other users. Multipath is caused by a reflection of the transmitted signal from multiple scatters and due to motion of the mobile receivers and transmitters. This may result in more than one version of the transmitted signal arriving at the receiver at slightly different amplitudes, phases, and times. Hence, increasing the time

required for the transmitted signal to reach the receiver. The constantly changing channel characteristics may cause inter-symbol interference (ISI). The channel characterization may be viewed in the frequency or time domain or both.

In the frequency domain, the characterization of the channel is dependent on its coherence bandwidth. The coherence bandwidth, which is a function of the delay spread, is a measure of the transmission bandwidth for which the signal distortion across the channel becomes noticeable. If the signal to be transmitted has a much large bandwidth than the channel coherence bandwidth, the received signal is distorted and the multipath channel is said to be frequency selective. However, if the channel coherence bandwidth is lager than that of the transmitted signal, the channel is said to be frequency non-selective, or frequency flat.

Alternatively, if the channel characterization is in the time domain, the parameter of concern is coherence time. Coherence time, which is a function of Doppler spread, can be defined as the duration of time in which the channel impulse response is effectively invariant. Doppler spread is a measure of Doppler frequency (shift) caused by relatively high mobility of the wireless propagation channel, transmitter and the receiver. The Doppler frequency f_D can be as

$$f_D = \frac{\upsilon}{\lambda}\cos\theta, \tag{1.1}$$

where λ is the wavelength, υ is the velocity of the mobile receiver and θ is the angle-of-arrival (AOA). The fading channel is said to be time selective if its coherence time is small compared to the duration of the received signal, otherwise, time non-selective (time invariant).

1.3 MIMO and OFDM

1.3.1 Orthogonal Frequency Division Multiplexing (OFDM)

OFDM is a multicarrier modulation technique known to support high speed transmission while mitigating the effects of multipath in wireless broadband communication systems. It has been used in standards such as digital audio/video broadcasting (DAB/DVB) [8], wireless fidelity (Wi-Fi) IEEE 802.11 group of standards

[9], worldwide interoperability for microwave access (WiMAX) IEEE 802.16 group of standards [10], [13] and high speed digital transmission over twisted pair cables (ADSL) [11], [12].

In OFDM, the symbol sequence to be transmitted is split into a large number of low speed symbol streams such that each modulates a separate carrier. The carrier spacing is chosen such that the modulated carriers are orthogonal over a symbol interval and a guard interval (commonly known as a cyclic prefix) is inserted to combat frequency-selective fading. Hence, OFDM is used to transform a frequency-selective channel into a set of independent parallel frequency-flat subchannels. The transmitter and receiver employing OFDM techniques can be implemented efficiently by use of fast Fourier transform methods.

1.3.2 MIMO-OFDM

The key feature of MIMO systems, is the ability to turn multipath propagation, traditionally a pitfall of wireless communications, into diversity gain. Despite the fact that space-time (ST) codes have successfully increased the channel capacity and reliability of a wireless communication system, they were designed for narrowband wireless systems i.e. flat fading. Their performance is degraded when applied to broadband channels mainly due to multipath fading which generally exhibits time selectivity and frequency selectivity [14]. In multipath, the signal power is carried by several propagation paths with different powers and delays which may result in inter-symbol interference. This necessitates use of a channel equalizer along with a space-time decoder when applied to broadband channels. Extending classical equalization methods such as minimum mean square error linear equalizer, decision feedback equalizer and maximum likelihood sequence estimation used for a single antenna system [39] to space-time coding is a challenging problem. A combination of ST codes and orthogonal frequency division multiplexing (OFDM) has been proposed to combat the effect of frequency-selective fading by increasing the duration of the transmitted symbol [113], [144], [145], [146], [147], [148]. Hence OFDM eliminates the need for high complex equalization techniques while offering high spectral efficiency.

Although OFDM is robust against frequency-selective channels, any time variations in the channel characteristics will cause performance degradation. OFDM combats

frequency-selective fading by splitting the symbol sequence to be transmitted into low speed symbol streams such that each modulates a separate carrier. Increasing the number of subcarriers increases the symbol duration. This makes the ST-OFDM system more sensitive to time-selective fading which may lead to loss of orthogonality among the subcarriers. Without orthoganality, when the signals arriving are down converted to their baseband equivalent at the receiver, inter-carrier interference (ICI) occurs. This is because signals from one carrier cause interference to the others especially to the neighbouring subcarriers. In some instances, the ST-OFDM signal reflections from far obstacles will generate inter-block interference due to long time delays. However, in most applications, the cyclic prefix is assumed longer than the maximum delay spread. Hence interference from previous OFDM symbols is restricted to the cyclic prefix which is discarded at the receiver, leaving ICI as the only consideration. Therefore the large ST-OFDM symbol duration used to combat frequency-selectivity is limited by time-selectivity.

Applying OFDM to broadband multiple-input multiple-output (MIMO) channels not only offers spatial diversity due to multiple antennas, but also frequency diversity due to delay spread. Space-frequency (SF) coding has emerged as a technique that aims to combine advantages of ST coding and MIMO-OFDM. Space-frequency coded MIMO-OFDM basically consists of coding across transmit antennas and OFDM tones while exploiting both spatial and frequency diversity. SF was first proposed in [149] where bandwidth was divided into several overlapping subbands equal to the number of multipaths. Other SF schemes utilizing already existing space-time codes by simply applying techniques such as delay diversity, multicarrier and permutation diversities to transform signals from space-time to a space-frequency were proposed in [150], [151], [152], [153], [154], [156], [157]. Although these schemes were able to achieve spatial diversity, frequency diversity was not guaranteed. SF schemes that have since been developed are able to achieve both spatial and frequency diversities. Techniques such as linear precoders or constellation rotation [155], [158], [161], [162], linear constellation decimation [164], or simply repetition codes [160] are used to code across multipaths, hence maximizing frequency diversity.

Although SF coding is well suited for fast fading, variations within subcarrier for large OFDM blocks and channels with large delay spreads may result in performance degradation. Whereas ST-OFDM is limited by time-selective fading, SF is limited by

frequency-selectivity fading. Hence space-time-frequency (STF) coding has been proposed in an attempt to integrate the advantages of ST-OFDM and SF coding [159].

1.4 Signal Detection and Error Correction

Transmission schemes over MIMO channels have been divided into either data rate maximization schemes or diversity maximization schemes. The first category focuses on improving the average capacity hence efficient use of the very expensive/valuable communication resource i.e. bandwidth, while the second category focuses on outage probability (reliability) of the system. The reliability of the MIMO system can further be improved through error control coding. Since the actual performance of a communication system is evaluated by the average bit error rate (BER) or symbol error rate (SER) versus signal-to-noise ratio (SNR), in MIMO systems, the receiver can coherently combine the received signal to increase the SNR, a technique known as "array gain". Hence the channel state information available at the receiver plays a significant role in the performance of MIMO systems.

1.4.1 Channel Coding

Error correcting codes also known as channel coding play a significant role in correcting errors incurred during transmission. They are divided into forward error correction (FEC) codes or automatic repeat request (ARQ). FEC is a one way error control strategy in which redundancy is added to the transmitter and automatically corrects errors detected at the receiver. Most coded systems use forward error correction which includes block codes and convolution codes as well as concatenated codes which build upon block and convolutional codes [37], [38], [39]. TCM codes [39] were invented in the 80's with the aim of combining coding and modulation as a single entity for better bandwidth efficiency. Most of these FEC schemes use hard decision decoding where the demodulator judges what the modulator input was and then passes its decision on to the decoder.

In 1993, Berrou et *al* [34], [35] introduced "turbo codes", a concatenation of two recursive convolutional codes whose performance was close to Shannon's limit. Turbo codes use the maximum a posteriori (MAP) algorithm introduced by Bahl et *al* [36] to decode convolution codes. Prompted by the discovery of turbo codes which may also be

used in a parallel concatenated codes (PCCs) configuration, serial concatenated codes (SCCs) and hybrids were constructed with same component convolutional codes to provide similar coding gains [40], [41], [63]. Turbo codes combine random like behaviour with relative simple structure obtained by concatenating low complex compound codes e.g. convolutional codes, block codes such as BCH and RS codes.

The performance of a coded system can be measured in terms of the probability of error. In the high SNR region, the average error probability of a system over a communication channel is given by [6],

$$P(\text{error}) \approx G_c \cdot \text{SNR}^{-G_d} \tag{1.2}$$

where G_c is the coding gain/advantage while G_d is the diversity gain/order.

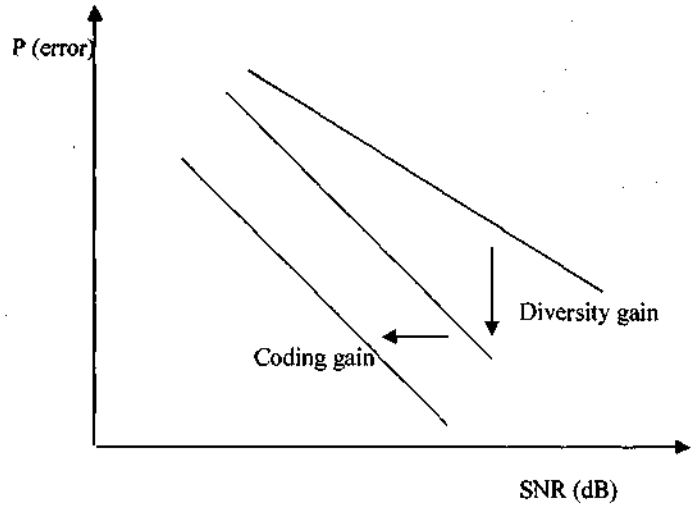

Figure 1.1: Difference in coding and diversity gain.

The sketch of the probability of error versus the SNR is as shown in Figure 1.1. The slope of the curve reflects the diversity gain while the horizontal shift in the curves can be interpreted as the coding gain. It can also be seen from (1.2) that the diversity gain dominates the error performance at high SNR.

However, at low SNR, the coding gain plays a significant role in the error performance of the code. The turbo decoding principle accentuates the coding gain by iteratively passing on soft information to the decoder.

1.4.2 Coherent and Noncoherent Detection

Shannon's coding theorem [1] assumed that for a given spectral efficiency, one is free to choose a modulation scheme that results in the best possible performance. However, the choice of a signalling scheme in real communication systems depends on practical considerations. Communication systems that are sensitive to power amplifications require constant signalling schemes such as M-ary phase shift-keying (MPSK) and frequency shift-keying (FSK), while those that are not, may use amplitude shift-keying (ASK) [39]. MPSK is a popular digital modulation technique whereby the information signal is encoded in the phase of the carrier signal. For optimum MPSK performance, coherent detection which necessitates accurate maintenance of carrier phase synchronization across the channel is paramount. At the receiver, the fading process needs to be known or estimated in order to recover the carrier and compensate for the corrupted signal. Digital signal transmission over fading channels not only suffers from varying loss but also from phase ambiguities. This can be overcome by inserting training symbols multiplexed in the data stream. However, the power and bandwidth efficiencies are somewhat reduced due to overhead. In fast fading, however, the channel characteristics of the fading process are changing rapidly and are therefore very difficult to track.

Noncoherent detection using differential modulation (DM) is very attractive for M-ary phase-shift-keying (MPSK) signalling over rapid fading channels because of its robustness against phase ambiguities and impairments of the received signal [64], [65]. There is no channel information required at the receiver, hence, eliminating the need for a tedious, impractical channel estimation process for rapidly changing channel characteristics.

Differential space-time modulation has been proposed for multiple antenna systems where neither the transmitter nor the receiver knows the fading coefficients [114], [115], [116]. This can be generalized as standard differential phase-shift-keying used in the single antenna unknown channel link. The success of differential space-time modulation is critical to the design of unitary space-time signal constellations [117], [118], [119], [120], [121].

1.5 Motivation

With the ever increasing demand for fast and reliable communication over wireless channels, broadband communication systems are required to provide faster data processing and higher data throughput at low complexity. One technology that has shown promising results is the use of multiple transmit and receive antennas known as multiple-input multiple-output (MIMO) communications system.

A core idea in MIMO systems is space-time signal processing. Multiple transmit space-time (ST) coding has evolved as one of the promising diversity technique for flat fading channels [5], [13]. However, broadband wireless channels are characterized by multipath fading which is a design challenge for any communication system [14]. In order to eliminate the effects of multipath fading and increase data transmission, a combination of ST coding and orthogonal frequency division multiplexing (OFDM) has been deployed [13].

MIMO systems take advantage of random fading while utilizing multipath delay spread, traditionally a pitfall to wireless communications. The prospect of several propagation paths at no extra spectrum has opened up new studies to investigate the diversity potential of MIMO systems. Space-frequency (SF) coding emerged as a technique that combines advantages of both transmit diversity and OFDM while utilizing multipath diversity. In SF coding, two dimensional coding is used to spread information across space (transmit antennas) and frequency. Although SF coding is well suited for fast fading, variations within subcarriers for large OFDM blocks and channels with large delay spreads may result in performance degradation. Hence space-time-frequency (STF) coding has been proposed [159]. However, STF coding does not necessarily offer additional diversity advantages compared to SF coding. This thesis therefore addresses maximizing the diversity gain offered by STF coding through the use of residue number system code as a frequency encoder.

In MIMO wireless communication systems, channel estimation is a tedious and impractical process because of the rapidly changing channel characteristics and several propagation paths. To circumvent the need for channel estimation, we resort to noncoherent differential modulation. In conventional differential modulation (CDM) the channel characteristics for at least two consecutive symbols $N = 2$ are considered

constant [64], [65], [66]. Multi-symbol differential modulation (MSDM) for M-ary phase shift keying (MPSK) was proposed to reduce the error floor effect, and hence improve the performance of CDM [68]. MSDM was extended to space-time block codes (STBC) [122], [123], [125]. In MSDM for STBC, the performance improves not only with increasing observation period i.e. $N > 2$, but also with the number of antennas. A less complex but suboptimal decision feedback differential modulation (DFDM) scheme was proposed for STBC [124], [126], [129]. This thesis therefore extends decision feedback differential modulation to STF coding.

Bit-interleaved coded modulation is a concatenation of a channel encoder and symbol mapper through an interleaver. This technique was shown to be well suited for bandwidth efficient transmissions over fading channels [55], [56], [58], [59]. The performance of bit-interleaved coded modulation can be greatly improved through iterative information exchange between the decoder and the demapper [58], [60]. It is a low complexity alternative to turbo codes rendering it attractive for MIMO systems [61]. To maximize the coding gains for bit-interleaved coded modulation, low rate convolutional codes are often used, hence reducing the overall rate of the system. This is further complicated by the necessity to exchange soft information at bit level, hence making convolutional codes easy to decode using already existing algorithms such as the Viterbi decoder [62], [63] compared to high rate block (binary or non-binary) codes. Through the pioneering work of Pyndiah [45], [46], [47], a soft decision decoding algorithm for linear block turbo codes was developed. An approximate maximum likelihood decoding algorithm based on list decoding method is described in [45] and the references therein. This implies that non-binary linear block codes with higher code rates can be used in place of convolutional codes and still achieve approximately the same coding gains. This thesis therefore proposes the use of residue number system codes as the channel encoder.

1.6 Thesis Overview

This thesis is divided into six chapters. It is aimed at developing a technique for combining channel coding, frequency diversity and spatial diversity into a bandwidth efficient communication scheme, and characterizing the performance of such a system in a wireless broadband environment.

In Chapter 1, Wireless MIMO and its functionalities are discussed, focussing on attributes that render it attractive as a wireless technology for broadband communications systems. Motivation for the work done in this thesis is also discussed.

In Chapter 2, residue number system (RNS) channel encoding is introduced. We discuss RNS codes redundancy properties and error control when applied to communication systems. Different encoding and decoding algorithms for hard decision are outlined. The already existing soft decoding algorithms for block codes are extended to RNS codes. A bit-interleaved coded modulation for noncoherent MPSK modulation is proposed and its performance investigated. It is shown in some applications that the residue number system codes can achieve similar or better bit error rate performance than convolutional codes of the same rate and asymptotic coding gain.

Chapter 3 presents a comparative study of different MIMO systems, i.e. space-time coding, space-frequency coding and space-time-frequency coding. The different design criteria for the MIMO systems in multipath fading channels are discussed and their performance investigated.

In Chapter 4, an RNS based space-time-frequency (STF) coding scheme is proposed. A design criterion similar to already existing space-time-frequency coding schemes is presented. It is shown that the proposed RNS space-time-frequency coding scheme offers additional frequency diversity independent of the selective nature of the fading channel. We investigate the performance of the proposed RNS space-time-frequency coding scheme over a rapid fading channel and show its flexibility over different space-time code designs.

In Chapter 5, an RNS coded iterative noncoherent differential space-time-frequency modulation scheme is presented and its performance characterized. RNS differential coding from single antennas systems is extended to MIMO systems. Analytical expressions are derived for both the hard and soft decision metric and the decision feedback differential space-time-frequency modulation. It is shown that increasing diversity can reduce or eliminate the flooring effect in conventional differential detection. Results show that significant coding gains can be achieved by passing not only hard decisions but also soft information.

Chapter 6 presents a summary and conclusions drawn in the thesis. Comments on future extensions of the work done in the thesis are also suggested.

1.7 Original Contribution

In Chapter 2, a near optimal bit-interleaved coded decision feedback differential modulation for single antenna is proposed. This uses a residue number system code instead of the convolutional code traditionally used in bit-interleaved coded modulation. This scheme achieves high data rates with minimal complexity, in contrast to the convolutionally coded schemes.

An RNS based space-time-frequency coding scheme is proposed in Chapter 4. The key feature of the proposed STF coding scheme is the frequency encoder. Most STF schemes in the literature use coding across multipaths and OFDM modulation techniques to maximize frequency diversity. The main challenge is the code construction involving a large number of OFDM carriers in a practical system. By dividing the available bandwidth into several non-overlapping subchannels equal to the code length, the proposed scheme codes across a number of subcarriers with space-time signalling on each subcarrier. Hence the signal design on each subcarrier is the same as that of space-time codes and multipath diversity is merely a trivial extension.

The proposed space-time-frequency code design in Chapter 4 can achieve full rate and diversity gain of $M_t M_r M_b N_c$ over quasi-static fading channels, where M_t and M_r are the number of transmit and receive antennas respectively, M_b is the time diversity and N_c the number of OFDM tones. The diversity order incorporates the number of subcarriers (OFDM tones) previously not considered in the design of already existing space-time-frequency architecture. Hence the proposed STFC scheme can achieve up to a maximum possible diversity gain of $M_t M_r M_b N_c L$, where L is the channel order.

The assumption of block fading is not ideal when transmitting over broadband wireless communication channels and channel state information is not easy to track. In Chapter 5, a residue number system based iterative noncoherent differential STF coding scheme for a frequency flat fast Rayleigh fading channel is proposed. The differential STF decision feedback metric is derived and the performance characterized.

A soft decision decoding for bit-interleaved decision-feedback differential modulation is presented and its bit metric derived in Chapter 5. It is shown that this scheme can achieve significant coding gains over the hard decision bit-interleaved decision-feedback differential modulation. The decoding process is not limited to RNS scheme but can be used in any iterative decision feedback differential modulation system a with channel encoder e.g. convolutional codes.

1.8 Publications

Part of the material in this thesis has been published, or submitted for possible publications as follows:

1. R.N. Akol and F. Takawira, "A comparative study for space-time-frequency coded systems for broadband channels", in *Proceedings Of the South African Telecommunications Networks and Applications Conference* (SATNAC), George, South Africa, Sept. 2003.
2. R.N. Akol and F. Takawira, "BER performance for residue based space-time-frequency coding in a rapid fading channel", in *Proceedings Of the South African Telecommunications Networks and Applications Conference* (SATNAC), Stellenbosch, South Africa, Sept. 2004.
3. R.N. Akol and F. Takawira, "Maximizing diversity for space-time frequency coding in a rapid fading channel", in *Proceedings of the 12th International Conference on Telecommunications* (ICT), Cape Town, South Africa, May 2005.
4. R.N. Akol, F. Takawira, "Performance of coded residual arithmetic differential MPSK modulation," in *Proceeding of the IEEE Wireless Communications and Networking Conference*, Las Vegas, Nevada, USA, pp. 1927-1932, Apr. 2006.
5. R.N. Akol, F. Takawira, "On performance of arithmetically coded differential space-time-frequency coding," submitted to *IEEE International Conference on Communications*, to be held in Glasgow, Scotland, United Kingdom, Jun. 2007.
6. R.N. Akol, F. Takawira, "Soft-in soft-out decision feedback differential space-time-frequency coding," Submitted to *IEEE Transactions on Vehicular Technology*, Sept. 2006.

CHAPTER 2

REDUNDANT RESIDUE NUMBER SYSTEM CODED DIFFERENTIAL MODULATION

2.1 Introduction

A residue number system (RNS) code is a non-weighted number system, with inherent carry-free operations and lack of ordered significance features among its residues [15], [16], [17], [18], [19], [20]. The carry-free feature implies that the operations related to the different residues such as additions, subtraction or multiplication are mutually exclusive, ensuring that errors are not propagated from one residue to another. Therefore, it is possible to perform arithmetic on long numbers at the same speed as short ones. The arithmetic advantage is due to the ability of RNS to add, multiply or subtract in parallel without generating intermediate carry forward digits or internal delays. Hence RNS find wide application in high speed arithmetic operations such as in general purpose computers [20], [22]. The residues are simply a remainder representation of the operand divided by pairwise relatively prime positive integers known as moduli. In RNS an integer is represented by a group of residues and can be recovered from any combination of subsets formed provided there is sufficient information. The lack of ordered significance feature among residue digits implies that some residues can be discarded without affecting the final outcome. This property heralds redundancy and forms the basis of error control design in RNS. RNS have been studied widely in tolerance protection of arithmetic operations such as digital filters and their redundancy property has been exploited in theoretical computer science [22]. Due

to their flexible data rates, RNS codes are currently being considered for adaptive systems [30] and cross layer design [173].

The error correction and detection properties of RNS are well established [17], [18], [19], [21], [26], [27], [28], making them attractive for channel coding in communication systems. These codes belong to maximum distance separable codes and hence have similar coding properties to Reed Solomon codes [33]. Liew, Yanga and Hanzo [31] showed that the Chase algorithm can be invoked to provide soft input to the hard decision RNS decoder and consequently applied the Pyndiah block turbo coding principle [29], [32]. These codes were shown to have tremendous improvement when the iterative decoding is applied in additive white Gaussian noise (AWGN).

Noncoherent detection using differential modulation (DM) is very attractive for M-ary phase-shift-keying (MPSK) signalling over rapid fading channels because of its robustness against phase ambiguities and impairments of the received signal. There is no channel information required at the receiver, hence, eliminating the need for a tedious, impractical channel estimation process for rapidly changing channel characteristics. Initially noncoherent DM was applied to quasi-static fading channels where the channel characteristics for at least two consecutive symbols $N = 2$ are considered constant [64], [66], [67]. Noncoherent DM has been adopted for continuous or fast fading channels. However, conventional noncoherent differential modulation leads to a 3 dB loss over coherent modulation due to variations in the autocorrelation function of the fading process. Multi-symbol differential modulation (MSDM) for MPSK was proposed to improve the performance of noncoherent DM [65], [68]. In MSDM the observation period $N > 2$ is considered for maximum likelihood sequence detection instead of symbol-by-symbol detection as in conventional differential modulation (CDM). The performance of MSDM improves with increasing observation period. This leads to increased complexity at the receiver. Hence, a suboptimal but less complex decision feedback differential modulation (DFDM) scheme was proposed [69], [70], [71]. This uses maximum likelihood detection for a symbol-by-symbol detection (rather than the entire block of N observations) by feeding back previous $N-1$ hard decisions. It was also shown that the performance of DFDM could be further improved through iterative decoding of bit-interleaved coded modulation [72]. In [72], an outer convoltional code is serially concatenated with an inner differential encoder. This

method was shown to offer comparable performance to the more complex iterative schemes proposed in [73], [74], [75], [78], [80], [81]. This method also outperformed the less complex coded CDM [76], [77]. The channel encoders employed in iterative DFDM and coded CDM schemes are convolutional codes which may require low rates or long constraint length to reduce the error floor effect.

Motivated by the performance of low complex iterative DFDM and soft decoding of RNS codes in AWGN, we propose a redundant residue number system iterative coding scheme for noncoherent differential MPSK modulation in a Rayleigh fast fading channel. Since RNS codes can offer high and flexible data rates, a key parameter in the design for today's multimedia communication systems, this research follows a novel path. In this scheme, the RNS code is used as a channel encoder and is concatenated with the inner differential encoder. Bit-interleaved coded modulation is applied to break the error dependence of the channel, hence increasing the code diversity. The soft values from the DFDM decoder are fed to the Chase like RNS decoder. Simulation results show that the RNS codes can achieve similar or better bit error rate (BER) performance than convolutional codes at approximately the same rate and asymptotic coding gain for $t = 1, 2$ error correction capability.

This chapter is organized as follows; in Section 2.2 we describe RNS representation and simple arithmetic. Section 2.3 highlights the RNS coding theory and the encoding process followed by the proposed bit-interleaved differential MPSK in Section 2.4. We present simulation results in Section 2.5 and conclude in Section 2.6.

2.2 Residue Number System (RNS)

2.2.1 Representation

The decimal number system is the most widely used number system. This system is linear, positional and weighted such that all positions derive their weights from the same radix (base) i.e. 10. Hence an integer X can be represented by

$$\begin{aligned} X &= a_{k-1}10^{k-1} + a_{k-2}10^{k-2} + \cdots + a_1 10 + a_0 \\ &= \sum_{j=0}^{K-1} a_j r^j, \end{aligned} \tag{2.1}$$

where $r = 10$ for decimal number system. The binary number system is another widely used number system with positional weights $2^0, 2^1, 2^2$, etc.

The residue number system is a mixed radix system with positional bases that are usually relative prime numbers to each other, for example 2, 3, and 5. An integer $X = 17$ is then represented by the bases 2, 3 and 5 by dividing it with the bases and retaining the remainder known as the residue digit in their respective positions. To convert a decimal number 17 to a residue number, we compute:

$$\begin{aligned} x_1 &= 17 \bmod 2 = 1, \\ x_2 &= 17 \bmod 3 = 2, \\ x_3 &= 17 \bmod 5 = 2, \end{aligned}$$

hence the decimal 17 is represented by $[1,2,2]$ in the above residue number system. This residue number system offers a unique representation of X in the range $0 \le X < 30 = 2 \times 3 \times 5$. Note that the integer $X = 17$ can be represented in the decimal number system as

$$17 = 1 \times 10^1 + 7 \times 10^0.$$

The weighted number system uses constant weights which is the power of the radix (e.g. 10 in decimal number system) and is referred to as a fixed radix system.

2.2.2 Operations in Residue Number System

Suppose X_1 and X_2 are two decimal numbers, the operation $X_1 \bullet X_2$ results in a third decimal number X_3, where $\bullet$ denotes addition, subtraction or multiplication. Likewise if $X_1 \leftrightarrow (x_{11}, x_{12}, \cdots, x_{1k})$ and $X_2 \leftrightarrow (x_{21}, x_{22}, \cdots, x_{2k})$ are uniquely represented in the RNS then $X_3 = X_1 \bullet X_2$ can be uniquely represented provided X_3 is in the range $[0, M-1]$, where M is the product of the radices in RNS. Hence

$$\begin{aligned} &X_3 = X_1 \bullet X_2, \\ &X_3 \leftrightarrow \left((x_{11} \bullet x_{21})_{\bmod m_1}, (x_{12} \bullet x_{22})_{\bmod m_2}, \cdots, (x_{1k} \bullet x_{2k})_{\bmod m_k} \right), \\ &X_3 \leftrightarrow (x_{31}, x_{32}, \cdots, x_{3k}). \end{aligned} \tag{2.2}$$

The following example illustrate the three arithmetic operations namely addition, subtraction and multiplication for RNS with radices $m_1 = 5$, $m_2 = 3$ and $m_3 = 2$, respectively.

9	$\leftrightarrow$	$[4,0,1]$	7	$\leftrightarrow$	$[2,1,1]$	7	$\leftrightarrow$	$[2,1,1]$
+ 16	$\leftrightarrow$	$[1,1,0]$	$\times$ 4	$\leftrightarrow$	$[4,1,0]$	$-$ 4	$\leftrightarrow$	$[4,1,0]$
25	$\leftrightarrow$	$[0,1,1]$	28	$\leftrightarrow$	$[3,1,0]$	3	$\leftrightarrow$	$[3,0,1]$
decimal		*residue*	*decimal*		*residue*	*decimal*		*residue*

There is no information carried forward between the residue digits resulting in high speed operations. In the event that an error occurs it is confined within the corresponding residue digit and does not affect other operations.

2.3 Using RNS in Channel Encoding

A residue number system (RNS) code is defined by a set of V pairwise relatively prime positive integers $m_i (i = 1,2,\cdots,V)$ known as moduli [15], [16], [17], [18], [19], [20]. The product of the moduli is called the dynamic range M_v which determines the maximum number of bits $(\log_2 M_v)$ that can be transmitted using the RNS code,

$$M_v = \prod_{i=1}^{V} m_i . \tag{2.3}$$

Any positive integer X in the range $0 \le X < M_v$ can be uniquely and unambiguously mapped to a set of residue sequence $(x_1, x_2, \cdots, x_v)$, such that $x_i = X (\mathrm{mod}\, m_i)$. From the Chinese remainder theorem (CRT) [26],[33], for a given set of residues, there exists one and only one integer X in the range $0 \le X < M_v$. This allows unique recovery of the information data X from a set of received residues. The CRT is expressed as

$$X = \left(\sum_{i=1}^{V} M_i x_i L_i \right) \mathrm{mod}\, M_v , \tag{2.4}$$

where $M_i = M_v / m_i$ and L_i is the multiplicative inverse of $M_i \,\mathrm{mod}\, m_i$, such that $(L_i M_i) \,\mathrm{mod}\, m_i = 1$.

The mixed radix conversion (MRC) can also be used to represent integer X in the from

$$X = \sum_{i=1}^{V} a_i \prod_{j=1}^{i-1} m_j , \tag{2.5}$$

such that $0 \le a_i < m_i$ are known as radix coefficients and $\prod_{j=1}^{0} m_j = 1$.

To incorporate error control, $U - V$ redundant moduli are appended to form a redundant residue number system RRNS(U,V) code with $0 \le X < M_v$ being the legitimate dynamic range and $M_v \le X < M_u$, the illegitimate dynamic range, given $M_u = \prod_{i=1}^{U} m_i$ [21], [26]. Any received information X falling in the illegitimate range implies that an error has occurred. Hence RNS can be used for error detection.

From information theory, the minimum distance $d_{\min}$ is a key parameter in any error control coding. The redundant residue number system (RRNS) code has a minimum distance of $d_{\min}$ if and only if the product of the redundant moduli satisfies the following inequality [18], [19]

$$\max\left\{\prod_{i=1}^{d_{\min}} m_{j_i}\right\} > M_R \ge \max\left\{\prod_{i=1}^{d_{\min}-1} m_{j_i}\right\}, \tag{2.6}$$

where $M_R = \prod_{i=V+1}^{U} m_{j_i}$ and m_{j_i} is any of the U moduli and $1 \le j_i \le U$. Hence the error correcting capability of a RRNS code is given by [21], [33]

$$t = \left\lfloor \frac{d_{\min} - 1}{2} \right\rfloor, \tag{2.7}$$

where $\lfloor z \rfloor$ denotes the largest integer not exceeding z. It was also shown that for maximum distance separable RRNS code (i.e. $d_{\min} - 1 = U - V$), the necessary condition for the left hand side of (2.6) to be satisfied requires RRNS code to have the largest modulus of $d_{\min} - 1$ as the redundant modulus.

RRNS(U,V) code is a block code, since it takes in V information symbols and generates U coded symbols. RRNS codes are semi-linear block codes as the condition of linearity is satisfied under certain conditions only [18], [33]. The fundamental properties of linear block codes are that the all-zero vector is a valid codeword and the sum of two valid codewords is also a valid codeword [37], [38], [39].

2.3.1 Redundant Residue Number System (RRNS) Encoder

There are two coding strategies used in RRNS, namely systematic and non-systematic encoding. This can literally be viewed as in the case of convolutional codes where the information bits have either a direct bearing on the coded symbols i.e. systematic encoding, or not i.e. non-systematic encoding.

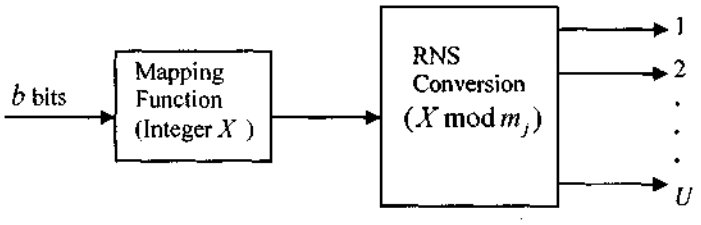

Figure 2.1: Non-systematic encoding

Figure 2.1 shows the block diagram of non-systematic RRNS encoding process. In non-systematic RRNS encoding, a block of b bits per encoding interval is mapped to an integer X such that

$$0 \le X < 2^b \le M_v, \tag{2.8}$$

where M_v is the legitimate dynamic range. Note that in most scenarios, the legitimate dynamic range is not a typical integer power of 2. Hence $2^b << M_v$, which implies that the dynamic range is not efficiently used. The residue digits corresponding to a given set of moduli are then generated using the convectional modular arithmetic

$$x_j = X \bmod m_j, \tag{2.9}$$

for $j = 1, 2, \cdots U$. Since the moduli are relatively prime to each other, the resultant codeword is unique for each given integer X. Each residue digit is converted to its binary equivalent such that there are n_j number of bits per residue

$$n_j = \log_2 m_j + 1, \tag{2.10}$$

hence the resultant number of coded bits at the output of the non-systematic encoder is

$$b' = \sum_{j=1}^{U} n_j . \tag{2.11}$$

The rate of the RRNS non-systematic code is given by b/b'. Since the residues do not directly represent the data, the above encoding process is referred to as non-systematic.

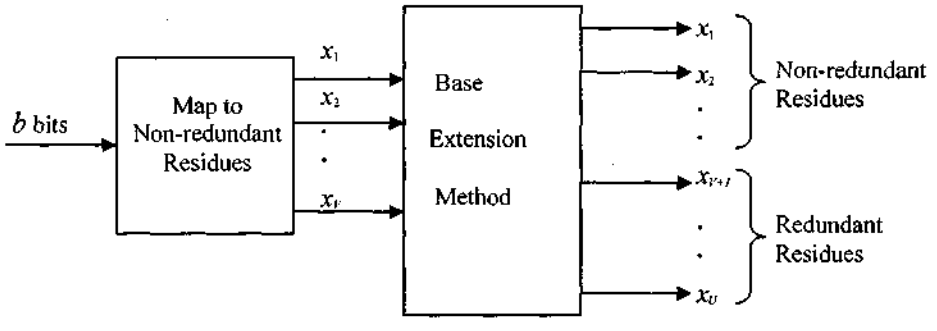

Figure 2.2: Systematic encoding

Figure 2.2 shows the block diagram of systematic RRNS encoding process. In a systematic RRNS encoding, a block of b information bits is divided into smaller groups of $b_j = \log_2 m_j$ bits and mapped to non-redundant residues $x_1, x_2, \cdots, x_V$ such that

$$b = \sum_{j=1}^{V} b_j . \tag{2.12}$$

The redundant residues are generated using the base extension (BEX) method [29], [33]. Mapping each redundant residue to its binary equivalent, yields $b_j = \log_2 m_j + 1$ bits and

$$b' = \sum_{j=V+1}^{U} b_j , \tag{2.13}$$

where b' is total number of redundant bits. Hence the rate of a RRNS systematic code is $b/(b+b')$. From (2.5), we can expand the MRC representation of integer X to form

$$X = a_1 + a_2 m_1 + a_3 m_1 m_2 + \cdots a_{k-1} \prod_{j=1}^{k-2} m_j + a_k \prod_{j=1}^{k-1} m_j , \tag{2.14}$$

where a_j are the mixed radix coefficients. Recall from the definition of the dynamic range i.e. the product of moduli, and assuming that the moduli are arranged in ascending order (which is a necessary condition for the inequality in (2.6) to be satisfied) i.e. $m_1 < m_2 < \cdots < m_k$. It can easily be seen that the terms in (2.14) are all multiples of X except for m_1, hence the radix coefficient $a_1 = X \bmod m_1$. To solve for a_2, first subtract a_1 from (2.14) and then divide by m_1,

$$\frac{X - a_1}{m_1} = a_2 + a_3 m_2 + \cdots a_{k-1} \prod_{j=2}^{k-2} m_j + a_k \prod_{j=2}^{k-1} m_j . \tag{2.15}$$

Likewise all the terms in (2.15) are multiples of $\frac{X - a_1}{m_1}$ except for m_2. The whole procedure can be repeated until all the radix coefficients are obtained. Hence

$$\begin{aligned} a_1 &= X \bmod m_1, \\ a_2 &= (X / m_1) \bmod m_2, \\ a_3 &= (X / m_1 m_2) \bmod m_3, \\ &\vdots \\ a_k &= (X / m_1 m_2 \cdots m_{k-1}) \bmod m_k. \end{aligned} \tag{2.16}$$

If another term is added to (2.14), the mixed radix representation would be

$$X = a_1 + a_2 m_1 + a_3 m_1 m_2 + \cdots a_{k-1} \prod_{j=1}^{k-2} m_j + a_k \prod_{j=1}^{k-1} m_j + a_{k+1} \prod_{j=1}^{k} m_j , \tag{2.17}$$

with $0 \le X < \prod_{j=1}^{k} m_j - 1$ being the legitimate dynamic range. Therefore, if the integer X is to be represented in the extended MRC form, its coefficients beyond k are equal to zero. Since the set of moduli is always predetermined, and the non-redundant residues are a result of direct mapping from the corresponding bits, the task of representing

integer X in the extended MRC form amounts to finding the radix coefficients. The fact that coefficients beyond k are equal to zero is used to find the residue digit of the extend moduli $X \bmod m_{k+1}$. Hence, redundant residue are generated from (2.16) by performing modulus operations since the non-redundant residues are known. The process of representing the integer in the extended MRC form is known as BEX.

2.3.2 Error Detection and Hard-Decision Decoding Algorithm

The decoding process is dependent on which encoding was used, i.e. systematic or non-systematic RRNS encoding. From the received residue vector, an integer $\bar{X}$ is computed using either the CRT or the MRC. If $\bar{X} \geq M_v$, it implies that the received residue vector is an invalid codeword, hence an error has been detected. Once errors have been detected, their respective positions have to be determined and subsequently corrected. An RRNS(U,V) code is able to detect up to $U-V$ residues if they are in error and correct up to $t=(U-V)/2$ residues in error. Any valid codeword represents a unique integer which falls within the legitimate range $0 \leq X < M_v$ of the RRNS code and any invalid codewords are in the illegitimate range $M_v \leq X < M_u$. An algorithm for single residue error correction based on modulus projection and the CRT was proposed [18] and has been extended to correct multiple residues in [19] and [20].

In this subsection we outline the error detection and hard decision decoding procedure that will be used to decode RNS codes throughout this thesis. The hard decision decoding algorithms are based on BEX and MRC for multiple error correction proposed in [33].

At the RRNS decoder, the MRC is applied on the set of the received residue vector to solve for radix coefficients. If the radix coefficients $a_{v+1} \cdots a_u$ are equal to zero, there is no error in the received residue vector. However, if any of the radix coefficients $a_{v+1} \cdots a_u$ are not equal to zero, there is at least one residue digit in error. The next step is to locate the error positions. An RRNS code can correct up to $t=(d_{\min}-1)/2=(U-V)/2$ residues in error. First, t residue positions are assumed to be in error and a new set of moduli is obtained by deleting the corresponding t moduli, hence a new legitimate and illegitimate dynamic range. MRC is then applied to

determine the values of the new radix confinements using the deleted residues and their corresponding moduli as the new redundant set. If all the radix coefficients $a_{v+1} \cdots a_{v+t}$ are zero, correct the error using the BEX method and stop. If not, the above process is repeated for all $\binom{U}{t}$ different combinations. If no zero radix coefficients are found after $\binom{U}{t}$ trials, there are more than t errors in the received residue vector and the decoding process is stopped.

2.4 Bit-Interleaved RRNS Differential Modulation

In this subsection we describe the system model for the proposed redundant residue number system iterative coding scheme for non-coherent differential modulation. The baseband representation of the system model is depicted in Figure 2.3.

2.4.1 System Model

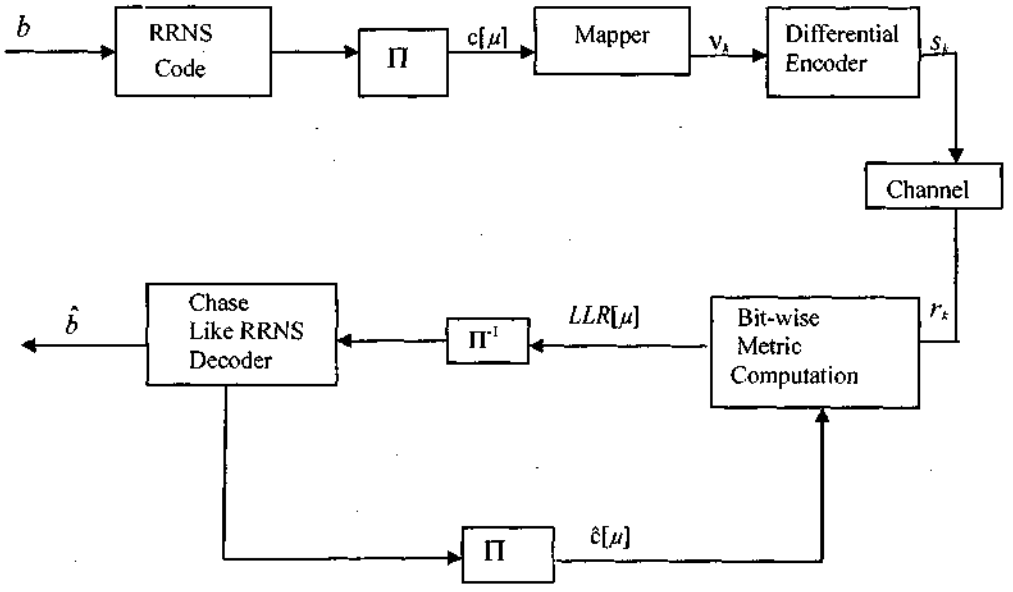

Figure 2.3: System model of RNS bit-interleaved differential MPSK

The binary information stream to be transmitted is first grouped into blocks of b bits M-ary symbols, which are then encoded by the outer RRNS(U,V) code to a set of U parallel residues as described in the preceding subsection. This implies that for b information bits to be transmitted using RRNS(U,V) code, the legitimate dynamic range should be equal or greater than 2^b (i.e. $b = \log_2 M_r$). In this chapter we use systematic RRNS encoders that were proposed in [29], [31], [33]. In a systematic RRNS encoding, the b block of bits is divided into smaller groups each with $b_i = \log_2 m_i$ which are mapped to non-redundant residues and the redundant residues are generated using the base extension (BEX) method. A block of L residues (with U parallel residues per coding interval) is serially converted to its binary equivalent and bit-interleaved. The coded bit stream is then mapped to a $\tilde{b}$ bit MPSK symbol such that $\tilde{b} = \log_2 \mathrm{M}$. The MPSK symbols are then differentially encoded and transmitted over rapidly fading Rayleigh frequency non-selective channel.

Consider a differentially coded symbol s_k propagating over a fast fading Rayleigh fading channel during the kth symbol interval. The output of the differential encoder is given by

$$s_k = v_k s_{k-1}, \tag{2.18}$$

where v_k is the data carrying symbol and is drawn from $v_k \in \mathrm{A} = \left\{\exp(j2\pi v/\mathrm{M}) \middle| v = 0,1,\cdots,\mathrm{M}-1\right\}$ MPSK signal constellation. At the receiver, the received signal can then be expressed as

$$r_k = s_k h_k + n_k \tag{2.19}$$

where n_k is the additive white Gaussian noise (AWGN) with zero mean and double spectral density $N_o/2$. The zero-mean complex Gaussian random correlated fading process h_k is based on Jakes model [174] with a normalized autocorrelation function given by

$$\varphi_h(\tau) = E_h\left\{h_k h_{k+\tau}^*\right\} = \sigma_h^2 J_o\left(2\pi f_D T\right), \tag{2.20}$$

where σ_h^2 is the variance, $E_h\{.\}$ and (.)* denotes the expectation with respect to h and complex conjugate respectively, $J_0(.)$ is the Bessel function of the first kind, f_D is the maximum Doppler frequency and T is the symbol duration.

2.4.2 Decision Feedback Differential Modulation

The maximum likelihood decoding process follows decision feedback differential modulation (DFDM) which is derived from multi-symbol differential modulation (MSDM) for $N > 2$ observation period [69], [70]. Given that there is no channel state information at the receiver, the conditional probability density function (pdf) of the received vector $\mathbf{r}_k = [r_k, r_{k-1}, \cdots, r_{k-N+1}]^T$ given the data carrying symbol vector $\mathbf{v}_k = [v_k, v_{k-1}, \cdots, v_{k-N+2}]^T$ for the differentially coded symbol vector $\mathbf{s}_k = [s_k, s_{k-1}, \cdots, s_{k-N+1}]^T$ is

$$p(\mathbf{r}_k / \mathbf{v}_k) = \frac{e \exp\left(-\mathbf{r}_k^{\mathcal{H}} \mathbf{\Lambda}^{-1} \mathbf{r}_k\right)}{\pi^N |\mathbf{\Lambda}|}, \tag{2.21}$$

where $\mathcal{T}$ is the transpose, $\mathcal{H}$ is the conjugate transpose and $\mathbf{\Lambda}$ is an $N \times N$ correlation matrix. The correlation matrix is derived from the autocorrelation matrix $\boldsymbol{\varphi}_h$ of the fading process and AWGN over $N > 2$ observation periods as

$$\begin{aligned} \mathbf{\Lambda} &= \mathbf{r}_k^{\mathcal{H}} \mathbf{r}_k / \mathbf{v}_k \\ &= \mathbf{s}_k^{\mathcal{H}} \boldsymbol{\varphi}_h \mathbf{s}_k + \frac{N_o}{2} \mathbf{I}_N, \end{aligned} \tag{2.22}$$

where the elements of $\boldsymbol{\varphi}_h$ are given by (2.20), $\mathcal{H}$ denotes the complex conjugate transpose and $\mathbf{I}_N$ is an $N \times N$ identity matrix. If the symbols v_k are taken from a unitary MPSK signal constellation, then $\mathbf{s}_k^{\mathcal{H}} \mathbf{s}_k = \mathbf{I}_N$ and the correlation matrix can be expressed as

$$\begin{aligned} \mathbf{\Lambda} &= \mathbf{s}_k^{\mathcal{H}} \left(\boldsymbol{\varphi}_h + \frac{N_o}{2} \mathbf{I}_N \right) \mathbf{s}_k \\ &= \mathbf{s}_k^{\mathcal{H}} \mathbf{R}_h \mathbf{s}_k, \end{aligned} \tag{2.23}$$

and is independent of the transmitted symbol sequence. Neglecting the constant terms and substituting for $\mathbf{A}$ in (2.21), the conditional pdf can be rewritten as [70], [71], [72]

$$\begin{aligned} p(\mathbf{r}_k / \mathbf{v}_k) &= e \exp\left[-\mathbf{r}_k^{\mathcal{H}} \left(\mathbf{s}_k^{\mathcal{H}} \mathbf{R}_h \mathbf{s}_k \right)^{-1} \mathbf{r}_k \right] \\ &= e \exp\left[-\mathbf{r}_k^{\mathcal{H}} \mathbf{s}_k \mathbf{R}_h^{-1} \mathbf{s}_k^{\mathcal{H}} \mathbf{r}_k \right]. \end{aligned} \tag{2.24}$$

The conditional pdf in (2.24) can further be expanded and expressed as

$$p(\mathbf{r}_k / \mathbf{v}_k) = \exp\left(\sum_{i=0}^{N-1} \sum_{j=0}^{N-1} t_{ij} r_{k-i}^{*} s_{k-i} s_{k-j}^{*} r_{k-j} \right), \tag{2.25}$$

where t_{ij} are elements of the inverse of the correlation matrix $\mathbf{R}_h$ in (2.23) defined as

$$\mathbf{T} = -\mathbf{R}_h^{-1} = -\left(\boldsymbol{\varphi}_h + \frac{N_0}{2} \mathbf{I}_N \right)^{-1} = \begin{bmatrix} t_{00} & t_{01} & \cdots & t_{0N-1} \\ t_{10} & t_{11} & \cdots & t_{1N-1} \\ \vdots & \vdots & \ddots & \vdots \\ t_{N-10} & t_{N-11} & \cdots & t_{N-1N-1} \end{bmatrix}. \tag{2.26}$$

By expanding (2.25) and substituting for $s_k s_{k-1}^{*} = v_k$, the multi-symbol differential pdf can be expressed as

$$p(\mathbf{r}_k / \mathbf{v}_k) = \exp\left[\mathrm{Re}\left(\sum_{i=0}^{N-1} t_{ii} r_{k-i}^{*} s_{k-i} s_{k-i}^{*} r_{k-i} \right) + 2\,\mathrm{Re}\left(\sum_{i=1}^{N-1} \sum_{j=0}^{i-1} t_{ij} r_{k-i}^{*} r_{k-j} \prod_{\zeta=j}^{i-1} v_{k-\zeta} \right) \right]. \tag{2.27}$$

Note that the first term of the exponential function is a constant and can be ignored, hence

$$p(\mathbf{r}_k / \mathbf{v}_k) \approx \exp\left[2\,\mathrm{Re}\left(\sum_{i=1}^{N-1} \sum_{j=0}^{i-1} t_{ij} r_{k-i}^{*} r_{k-j} \prod_{\zeta=j}^{i-1} v_{k-\zeta} \right) \right]. \tag{2.28}$$

The maximum likelihood decoding for symbol v_k is taken over the entire N block symbols by choosing the metric that maximize the conditional pdf in (2.28). To minimize the receiver complexity, $N-1$ previous hard decisions are fed back [69], [70], hence, the term decision feedback differential modulation (DFDM). The conditional pdf in (2.27) reduces to

$$p(\mathbf{r}_k / \mathbf{v}_k) = \exp\left(2\,\mathrm{Re}\left\{ r_k^* v_k \sum_{j=1}^{N-1} t_{0j} r_{k-j} \prod_{\zeta=1}^{j-1} \tilde{v}_{k-\zeta} \right\} \right), \tag{2.29}$$

where $\tilde{v}_{k-\zeta}$ are the hard symbol decisions from the previous detection except for the kth symbol interval. From (2.29) the maximum likelihood decoding for v_k chooses the symbol from the MPSK signal constellation that maximize the conditional pdf in (2.29). Since the logarithmic function is a monotonically increasing, maximizing $p(\mathbf{r}_k / \mathbf{v}_k)$ over $\mathbf{v}_k$ is equivalent to maximizing $\log\left(p(\mathbf{r}_k / \mathbf{v}_k)\right)$ over $\mathbf{v}_k$. Hence the bit metric from the kth label can be obtained by averaging over signal constellation whose symbol metrics have $b \in \{0,1\}$ in the μth bit position as

$$\lambda_b^k[\mu] = \log \sum_{v_k \in A_b^\mu} \exp\left(2\,\mathrm{Re}\left\{ r_k^* v_k \sum_{j=1}^{N-1} t_{0j} r_{k-j} \prod_{\zeta=1}^{j-1} \tilde{v}_{k-\zeta} \right\} \right). \tag{2.30}$$

Thus the bit log-likelihood-ratio (LLR) metric for the kth label in the μth bit position is given by

$$LLR_k[\mu] = \lambda_0^k[\mu] - \lambda_1^k[\mu]. \tag{2.31}$$

The LLR are first deinterleaved and fed to a chase like RRNS decoder. The deinterleaved LLR values are the soft input to the Chase RRNS decoder which outputs hard decisions. The hard decisions are interleaved and fed back to the bit-wise metric computer. The procedure is repeated for several iterations.

2.4.3 Chase and Iterative Decoding Algorithm

The hard decision decoding algorithms used in this thesis are based on BEX and MRC for multiple error correction as outlined in Section 2.3.2. We invoke the Chase algorithm similar to [31] but differ in the generation of soft input to the chase decoder and the error pattern.

For every decoding interval, $b+b'$ LLR values are fed to the Chase like RRNS decoder. A hard decision z_μ associated to the soft information $y_\mu = \hat{\lambda}_\mu^{n,k} N_0 / 2$ is made [47]. The confidence values $|y_\mu|$ are then sent to the Chase algorithm which generates

a set of 2^l error patterns according to the l least reliable confidence values $|y_\mu|$. The error patterns are each added to $\mathbf{Z} = [z_1 z_2 ... z_{b+b'}]$ by modulo two addition to produce a new sequence $\mathbf{Z}'$ which is mapped to corresponding residues and sent to hard decision RRNS decoder. At the output of the hard decision decoder a set of valid codewords is searched according to (2.32), and the codeword with the minimum metric is decoded as the transmitted codeword

$$\hat{v}_i = \sum_{\mu=1}^{b+b'} \left| y_\mu - \overline{z}_\mu^i \right|^2, \tag{2.32}$$

where $\overline{z}_\mu^i \in \{+1, -1\}$ in the μth bit position of the ith codeword at the output of the hard decision decoder.

If no valid codeword is found, $\mathbf{Z}$ is then decoded as the transmitted codeword. The decoded codeword is mapped to non-redundant residues as described in Section 2.3.1 for systematic RRNS encoding. Redundant residues are generated through BEX method and the whole process is repeated for the entire block. The residues are then converted to their binary equivalent and bit-interleaved. After bit-interleaving the bits are mapped to MPSK symbols, which are then differentially encoded and fed back to the DFDM decoder for a new metric computation as shown in Figure 2.3.

For the iterative decoding process, the re-modulated fed back symbols are generated from bit decision at the output of the Chase RRNS decoder. For the first iteration, as there are no previous decisions available, we use conventional differential modulation i.e. $N = 2$ for the first iteration [72]. For further iterations, re-modulated fed back symbols from previous iterations are used to calculate the bit LLR values as in (2.30) and (2.31) for $N > 2$ observations period.

2.4.4 Complexity Issues

In this subsection, we comment on the complexity of the proposed system model versus the convolutionally coded differential scheme in [72]. Since both schemes use decision feedback differential modulation for their differential decoding, our comparisons are based on the channel encoders i.e. convolutional code (CC) versus RRNS code.

Although the $d_{\min}$ for the block code is different from the minimum free distance (d_{free}) for a CC, they both have the same effect on the asymptotic coding gain.

For sequential decoding using the standard soft-in hard-out Viterbi decoding algorithm for CC, the complexity C_{cc} is dependent on the number of states (S_{st}), number of input bits (b) to the code and frame length (L) as follows [39]

$$C_{cc} \propto LS_{st}\left(2^b / b\right), \tag{2.33}$$

where $S_{st} = 2^c$ and c is the constraint length. It can be seen from (2.33), that C_{cc} increases exponentially with increasing c and b. Moreover to obtain low BER, large constraint lengths are used, hence increasing the complexity. The CC used in [72] are low complexity, low rate $1/b$ [38], [39]. Even though puncturing increases the rate of $1/b$ CC, the BER performance is not as good as the parent code.

On the other hand, an approximate maximum likelihood decoding based on the Chase algorithm is used for block codes. In [33] the complexity for RRNS code was determined and shown to be dependent on the error pattern 2^t, the code length U and the error correction capability t as

$$C_{RNS} \propto 2^{t-1}\left(U\left(U-t-1\right)-\sum_{i=1}^{U-t-1} i\right)\frac{U!}{(U-t)!t!}. \tag{2.34}$$

Although the CC may appear to be less complex than RRNS code, the decision on the transmitted sequence is based on the entire frame length as opposed to RRNS code where a decision is made per decoding interval. The length of the random interleaver is key and the larger it is, the lower BER performance. The complexity equations in (2.33) and (2.34) are independent of the length of the interleaver even if it is assumed to be the same in both cases for comparison purposes. Therefore, with minimal error patterns, for low error correction capability t, the complexity for short RRNS codes becomes comparable to CC. Since RRNS codes can achieve high data rates for the same complexity, this makes them attractive over CC.

2.5 Simulation Results and Discussion

In this section we demonstrate the performance through simulated results of the proposed redundant residue number system bit-interleaved differential MPSK modulation as described in Section 2.4.1 compared to the one with convolutional codes in [72]. The comparison is based on RRNS and CC with $d_{\min} = d_{free}$ respectively and approximately equal code rates. This implies that the two codes have approximately the same asymptotic coding gain, since it is only dependent on the code rate and minimum distance of the code. The simulation model is as shown in Figure 2.3.

Correlated Rayleigh fading coefficients were generated based on Jake's model [174] and assumed to be flat over a symbol interval. The RRNS codes used in the simulations are systematic and the moduli 211, 217, 223, 227, 229, 233, 239, 241, 247, 251, 253, 255, 256 were taken from [33]. Error correcting capability of t = 1, 2, 3 according to (2.7) for RRNS(5,3), RRNS(9,5), RRNS(13,7) codes respectively were considered. For all our simulations, the input to the differential encoder is mapped to QPSK symbols with Gray labelling. A random bit-interleaver for each frame of 4000 (or approximately 4000 for RRNS codes) bits was used. A normalized Doppler frequency was taken to be $f_D T = 0.01$ and the measured BER are presented as a function of SNR (E_b/N_o) in dB. The CC simulation model is based on Figure 2.3 by simply replacing RRNS code with the CC. The decoding algorithm for the CC is based on standard Viterbi decoder [72] and Chase like decoder was invoked as described in Section 2.4.3 for the RRNS code.

2.5.1 Effect of Test Patterns on the BER Performance of RRNS vs. Convolutional Code

Figure 2.4 shows the bit error rate performance comparison of the proposed system with RRNS(5,3) and rate 1/2 CC with a $d_{\min}$ = 3 in a rapid correlated flat Rayleigh fading channel for CDM i.e. $N = 2$. The RRNS(5,3) moduli are m_1 = 227, m_2 = 229 m_3 = 233, m_4 = 239, m_5 = 241, with m_1, m_2, m_3 non-redundant and m_4, m_5 redundant moduli, hence a code rate of $b/(b+b')$ = 21/37. The CC is non-systematic two states code with generators $g_0 = 3$ and $g_1 = 1$ in octal form and are taken from [38].

It can be seen from Figure 2.4 that as the number of test patterns 2^l (l = 0, 2, 4, 6) increases, the BER performance of the RRNS code improves tremendously and becomes comparably to CC. We also see that that for l = 4, and l = 6, the RRNS code performs better than CC at SNR higher than 8 and 5 dB respectively. This is due to the repetitive nature of RRNS codes since the same information is transmitted on several residues.

Figure 2.5 shows the bit error rate performance comparison of the proposed system with RRNS(9,5) and rate $1/2$ CC with a $d_{min} = 3$ in a rapid correlated flat Rayleigh fading channel for CDM i.e. $N = 2$. The RRNS(9,5) moduli are m_1 = 227, m_2 = 229, m_3 = 233, m_4 = 239, m_5 = 241, m_6 = 247, m_7 = 251, m_8 = 253, m_9 = 255, with m_1, m_2, m_3, m_4, m_5 non-redundant and m_6, m_7, m_8, m_9 redundant moduli, hence a code rate of $b/(b+b') = 35/67$. The CC is a non-systematic two states code with generators $g_0 = 5$, $g_1 = 7$ in octal form taken from [38].

It can be seen from Figure 2.5 that increasing the number of error patterns 2^l for (l = 0, 2, 4, 6, 8) improves the BER performance of the RRNS code tremendously. However, the RRNS code achieves comparable BER performance to CC at high error patterns 2^l, for l = 8. This is because bit-interleaving spreads errors and destroys the mutually exclusive property of residues in fading channels and hence the low coding gains for RRNS codes which is a dominant performance factor at low SNR and increasing length of the code. However at high SNR, the diversity gain of the RRNS code becomes dominant. Hence, the RRNS code performs better than CC at high SNR.

2.5.2 BER Performance of Iterative DFDM of RRNS vs. Convolutional Code

Figure 2.6 shows the BER performance of the proposed decision feedback differential modulation (DFDM) scheme with $N > 2$ for RRNS(5,3) code at 2^l, l = 6 error patterns and rate $1/2$ CC at four iterations and $d_{min} = 3$. The RRNS has the same moduli as in Figure 2.4. It can be seen that the BER performance increases with increasing observation period $N > 2$ as expected. It can also be seen that RRNS code performs better than the CC at high SNR.

2.5.3 Effect of Increasing the RRNS Error Correction Capability

Figure 2.7 shows the BER performance of the proposed system at different error correcting capabilities (t = 1, 2, 3) for a hard decision decoding of the RRNS code. The different RRNS codes employed are as follow: The RRNS(5,3) moduli are m_1 = 227, m_2 = 229, m_3 = 233 non-redundant and m_4 = 239, m_5 = 241 redundant, code rate of $21/37$; while RRNS(9,5) has m_1 = 227, m_2 = 229, m_3 = 233, m_4 = 239, m_5 = 241 non-redundant and m_6 = 247, m_7 = 251, m_8 = 253, m_9 = 255 redundant moduli, code rate of $35/67$; the RRNS(13,7) has m_1 = 211, m_2 = 217, m_3 = 223, m_4 = 227, m_5 = 229, m_6 = 233, m_7 = 239 non-redundant and m_8 = 241, m_9 = 247, m_{10} = 251, m_{11} = 253, m_{12} = 255, m_{13} = 256 redundant moduli, code rate of $49/97$.

It can be seen that as the error correction capability increases from t = 1 to t = 2, the BER performance improves for a hard decision RRNS code. However, there is no significant improvement from t = 2 to t = 3. This is consistent with [33], where it was shown that there are no significant coding gains beyond $t > 5$ for an additive white Gaussian noise channel.

2.5.4 Effect of Increasing the RRNS Code Rate vs. Convolutional Code

Figure 2.8 shows the BER performance for RRNS at different code rates and 2^l, l = 6 error pattern in comparison to rate $1/2$ CC with the same minimum distance $d_{min} = 3$ for conventional differential modulation (CDM) i.e. $N > 2$. It can be seen from Figure 2.8 that the RRNS code can reduce the effect of CDM at a higher code rate compared to the CC for $d_{min} = 3$.

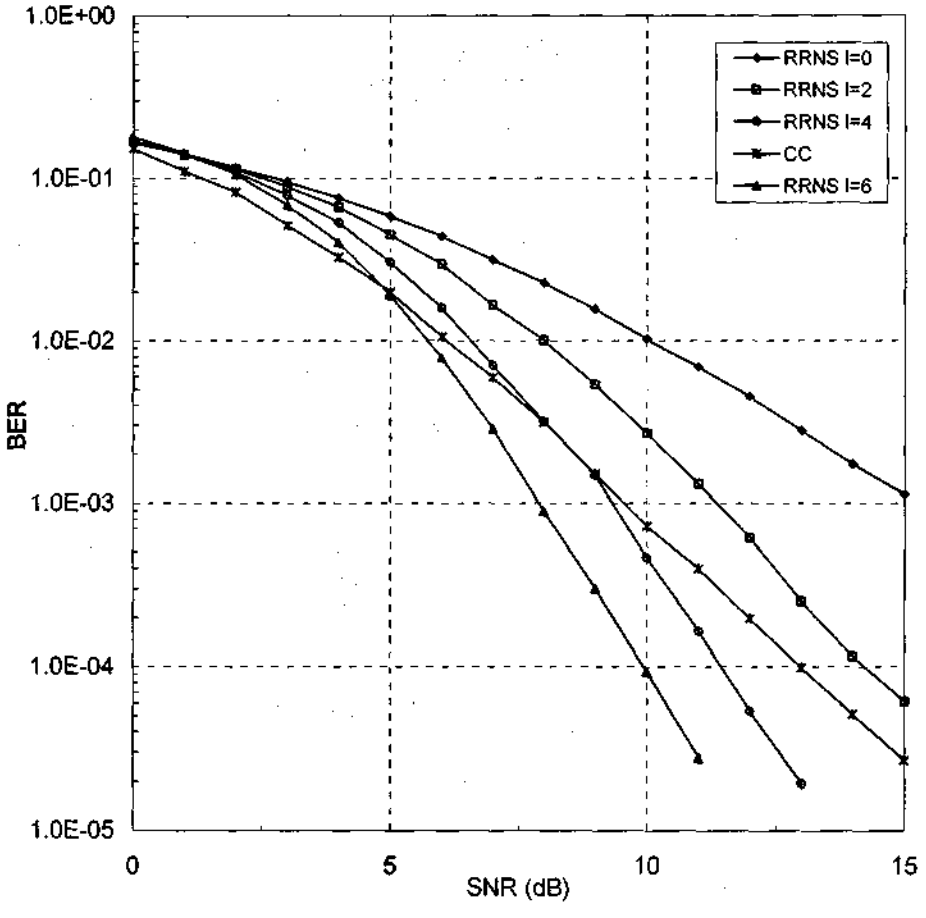

Figure 2.4: BER performance comparison of RRNS(5,3) with error patterns 2^l, l = 0, 2, 4, 6 and rate 1/2 CC for conventional differential modulation i.e. $N = 2$, and minimum distance $d_{\min} = d_{free} = 3$.

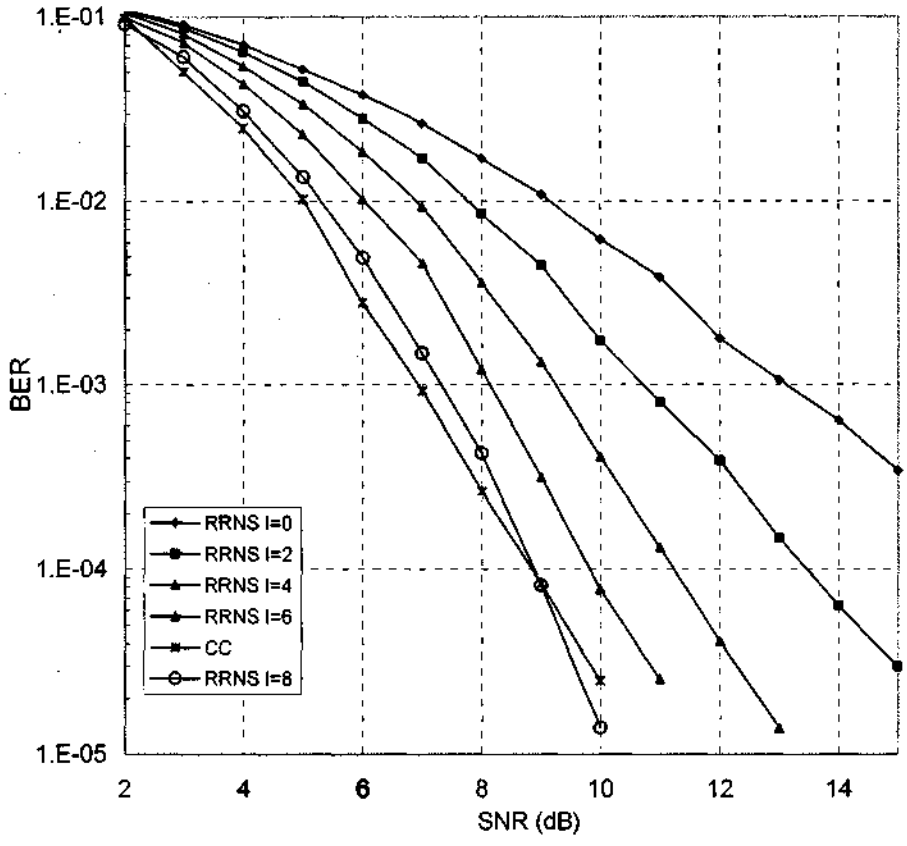

Figure 2.5: BER performance comparison of RRNS(9,5) with error patterns 2^l, $l = 0$, 2, 4, 6, 8 and rate $1/2$ CC for conventional differential modulation i.e. $N = 2$, and minimum distance $d_{\min} = d_{free} = 5$.

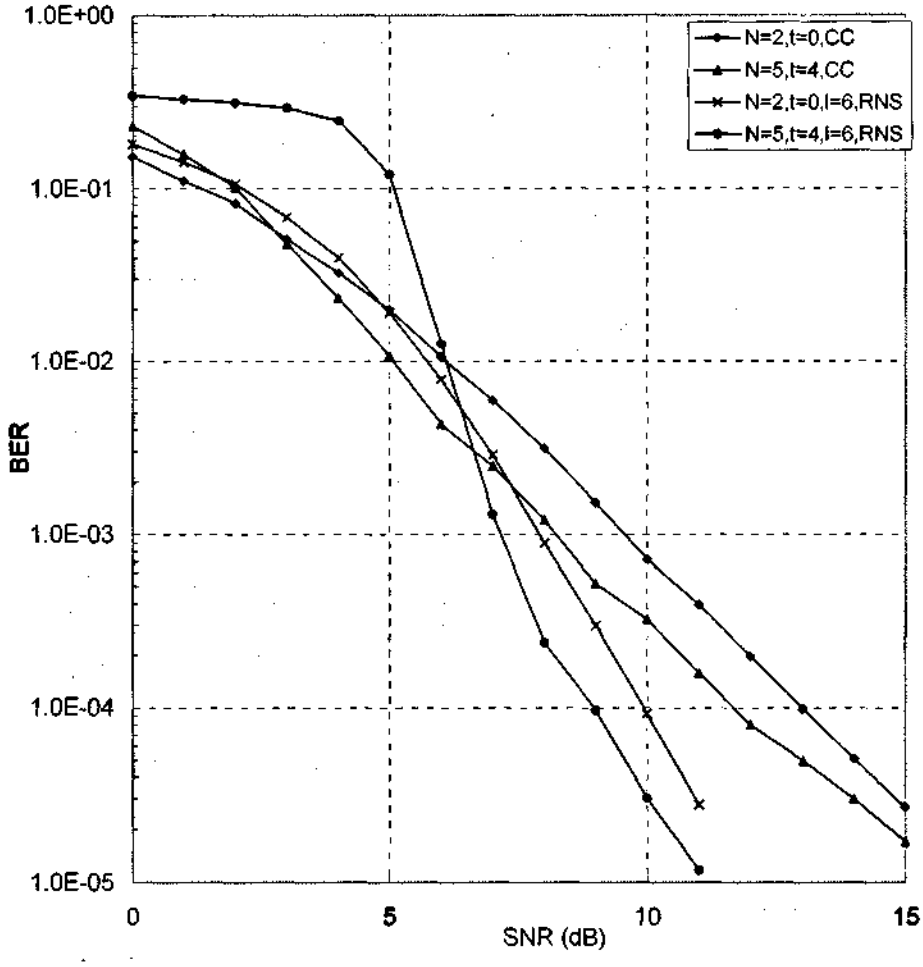

Figure 2.6: BER performance comparison of decision feedback differential modulation i.e. $N > 2$ for RRNS(5,3) code with 2^l, $l = 6$ error patterns and rate $1/2$ CC for four iterations, and $d_{min} = d_{free} = 3$

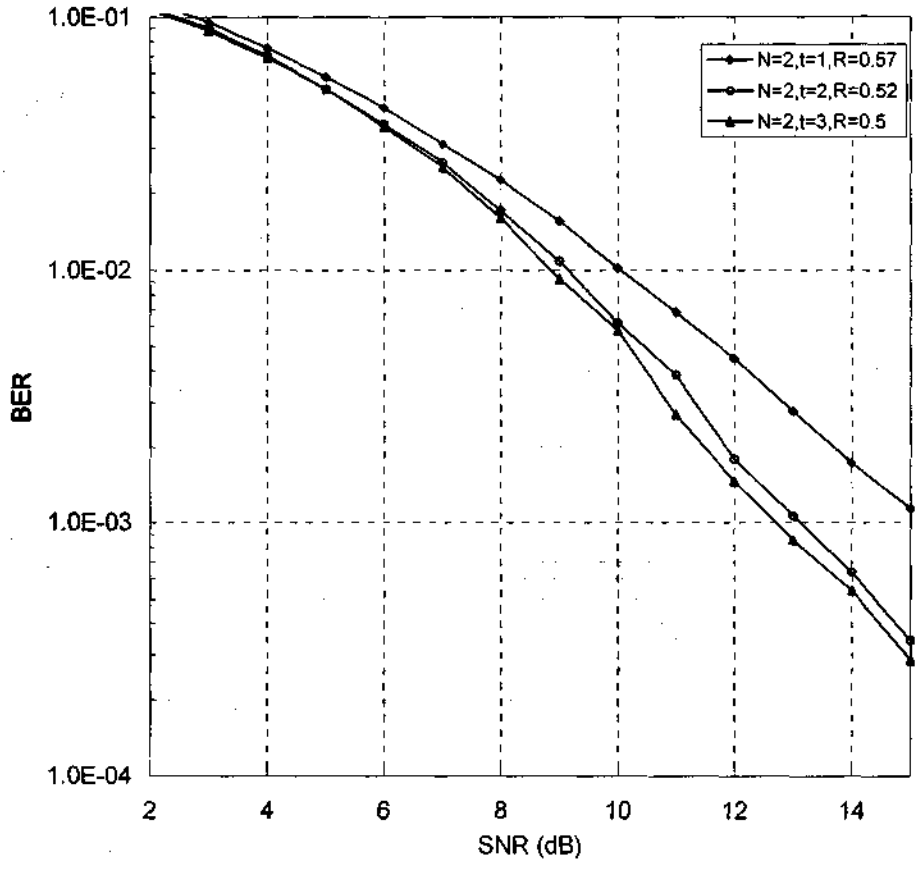

Figure 2.7: BER performance of a hard decision decoding of the proposed system at t = 1, 2, 3 error correcting capability for conventional differential modulation i.e. $N = 2$.

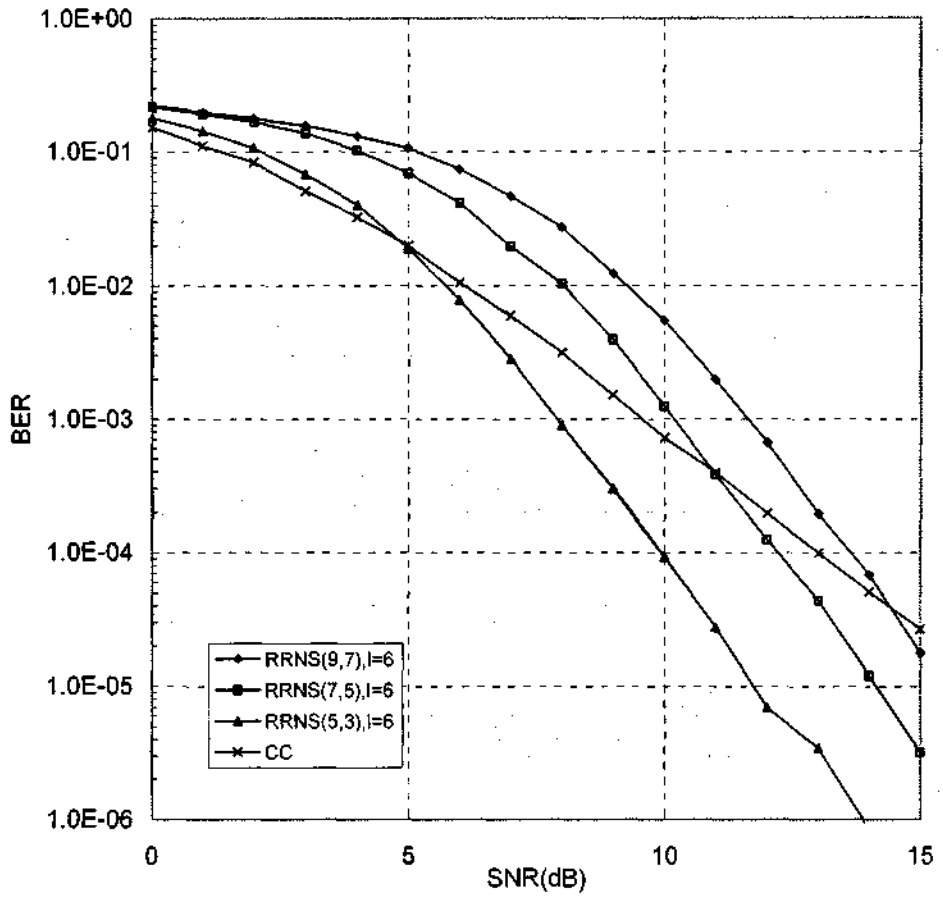

Figure 2.8: BER performance of RRNS at different code rates and 2^l, $l = 6$ error pattern in comparison to rate $1/2$ CC with same minimum distance $d_{\min} = d_{free} = 3$ for conventional differential modulation i.e. $N = 2$.

2.6 Conclusion

In this chapter, residue number system channel encoding and decoding was introduced. We discussed residue number system codes redundancy properties and error control when applied to communication systems. The encoding and decoding algorithms for hard decision were outlined. We extend already existing soft decoding algorithms for block codes to residue number system codes. A bit-interleaved coded modulation for noncoherent MPSK modulation was proposed and its performance investigated.

It is shown through simulation results that, in some applications the residue number system codes can achieve similar or better bit error rate performance than convolutional codes at approximately the same rate and asymptotic coding gain.

CHAPTER 3

MIMO SYSTEMS

3.1 Introduction

Providing fast and reliable transmission over a wireless link at low complexity has been the centre of attention in the communication industry in the recent past. This is mainly due to the fact that a wireless channel is characterized by multipath [14], which may result in the received signal adding destructively, hence performance degradation. This can be overcome by introducing diversity into a wireless system. Temporal diversity can be achieved through employing error correcting coding schemes combined with interleaving, an example of which was discussed in the previous Chapter. If two or more diversity schemes are combined, more independent dimensions become available for information transfer.

In the last decade, MIMO systems have been found not only to provide spatial diversity but also to offer larger channel capacity [2], [3], [4], [87]. The culmination of MIMO systems with OFDM has turned multipath propagation, traditionally a pitfall for wireless communications, into diversity gain. Space-time (ST) coding forms an integral part of MIMO schemes and architectures. A lot of research has been devoted to the design and construction of space-time codes (STC) [86], [88], [89], [90], [94]. STC have been extend to OFDM systems [145], [146], [147], [148], [149]. The possibility of MIMO and OFDM has prompted a completely new area of research with the aim of optimizing/maximizing the potential frequency diversity due to the inherent frequency selective nature of the wireless fading channel. This has led to new coding schemes

analogous to space-time coding such as space-frequency coding [150], [151], [152], [153], [154], [155], [156] and space-time-frequency coding [159], [163], [164], [165].

This chapter presents a comparative study of the performance of space-time coded OFDM, space-frequency coding and space-time-frequency coding. It is shown that space-frequency block codes (SFBC) perform better than space-time block coded OFDM when the effect of Doppler spread is large and the effect of delay spread is small. However, when the effect of delay spread is small and the effect of Doppler spread is small, space-time block coded (STBC) OFDM and SFBC have the same bit error rate performance. It is also shown that STF does not necessarily offer extra frequency diversity gain than the already existing space-frequency coding.

This chapter begins with a discussion on the existing space-time coding approaches for MIMO flat fading channels in Section 3.2, followed by space-frequency coding techniques in Section 3.3. Existing space-time-frequency coding schemes are discussed in Section 3.4 followed by a comparative simulation results and discussion in Section 3.5. A conclusion is then drawn in Section 3.6.

3.2 Space-Time Block Codes

This subsection presents a brief overview of space-time block codes (STBC) and OFDM. Note that although space-time trellis codes (STTC) can be or have been used along with OFDM to offer the same advantages, not many architectures have found wide applications in the current research involving space-frequency or space-time-frequency coding. This is mainly due to the easy construction and implementation of STBC, allowing for its application in several diversity techniques while still achieving full spatial diversity. Although our discussion throughout this thesis will not be limited to STBC, many examples will be based on them.

3.2.1 Signal Model and Performance Criteria

Consider a MIMO system with M_t transmit and M_r receive antennas. A STBC is a collection of some matrices each with size $P \times M_t$, where P is number of time slots or time delay for transmitting a codeword. A block of K information symbols

$\mathbf{X} = [x_1 x_2 \cdots x_K]$ drawn from an arbitrary constellation is encoded by a STBC to a codeword

$$\mathbf{V} = \begin{bmatrix} v_1^1 & v_2^1 & \cdots & v_{M_t}^1 \\ v_1^2 & v_2^2 & \cdots & v_{M_t}^2 \\ \vdots & \vdots & \ddots & \vdots \\ v_1^P & v_2^P & \vdots & v_{M_t}^P \end{bmatrix}, \tag{3.1}$$

such that v_i^t denotes the coded symbol to be transmitted on the ith transmit antenna during the tth time slot. The entries of $\mathbf{V}$ are complex linear combination of information symbols $x_1, x_2, \cdots, x_K$ or their complex conjugate. The symbol transmission rate $\Re_{ST}$ which is defined as the ratio of symbols at the input of the encoder and the output of the ST coded symbols are transmitted from each antenna as

$$\Re_{ST} = K / P, \tag{3.2}$$

where K information symbols are transmitted in one block with P time delay.

The received signal collected over M_r receive antennas can be modelled as

$$\mathbf{R} = \mathbf{VH} + \mathbf{N}, \tag{3.3}$$

where $\mathbf{R}$ is a $P \times M_r$ received signal matrix and $\mathbf{N}$ denotes a $P \times M_r$ zero mean additive white Gaussian noise (AWGN) matrix. The channel $\mathbf{H}$ is assumed to be an independent identically distributed Gaussian random process with quasi-static fading, i.e. the channel remains constant over the length of the STBC, and is given by

$$\mathbf{H} = \begin{bmatrix} h_{1,1} & h_{1,2} & \cdots & h_{1,M_r} \\ h_{2,1} & h_{2,2} & \cdots & h_{2,M_r} \\ \vdots & \vdots & \ddots & \vdots \\ h_{M_t,1} & h_{M_t,2} & \cdots & h_{M_t,M_r} \end{bmatrix}, \tag{3.4}$$

where $h_{i,j}$ is the channel gain between the ith transmit antenna and the jth receive antenna. Assuming that there is perfect channel state information available at the receiver, the maximum likelihood decoding metric can be expressed as

$$\begin{aligned}\hat{\mathbf{V}} &= \min_{\mathbf{V}} \|\mathbf{R}-\mathbf{VH}\|^2 \\ &= \min_{\mathbf{V}} tr\left[(\mathbf{R}-\mathbf{VH})^{\mathcal{H}}(\mathbf{R}-\mathbf{VH})\right] \\ &= \min_{\mathbf{V}} \left[tr\left(\mathbf{R}^{\mathcal{H}}\mathbf{R}\right) - tr\left(\mathbf{R}^{\mathcal{H}}\mathbf{VH}+\mathbf{V}^{\mathcal{H}}\mathbf{H}^{\mathcal{H}}\mathbf{R}\right) + tr\left(\mathbf{V}^{\mathcal{H}}\mathbf{VHH}^{\mathcal{H}}\right)\right]\end{aligned} \tag{3.5}$$

where $tr(\cdot)$ denotes the trace, $\mathcal{H}$ the conjugate transpose and $\|\cdot\|$ the norm of a matrix. The minimization is done over all the admissible codewords of $\mathbf{V}$. It can be seen in (3.5) that the first term is independent of the transmitted vector, the second and the third terms are linear combinations of the first order and second order respectively of information symbols $x_1, x_2, \cdots, x_K$ or their complex conjugate. Recall from the orthogonality property of STBC, since there are no terms $x_i x_j$, $x_i x_j^*$, and $x_i^* x_j^*$ with $i \neq j$ in the third term, the decision metric in (3.5) can be written as sum of function whose variable depend on each information symbol x_i, i.e.

$$\min_{\mathbf{V}} \|\mathbf{R}-\mathbf{VH}\|^2 = \sum_{i=1}^{K} f_i(x_i). \tag{3.6}$$

Hence the minimization can be done independently on each symbol which leads to fast maximum likelihood decoding of STBC.

The pairwise error probability for detecting a codeword $\hat{\mathbf{V}}$ assuming $\mathbf{V}$ was transmitted can be upper bound by [85], [86]

$$P\left(\mathbf{V},\hat{\mathbf{V}}\right) \leq \frac{1}{2}\left(\prod_{i=1}^{r}\lambda_i\right)^{-M_r}\left(\frac{\mathrm{SNR}}{4}\right)^{-rM_r}, \tag{3.7}$$

where r denotes the rank of a matrix $\left(\mathbf{V}-\hat{\mathbf{V}}\right)$ and $\lambda_1, \lambda_2, \cdots, \lambda_r$ are the nonzero eigenvalues of $\left(\mathbf{V}-\hat{\mathbf{V}}\right)\left(\mathbf{V}-\hat{\mathbf{V}}\right)^{\mathcal{H}}$. This leads to the rank or diversity and product criterion for STBC in quasi-static Rayleigh fading channels [86]. The diversity criteria is more attractive and for full diversity the difference matrix $\mathbf{V}-\hat{\mathbf{V}}$ should be full rank for any pair of distinct codewords $\mathbf{V}$ and $\hat{\mathbf{V}}$. It was shown that ST coding can exploit up to a maximum $M_t M_r$ diversity gain in flat fading channels [6], [7].

It was shown in [90] that a good STBC should achieve maximum diversity and possesses fast maximum likelihood (ML) decoding algorithm. Hence the special structure of orthogonal design not only guarantees maximum diversity but also provides for fast ML decoding. The transmitted matrix $\mathbf{V}$ is said to be orthogonal if it satisfies the following condition,

$$\mathbf{V}^{H}\mathbf{V} = \left(|x_1|^2 + |x_2|^2 + \cdots + |x_K|^2\right)\mathbf{I}. \tag{3.8}$$

One of the advantages of STC is increased channel capacity at no bandwidth expansion. It was shown that while the maximum symbol transmission rate of one can be reached for any number of transmit antennas for STBC from real orthogonal design, STBC from generalized complex orthogonal designs cannot achieve a symbol rate of one for more than two transmit antennas [89], [90], [7]. Spatial diversity is independent of transmission rate, hence full diversity does not imply full rate. It is therefore possible to sacrifice some data rate for more diversity and indirectly compensate through high level modulation formats.

3.2.2 Complex Orthogonal STBC

A well known example of STBC that achieves full diversity but no coding gains is the Alamouti scheme [88]. Originally designed for two transmit antennas, it has been extended to three and four transmit antennas with emphasis on the orthogonal construction of the signal constellation at the transmitter to ease the detection process at the receiver. The Alamouti STBC code matrix for two transmit antennas is given in (3.9). Clearly the rate of code matrix $\mathbf{G}_2$ is one.

$$\mathbf{G}_2(x_1, x_2) = \begin{bmatrix} x_1 & x_2 \\ -x_2^* & x_1^* \end{bmatrix} \tag{3.9}$$

Examples of the STBC code matrix for three and four transmit antennas are defined as

$$\mathbf{G}_3(x_1, x_2, x_3) = \begin{bmatrix} x_1 & x_2 & x_3 \\ -x_2^* & x_1^* & 0 \\ -x_3^* & 0 & x_1^* \\ 0 & -x_3^* & x_2^* \end{bmatrix}, \quad \mathbf{G}_4(x_1, x_2, x_3) = \begin{bmatrix} x_1 & x_2 & x_3 & 0 \\ -x_2^* & x_1^* & 0 & x_3 \\ -x_3^* & 0 & x_1^* & -x_2 \\ 0 & -x_3^* & x_2^* & x_1 \end{bmatrix}. \tag{3.10}$$

It can be seen from (3.10) that for three and four transmit antennas, the STBC rate is $3/4$. Note that the code matrix for three transmit antennas $\mathbf{G}_3$ is derived from the code matrix for four transmit antennas $\mathbf{G}_4$ by deleting one of the columns. These codes belong to the generalized complex orthogonal design for complex constellations such as QAM and PSK [7], [89], [90].

3.2.3 Quasi-Orthogonal STBC

It was shown that increasing the number of transmit antennas increases the spatial diversity and orthogonal STBC can achieve full spatial diversity [89], [90], [92]. However, complex orthogonal STBC could not guarantee rate one for more than two transmit antennas. Hence full rate quasi-orthogonal STBC were proposed [93], [7] by relaxing the orthogonality condition to achieve full rate. This however compromises the fast ML decoding as is it can no longer be carried out on each symbol but on the pairs of candidate symbols. An example of four transmit full rate quasi-orthogonal STBC in [7] was constructed as follows

$$G_4(x_1,x_2,x_3,x_4)=\begin{bmatrix}\mathbf{A} & \mathbf{B}\\ -\mathbf{B}^* & \mathbf{A}^*\end{bmatrix}=\begin{bmatrix}x_1 & x_2 & x_3 & x_4\\ -x_2^* & x_1^* & -x_4^* & x_3^*\\ -x_3^* & -x_4^* & x_1^* & x_2^*\\ x_4 & -x_3 & -x_2 & x_1\end{bmatrix}, \tag{3.11}$$

where

$$\mathbf{A}=\begin{bmatrix}x_1 & x_2\\ -x_2^* & x_1^*\end{bmatrix},\ \mathbf{B}=\begin{bmatrix}x_3 & x_4\\ -x_4^* & x_3^*\end{bmatrix}.$$

It was proved in [89] that the above code has a maximum rank of 2 over all the distinct codewords, hence diversity of $2M_r$ rather than a full diversity of $4M_r$. In [91] full rate full diversity quasi-orthogonal STBC were obtained by rotating the signal constellation for not more than four transmit antennas. Other full rate full diversity STBC can be found in [101], [102].

3.2.4 Space-Time Block Coded OFDM

Unfortunately STBC are very sensitive to delays. The orthogonality of the STBC is broken in multipath fading channels and inter-symbol interference (ISI) may occur, degrading their performance. In this subsection we briefly discuss the space-time block coded OFDM (STBC-OFDM) signal model.

Consider an OFDM communication system employing M_t transmit and M_r receive antennas propagating through a frequency-selective fading channel. A single stream of binary information data enters a ST encoder which transforms it into M_t parallel streams of baseband constellation symbols. Each stream is broken into OFDM blocks of constellation symbols of length N_c such that the nth block from the ith transmit antenna to be transmitted on the uth subcarrier is given by $v_i[n,u]$, for $u = 1,2,\cdots,N_c$. The data symbols are then modulated using inverse fast Fourier transform (IFFT) into OFDM symbols. After adding a guard interval, the OFDM symbols are then transmitted each stream from its corresponding antenna. Thus, all the M_t transmit antennas simultaneously transmit on N_c subcarrier. At the receiver after removing the guard interval, the received signal is demodulated by fast Fourier transform (FFT). Hence equation (3.3) for an OFDM symbol on the nth block becomes

$$\mathbf{R}[n] = \mathbf{V}[n]\mathbf{H}[n] + \mathbf{N}[n], \tag{3.12}$$

where $\mathbf{V}[n]$ is a collection of N_c STBC symbols and $\mathbf{N}[n]$ is a diagonal matrix whose elements are FFT of the channel AWGN defined the same way as in (3.3). The fading channel matrix on the nth OFDM symbol $\mathbf{H}[n]$ is a diagonal matrix whose diagonal elements are FFT of the impulse channel response. The channel frequency response between the ith transmit and the jth receive antennas in the nth OFDM block, on the uth subcarrier and lth path can be defined similarly to (3.4) as

$$h_{i,j}^{n}[u] = \sum_{l=0}^{L-1} \alpha_{i,j}^{l}[n] e^{-j2\pi ul/N_c}. \tag{3.13}$$

In (3.13), $\alpha_{i,j}^{l}[n]$ is an independent identically distributed fading coefficient on the lth tap delay line. The maximum number of resolvable paths is $L = \lceil \tau_m \Delta_u + 1 \rceil$ where τ_m is

the maximum delay spread and $\Delta_u = 1/(N_c T)$ is the tone spacing of the OFDM system. For STBC-OFDM to function normally i.e. no ISI, the channel coefficients of P consecutive OFDM symbols are considered constant, i.e, $h_{i,j}[1] = h_{i,j}[2] = \cdots = h_{i,j}[P]$. Hence an OFDM symbol period of PN_cT , where P is the delay time or the number of time slots required to transmit STBC code symbol. It is further assumed that all the path gains between any pair of transmit antenna and receive antenna follow the same power profile $E\left\{\left|\alpha_{i,j}^{l}\right|^2\right\} = \sigma_l$ for any given (i, j, l), and the powers of the L paths are normalized such that $\sum_{l=0}^{L-1} \sigma_l = 1$. The frequency selective fading channel is transformed into L flat multiplicative subchannels, hence the presence of multipath can lead to performance improvement.

Figure 3.1 shows an example STBC-OFDM based on the Alamouti two transmit one receive antennas scheme signalling through a frequency selective fading channel.

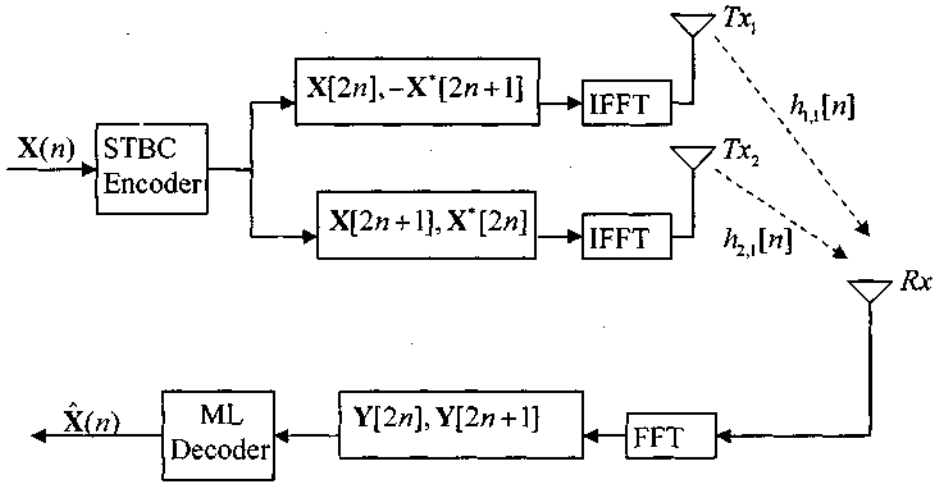

Figure 3.1: Space-time block coded OFDM with two transmit and one receive antennas.

At the transmitter after IFFT modulation, the nth STBC-OFDM symbol defined in terms of odd $\mathbf{X}[2n+1]$ and even $\mathbf{X}[2n]$ is given by

$$\begin{aligned}\mathbf{X}[n] &= IFFT\left[\left\{X_u[2n]\right\}_{u=1}^{N_c}\right],\\ \mathbf{X}[2n+1] &= IFFT\left[\left\{X_u[2n+1]\right\}_{u=1}^{N_c}\right],\end{aligned} \tag{3.14}$$

where n is the time instance. The received signal after removing the guard interval and performing OFDM demodulation can be expressed as

$$\begin{aligned}\mathbf{Y}[2n] &= X[2n]\mathbf{H}_{1,1}^{1}[2n] + X[2n+1]\mathbf{H}_{2,1}^{1}[2n+1] + \mathbf{N}[2n],\\ \mathbf{Y}[2n+1] &= -X^{*}[2n+1]\mathbf{H}_{1,1}^{2}[2n] + X^{*}[2n]\mathbf{H}_{2,1}^{2}[2n+1] + \mathbf{N}[2n+1],\end{aligned} \tag{3.15}$$

where $X[2n]$ and $X[2n+1]$ is a collection of STBC symbols, $\mathbf{N}[2n+1]$ and $\mathbf{N}[2n]$ are odd and even FFT of the channel AWGN respectively. For the STBC-OFDM example above to function normally i.e. without ISI, the channel coefficients of two consecutive OFDM symbols are considered constant, i.e. $\mathbf{H}_{1,1}^{1}[2n] \approx \mathbf{H}_{1,1}^{2}[2n]$ and $\mathbf{H}_{2,1}^{1}[2n+1] \approx \mathbf{H}_{2,1}^{2}[2n+1]$, hence an STBC-OFDM symbol period of $2N_cT$.

However, in a fast fading channel which is normally the case for mobile communication systems, the orthogonality condition that the channel response of P consecutive OFDM blocks are the same, cannot be satisfied. Any time variation will cause performance degradation as the channel coefficients from one OFDM block to another are no longer constant. From (3.13), the autocorrelation function of the channel coefficients assuming adequate subcarrier spacing and independent multipaths is

$$\begin{aligned}\Gamma_h &\approx E\left\{h_{i,j}[(n+\kappa)N_cT]h_{i,j}^{*}[nN_cT]\right\}\\ &= E\left\{\sum_{l=0}^{L-1}\alpha_{i,j}^{l}[(n+\kappa)N_cT]e^{-j2\pi lu/N_c}\sum_{q=0}^{L-1}\alpha_{i,j}^{l}[nN_cT]e^{-j2\pi qu/N_c}\right\}\\ &\approx \sum_{l=0}^{L-1}R_{\alpha_{i,j}^{l}},\end{aligned} \tag{3.16}$$

where $\alpha_{i,j}^{l}$ is the fading coefficients on the lth path, $E\{\cdot\}$ denotes the expectation, Γ_h is the autocorrelation function of the fading channel and $R_{\alpha_{i,j}^{l}}$ is the power profile. Assuming a normalized autocorrelation function based on Jakes' fading channel model [174], $R_{\alpha_{i,j}^{l}} = J_0(2\pi f_D \kappa N_c T)\sum_{l=0}^{L-1}\sigma_l$, where $\kappa = P$ for a STBC defined in (3.1), hence a

normalized Doppler frequency of $Pf_D N_c T$. Increasing the number of subcarriers N_c increases the OFDM period $PN_c T$ but unfortunately results in more correlations due to relatively high mobility of the wireless communication channel. It can be seen from (3.16) that even in time selective fading OFDM systems, the effect of multipaths is multiplicative and can lead to performance improvement.

3.3 Space-Frequency Coding

Although STBC-OFDM was successful in combating ISI, it could only exploit spatial diversity even though there is potential frequency diversity offered by the frequency-selective fading channels. To exploit the possible additional frequency diversity in MIMO-OFDM, several coding schemes were proposed, some of which involved concatenating narrowband coding with STBC [146], [152], [166]. Space-frequency coding emerged as a technique that aims to combine advantages of ST coding and MIMO-OFDM [153], [154]. The strategy of space-frequency (SF) coding is to distribute the information symbols over different antennas and OFDM tones. Hence the use of OFDM in STC as was illustrated in Section 3.2.4 above offers the possibility of coding in the frequency domain. Similar to STC, a good space-frequency code (SFC) should possess both full diversity and high coding gains. However, most existing SFC studies are focussed on exploring frequency and spatial diversities, hence we focus on the diversity component of SFC in this subsection.

3.3.1 Signal Model

In this subsection we present space-frequency codes from STBC. The incoming bit stream is mapped to K information symbols drawn from a discrete alphabet $S_K \in \mathrm{A}^K$. The source symbols are then parsed onto blocks and mapped onto space-frequency (SF) codewords. The SF codeword is simultaneously transmitted over N_c subcarriers and M_t transmit antennas. Each codeword is a $N_c \times M_t$ matrix and can be expressed as

$$\mathbf{C} = \begin{bmatrix} c_1(0) & c_2(0) & \cdots & c_{M_t}(0) \\ c_1(1) & c_2(1) & \cdots & c_{M_t}(1) \\ \vdots & \vdots & \ddots & \vdots \\ c_1(N_c-1) & c_2(N_c-1) & \vdots & c_{M_t}(N_c-1) \end{bmatrix}, \tag{3.17}$$

where $c_i(u)$ denotes the channel symbol transmitted over the uth subcarrier by the ith transmit antenna. The SF code is assumed to satisfy the energy constraint $E\left\{\|\mathbf{C}\|^2\right\} = N_c M_t$. The N_c point IFFT is then applied to each column of matrix $\mathbf{C}$ and after appending the cyclic prefix, each OFDM symbol is simultaneously transmitted from its corresponding transmit antenna. We define the SF code rate as the symbol rate per channel use and is given by

$$\Re_{SF} = K / N_c . \tag{3.18}$$

For proper OFDM operation, we assume that the path gains between each pair of transmit and receive antennas remains constant over one OFDM symbol period but is frequency selective with L independent paths. Hence after removing the cyclic prefix and performing FFT, the received signal at the jth receive antenna and uth subcarrier can be expressed as

$$y_j(u) = \sum_{i=1}^{M_t} c_i(u) h_{i,j}(u) + z_j(u), \tag{3.19}$$

with a frequency selective fading gain whose complex frequency channel response is defined as in (3.13). We rewrite the received signal in vector form as

$$\mathbf{Y} = \mathbf{DH} + \mathbf{Z}, \tag{3.20}$$

where $\mathbf{D}$ is an $N_c M_r \times M_t L M_r$ matrix derived from the SF codeword and is given by

$$\mathbf{D} = I_{M_r} \otimes \begin{bmatrix} D_1 & & & \\ & D_2 & & \\ & & \ddots & \\ & & & D_{M_t} \end{bmatrix}, \tag{3.21}$$

such that each $D_i = \left[diag(\mathbf{c}_i) W^{\tau_0} diag(\mathbf{c}_i) W^{\tau_1} \cdots diag(\mathbf{c}_i) W^{\tau_{L-1}} \right]$ for $i = 1, 2, \cdots M_t$, $W^{\tau_l} = \left[1^{\tau_l} e^{-j2\pi\tau_l/N_c} \cdots e^{-j2\pi\tau_l(N_c-1)/N_c} \right]^T$ and $\mathbf{c}_i$ is the OFDM symbol on the ith transmit antenna. The received vector $\mathbf{Y}$ and the noise vector $\mathbf{Z}$ are of the same size $N_c M_r \times 1$ and are given by

$$\mathbf{Y}=\left[y_1(0)y_1(1)\cdots y_1(N_c-1)y_2(0)\cdots y_2(N_c-1)y_{M_r}(0)\cdots y_{M_r}(N_c-1)\right]^T, \tag{3.22}$$

and

$$\mathbf{Z}=\left[z_1(0)z_1(1)\cdots z_1(N_c-1)z_2(0)\cdots z_2(N_c-1)z_{M_r}(0)\cdots z_{M_r}(N_c-1)\right]^T, \tag{3.23}$$

respectively. The channel vector $\mathbf{H}$ is of the size $M_tLM_r\times 1$ and is defined as

$$\mathbf{H}=\left[\mathbf{h}_{1,1}^T\cdots\mathbf{h}_{M_t,1}^T\mathbf{h}_{1,2}^T\cdots\mathbf{h}_{M_t,2}^T\cdots\mathbf{h}_{1,M_r}^T\cdots\mathbf{h}_{M_t,M_r}^T\right]^T, \tag{3.24}$$

where $\mathbf{h}_{i,j}=\left[\alpha_{i,j}^0\alpha_{i,j}^1\cdots\alpha_{i,j}^{L-1}\right]^T$.

3.3.2 Performance Criteria

Let $\mathbf{D}$ and $\hat{\mathbf{D}}$ be two different matrices derived from two different SF codewords $\mathbf{C}$ and $\hat{\mathbf{C}}$ respectively. Assuming that the receiver has perfect knowledge of the channel, the PEP between $\mathbf{D}$ and $\hat{\mathbf{D}}$ is upper bounded as [104], [160]

$$P(\mathbf{D},\hat{\mathbf{D}})\le\binom{2r-1}{r}\left(\prod_{i=1}^{r}\lambda_i\right)^{-1}\left(\frac{SNR}{M_t}\right)^{-r}, \tag{3.25}$$

where r is the rank of matrix $\left(\mathbf{D}-\hat{\mathbf{D}}\right)\boldsymbol{\Gamma}\left(\mathbf{D}-\hat{\mathbf{D}}\right)^{\mathcal{H}}$, $\lambda_1,\lambda_2,\cdots\lambda_r$ are nonzero eigenvalues of $\left(\mathbf{D}-\hat{\mathbf{D}}\right)\boldsymbol{\Gamma}\left(\mathbf{D}-\hat{\mathbf{D}}\right)^{\mathcal{H}}$ and $\boldsymbol{\Gamma}=E\left\{\mathbf{H}\mathbf{H}^{\mathcal{H}}\right\}$ is an $M_rM_tL\times M_rM_tL$ correlation matrix of $\mathbf{H}$. Based on the upper bound in (3.25), the design criteria for SF codes was proposed to be diversity and product criterion. The product criteria maximizes the coding advantage.

The primary interest of SF code design is the diversity gain. The diversity criteria state that to maximize the diversity advantage, the minimum rank of $\left(\mathbf{D}-\hat{\mathbf{D}}\right)\boldsymbol{\Gamma}\left(\mathbf{D}-\hat{\mathbf{D}}\right)^{\mathcal{H}}$ over all distinct codewords $\mathbf{C}$ and $\hat{\mathbf{C}}$ should be as large as possible. Hence

$$
\begin{aligned}
r &= rank\left[\left(\mathbf{D}-\hat{\mathbf{D}}\right)\boldsymbol{\Gamma}\left(\mathbf{D}-\hat{\mathbf{D}}\right)^{H}\right] \\
&= M_r rank\left[\sigma_0 diag\left(\mathbf{C}-\hat{\mathbf{C}}\right)\sigma_1 diag\left(\mathbf{C}-\hat{\mathbf{C}}\right)\cdots\sigma_{L-1} diag\left(\mathbf{C}-\hat{\mathbf{C}}\right)\right],
\end{aligned}
\tag{3.26}
$$

where $\sigma_l, l = 0,1,\cdots L-1$ is the power profile on the lth path. It can be easily seen that the rank of SF codes in MIMO frequency selective fading channels is given by

$$
r \le \min\left\{M_r N_c, LM_r M_t\right\}. \tag{3.27}
$$

In most scenarios, $N_c \ge M_t L$, hence the maximum achievable diversity gain is at most $r \le M_t M_r L$. However, for full diversity advantage, $r = M_t M_r L$ i.e. the maximum diversity gain for SF is the product of spatial diversity gain $M_t M_r$ and frequency diversity due to the L multipaths.

Note that from (3.27), the maximum achievable diversity gain is the same as that of ST coded OFDM [147], [153]. In SF the fading channel is assumed constant over one OFDM symbol in contrast to an entire STBC-OFDM codeword. Hence in the presence of time correlated fading, space-frequency block codes (SFBC) would perform better than STBC-OFDM which has a longer symbol period.

3.3.3 Example of SFBC from STBC

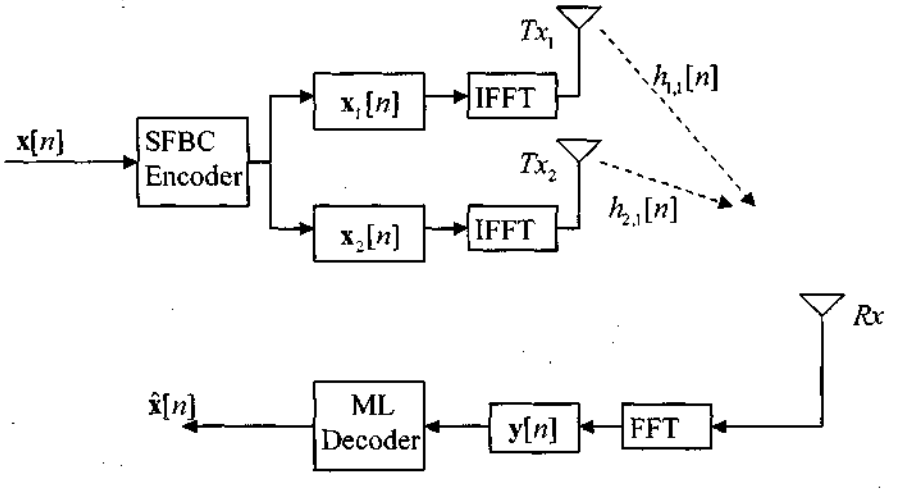

Figure 3.2: Space-frequency block coded OFDM.

Figure 3.2 shows an example of a two-branch SFBC scheme signalling through a frequency selective fading channel. The two-branch SFBC is an extension of a simple orthogonal transmitter diversity scheme first shown in [88]. The data symbol vector on the nth block $\mathbf{x}[n]$ is encoded by space-frequency block code (SFBC) to two vectors as

$$\begin{aligned}\mathbf{x}[n] &= \left[x_1(n)x_2(n)\cdots x_{N_c}(n)\right]^T \\ \mathbf{x}_1[n] &= \left[x_1(n)-x_2^*(n)\cdots x_{N_c-1}(n)-x_{N_c}^*\right]^T \\ \mathbf{x}_2[n] &= \left[x_2(n)x_1^*(n)\cdots x_{N_c}(n)x_{N_c-1}^*\right]^T\end{aligned}. \tag{3.28}$$

During the nth OFDM block instance, $\mathbf{x}_1[n]$ is transmitted from the first transmit antenna while $\mathbf{x}_2[n]$ is simultaneously transmitted from the second transmit antenna. SF encoding and decoding processes can be described in terms of odd $\mathbf{x}_o[n]$ and even $\mathbf{x}_e[n]$ component vectors of $\mathbf{x}[n]$ such that

$$\begin{aligned}\mathbf{x}_{1,o} &= \mathbf{x}_o \quad \mathbf{x}_{1,e} = -\mathbf{x}_e^* \\ \mathbf{x}_{2,o} &= \mathbf{x}_e \quad \mathbf{x}_{2,e} = \mathbf{x}_o^*\end{aligned}, \tag{3.29}$$

where $\mathbf{x}_{1,o}, \mathbf{x}_{1,e}$ and $\mathbf{x}_{2,o}, \mathbf{x}_{2,e}$ are odd and even vectors of $\mathbf{x}_1[n]$ and $\mathbf{x}_2[n]$ respectively. It can be seen from (3.29) that the Alamouti's equivalent SFBC transmission matrix is given by

$$G[n] = \begin{bmatrix} \mathbf{x}_o & \mathbf{x}_e \\ -\mathbf{x}_e^* & \mathbf{x}_o^* \end{bmatrix}. \tag{3.30}$$

At the receiver assuming perfect knowledge of the channel, the receive signal vector after removing the cyclic prefix can be expressed in terms of odd and even components as

$$\begin{aligned}\mathbf{y}_o[n] &= \mathbf{x}_o(n)\Lambda_{1,o}(n) + \mathbf{x}_e(n)\Lambda_{2,0}(n) + z_o(n) \\ \mathbf{y}_e[n] &= -\mathbf{x}_e^*(n)\Lambda_{1,e}(n) + \mathbf{x}_o^*(n)\Lambda_{2,e}(n) + z_e(n)\end{aligned}, \tag{3.31}$$

where $z_o(n), z_e(n)$ and $\Lambda_{1,o}(n), \Lambda_{1,e}(n)$ are odd and even components of the AWGN and the complex fading channel coefficients respectively. The channel coefficients are defined as in (3.13). To maintain SFBC orthogonality, the complex channel gains

between at least two adjacent subcarriers are assumed constant, i.e. $\Lambda_{1,o}(n) \approx \Lambda_{1,e}(n)$ and $\Lambda_{2,o}(n) \approx \Lambda_{2,e}(n)$, hence $N_c T$ OFDM symbol period. In the presence of time selective fading, SFBC-OFDM would perform better than STBC-OFDM which has a longer symbol period. The transmitted symbols are recovered from the received signal in a similar manner to the Alamouti scheme [88]. Since the above example uses the Alamouti structure, it thus reasonable to expect SFBC from STBC to have the same diversity performance as the STBC-OFDM in Figure 3.1. Hence, although the above example can achieve spatial diversity, it still fails to achieve frequency diversity offered by channel selectivity.

3.3.4 Full Diversity Space-Frequency Codes

The design parameters for good SFC are vastly different from those of STC in narrowband fading channels. Employing known STC as SFC by coding across space and frequency (rather than space and time) in general provides spatial diversity but fails to exploit the available frequency diversity [153], [151]. SF codes offering full diversity by coding across the multipaths, hence maximizing the frequency diversity have been proposed. These codes use techniques such as linear precoders or constellation rotation [161], [162], [163], linear constellation decimation [164], or simply repetition codes to code across multipaths in addition to space coding [160]. This subsection presents the signal design and criteria for SF codes derived from STC using repetition coding across multipath.

3.3.4.1 Signal Design

In order to achieve full diversity $M_t M_r L$, the matrix $\left(\mathbf{D}-\hat{\mathbf{D}}\right)\boldsymbol{\Gamma}\left(\mathbf{D}-\hat{\mathbf{D}}\right)^{\mathcal{H}}$ in (3.26) has to be full rank for every distinct pair of the SF codewords $\mathbf{C}$ and $\hat{\mathbf{C}}$. This subsection presents a derivation of how full diversity SF codes can be constructed from STBC designed for a narrowband fading channel using repetition coding similar to [160]. Note that constellation rotation, cyclic shift, or permutation techniques used to generate full diversity SF codes are a form of repetition coding with varying coding gains and code rates. Similar techniques have been used in the design of STBC to achieve full diversity or full rate [101], [102].

Suppose a STBC codeword $\mathbf{V}$ in (3.1) which is a $M_t \times M_t$ square matrix, i.e. $P = M_t$, an $N_c \times M_t$ SF codeword is formed by concatenating $\mathbf{V}$ STBC matrices L times. Hence a SF codeword is formed by repeating each row of the $\mathbf{V}$ matrix L times and adding some zero rows where $M_t L$ is less than the number of subcarriers N_c, i.e.

$$C = \begin{bmatrix} G_L(\mathbf{V}) \\ \mathbf{O}_{(N_c - LM_t)\times M_t} \end{bmatrix}. \tag{3.32}$$

The mapping G_L is defined as

$$G_L(\mathbf{V}) = \left[\mathbf{I}_{M_t} \otimes 1_{L\times 1}\right]^T \mathbf{V}, \tag{3.33}$$

where $\mathbf{I}_{M_t}$ is an $M_t \times M_t$ identity matrix, $1_{L\times 1}$ is an all one matrix with size $L \times 1$ and $\otimes$ denotes the tensor product [177]. It can be seen from (3.32) that the symbol rate per channel use $\Re_{SF} = LM_t / N_c$ is less than one if $LM_t < N_c$.

3.3.4.2 Diversity Criteria

From the performance criteria, the rank/diversity criteria states that the minimum rank of the matrix $\left(\mathbf{D} - \hat{\mathbf{D}}\right)\boldsymbol{\Gamma}\left(\mathbf{D} - \hat{\mathbf{D}}\right)^{\mathcal{H}}$ over all distinct codewords $\mathbf{C}$ and $\hat{\mathbf{C}}$ should be as large as possible,

$$\begin{aligned} r &= rank\left\{\left(\mathbf{D} - \hat{\mathbf{D}}\right)\boldsymbol{\Gamma}\left(\mathbf{D} - \hat{\mathbf{D}}\right)^{\mathcal{H}}\right\} \\ &= rank\left\{\left(\mathbf{I}_{M_r} \otimes \left[\left(\mathbf{C} - \hat{\mathbf{C}}\right)\left(\mathbf{C} - \hat{\mathbf{C}}\right)^{\mathcal{H}}\right]\right) \circ \boldsymbol{\Gamma}\right\}, \end{aligned} \tag{3.34}$$

where $\circ$ is the Hadamard product [177],

$$\left(\mathbf{C} - \hat{\mathbf{C}}\right)\left(\mathbf{C} - \hat{\mathbf{C}}\right)^{\mathcal{H}} = \begin{bmatrix} G_L\left(\mathbf{V} - \hat{\mathbf{V}}\right)\left[G_L\left(\mathbf{V} - \hat{\mathbf{V}}\right)\right]^{\mathcal{H}} & \mathbf{0}_{N_c - LM_t} \\ \mathbf{0}_{N_c - LM_t} & \mathbf{0}_{N_c - LM_t} \end{bmatrix}, \tag{3.35}$$

and since for quasi-static fading the channel characteristics for one OFDM smbol are assumed constant an $N_c \times N_c$ correlation matrix $\boldsymbol{\Gamma}$ is defined as

$$\Gamma = \mathbf{I}_{M_r} \otimes \begin{bmatrix} \mathbf{I}_{M_t} \otimes E\left\{\mathbf{h}_{i,j}\mathbf{h}_{i,j}^{\mathcal{H}}\right\} & \mathbf{0}_{N_c - LM_t} \\ \mathbf{0}_{N_c - LM_t} & \mathbf{0}_{N_c - LM_t} \end{bmatrix}, \tag{3.36}$$

given $\mathbf{h}_{i,j} = \left[\alpha_{i,j}^0 \alpha_{i,j}^1 \cdots \alpha_{i,j}^{L-1}\right]^T$ for $i = 1, 2, \cdots, M_t$.

The aim of this subsection is to prove that the matrix in (3.34) has a rank of at least LM_tM_r. Since ST codes achieve full diversity for quasi-static flat fading channels, $\left(\mathbf{V} - \hat{\mathbf{V}}\right)$ has M_t rank for any two distinct codewords. Note from (3.36) that

$$\Gamma = E\left\{\mathbf{h}_{i,j}\mathbf{h}_{i,j}^{\mathcal{H}}\right\} = diag\left\{\sigma_0, \sigma_1, \cdots, \sigma_{L-1}\right\}, \tag{3.37}$$

is an $L \times L$ diagonal matrix whose power profile on the lth path is given by σ_l. Hence for any number of transmit antennas M_t the correlation Γ has a minimum rank of L. Therefore the rank of the matrix in (3.34) is

$$\begin{aligned} r &= rank\left\{\mathbf{I}_{M_r} \otimes \left\{\left[\left(\mathbf{V} - \hat{\mathbf{V}}\right)\left(\mathbf{V} - \hat{\mathbf{V}}\right)^{\mathcal{H}}\right] \otimes \Gamma\right\}\right\} \\ &= rank\left(\mathbf{I}_{M_r}\right) rank\left\{\left(\mathbf{V} - \hat{\mathbf{V}}\right)\left(\mathbf{V} - \hat{\mathbf{V}}\right)^{\mathcal{H}}\right\} rank\left(\Gamma\right) \\ &= M_r M_t L, \end{aligned} \tag{3.38}$$

hence, achieving full diversity.

3.4 Space-Time-Frequency Coding

As was pointed out in the preceding subsection, SFC is predominantly focussed on achieving high diversity gains and hardly any coding gain. The performance of SF codes can be improved by coding across several OFDM blocks in what is known as "space-time-frequency" (STF) coding. When OFDM is used in wireless communications, the frequency diversity induced by the frequency selective channel characteristics can be exploited by interleaving and channel coding to maximize gains.

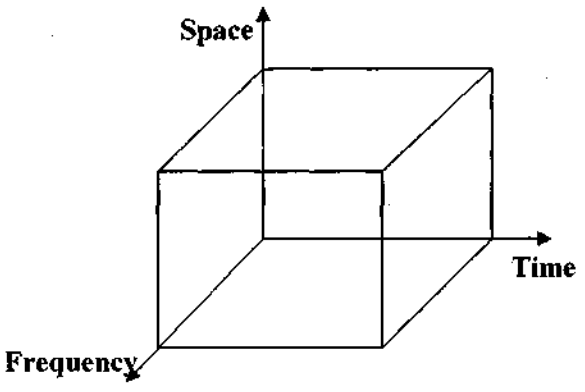

Figure 3.3: Illustration of STF coded transmissions

STF coding may be viewed as concatenating several OFDM words in the time domain or transmitting different ST codeword on several carriers as illustrated in Figure 3.3. STF coding combines the advantages of STC i.e. spatial and temporal diversities with frequency diversity from SFC. As the name STF coding suggests, coding is across three diversity dimensions i.e. space, time and frequency domains. In order to achieve high diversity gains from the three diversity domains, several coding approaches have been investigated for block fading channels.

In this subsection we review the signal design and performance criterion of space-time-frequency codes (STFC) [159], [164], [165], [167]. It is shown that although SFC can achieve maximum diversity of $M_r M_t L$, more gain can be realized through channel coding (temporal diversity).

3.4.1 Signal Design

Consider a STF coding MIMO system with N_c OFDM tones, M_t transmit and M_r receive antennas. A block of K information symbols drawn from a finite alphabet $\mathbf{S}_K \in \mathrm{A}^K$ is encoded by STFC to a codeword such that $\mathbf{C} \in C^{N_c \times M_t M_b}$ hence a code rate $\Re_{STF}$ of

$$\Re_{STF} = K / N_c M_b . \tag{3.39}$$

Thus one STF codeword contains $N_c M_b M_t$ transmitted symbols spanning over M_t transmit antennas, M_b OFDM symbols (intervals), and N_c subcarriers which can be organized as SF block matrices

$$\underline{\mathbf{C}} = \left[\mathbf{C}^1 \mathbf{C}^2 \cdots \mathbf{C}^{M_b}\right]^T \in C^{M_b N_c \times M_t}, \tag{3.40}$$

where $\mathbf{C}^n$ is the SF block matrix on the nth time instant defined as

$$\mathbf{C}^n = \begin{bmatrix} c_1^n(0) & c_2^n(0) & \cdots & c_{M_t}^n(0) \\ c_1^n(1) & c_2^n(1) & \cdots & c_{M_t}^n(1) \\ \vdots & \vdots & \ddots & \vdots \\ c_1^n(N_c-1) & c_2^n(N_c-1) & \vdots & c_{M_t}^n(N_c-1) \end{bmatrix} \in C^{N_c \times M_t}, \tag{3.41}$$

for $n = 1, 2 \cdots M_b$. After IFFT modulation and cyclic prefix insertion in the nth time instant, the OFDM symbols are simultaneously transmitted from the different transmit antennas. The STF codeword propagates through a quasi-static MIMO channel experiencing frequency selective fading and is assumed to have L independent paths between each pair of transmit and receive antennas. Under quasi-static fading conditions, the path gains between each pair of transmit and receive antennas is considered constant over N_c consecutive symbols but differ from one OFDM block to another.

At the receiver, assuming perfect timing and after removing the cyclic prefix and performing FFT demodulation, the received signal on the nth time instance can be expressed as

$$\mathbf{Y}^n = \mathbf{D}^n \mathbf{H}^n + \mathbf{Z}^n, \tag{3.42}$$

where $\mathbf{D}^n, \mathbf{Y}^n, \mathbf{Z}^n, \mathbf{H}^n$ are defined as in equations (3.20) to (3.24). The received vector collected over M_b fading blocks can be further defined as

$$
\begin{aligned}
\bar{\mathbf{Y}} &= \left[\left(\mathbf{Y}^{1}\right)^{T}\left(\mathbf{Y}^{2}\right)^{T}\cdots\left(\mathbf{Y}^{M_b}\right)^{T}\right]^{T},\\
\mathbf{X} &= diag\left[\mathbf{D}^{1},\mathbf{D}^{2},\cdots,\mathbf{D}^{M_b}\right],\\
\bar{\mathbf{H}} &= \left[\left(\mathbf{H}^{1}\right)^{T}\left(\mathbf{H}^{2}\right)^{T}\cdots\left(\mathbf{H}^{M_b}\right)^{T}\right]^{T},\\
\bar{\mathbf{Z}} &= \left[\mathbf{Z}^{1}\mathbf{Z}^{2}\cdots\mathbf{Z}^{M_b}\right],
\end{aligned}
\tag{3.43}
$$

hence,

$$
\bar{\mathbf{Y}} = \mathbf{X}\bar{\mathbf{H}} + \bar{\mathbf{Z}}, \tag{3.44}
$$

where $\bar{\mathbf{Y}} \in C^{N_c M_b M_r}$ is the received vector, the matrix $\mathbf{X} \in C^{N_c M_b M_r \times M_t L M_b M_r}$ is the transmitted signal, $\bar{\mathbf{H}} \in C^{M_t L M_b M_r}$ is the channel vector and $\bar{\mathbf{Z}} \in C^{M_r M_b M_r}$ denotes the zero mean AWGN vector.

3.4.2 Performance Criteria

From [104], [160] and (3.25), the diversity/rank criteria for STFC requires the minimum rank of $\left(\mathbf{X}-\hat{\mathbf{X}}\right)\bar{\Gamma}\left(\mathbf{X}-\hat{\mathbf{X}}\right)^{\mathcal{H}}$ over all distinct codewords $\mathbf{C}$ and $\hat{\mathbf{C}}$ to be as large as possible while the product criteria maximizes the product of the eigenvalues over all pairs of different codeword $\underline{\mathbf{C}}$ and $\hat{\underline{\mathbf{C}}}$, such that

$$
\bar{\Gamma} = E\left\{\mathbf{H}\mathbf{H}^{\mathcal{H}}\right\} = \mathbf{I}_{M_r} \otimes \mathbf{I}_{M_b} \otimes \left(diag\left\{\sigma_0,\sigma_1,\cdots,\sigma_{L-1}\right\} \otimes \mathbf{I}_{M_t}\right). \tag{3.45}
$$

Since the primary interest of the code design is diversity, it can easily be seen that the rank of STFC in MIMO frequency selective block fading channels is given by

$$
r \le \min\left\{M_r M_b N_c, M_r M_b M_t L\right\}. \tag{3.46}
$$

Since the number of subcarriers is usually greater than $M_t L$, $r \le M_r M_b M_t L$, and hence STFC can achieve up to a maximum diversity gain equivalent to the product of spatial diversity $M_r M_t$, temporal diversity M_b and frequency diversity L. Note however that STFC do not necessarily guarantee frequency diversity compared to SFC but simply add a temporal diversity domain. Therefore it is possible to achieve frequency diversity

without coding across multiple fading blocks. Let the matrix $\underline{\mathbf{D}} = diag\left(\mathbf{D}^1, \mathbf{D}^2, \cdots \mathbf{D}^{M_b}\right)$, and

$$\left(\mathbf{X}-\hat{\mathbf{X}}\right)\bar{\mathbf{\Gamma}}\left(\mathbf{X}-\hat{\mathbf{X}}\right)^{\mathcal{H}} = \mathbf{I}_{M_r} \otimes \left(\underline{\mathbf{D}}\underline{\mathbf{D}}^{\mathcal{H}}\right). \tag{3.47}$$

It can be seen that the rank of the matrix in (3.47) is the sum of the rank r_n of each nth matrix

$$r = \sum_{n=1}^{M_b} r_n = \sum_{n=1}^{M_b} \left(\mathbf{D}^n - \hat{\mathbf{D}}^n\right)\mathbf{\Gamma}_n^{1/2}, \tag{3.48}$$

and the product

$$\prod_{n=1}^{M_b}\prod_{i=1}^{r_n} \lambda_i^n. \tag{3.49}$$

Equations (3.48) and (3.49) are the sum-of-ranks and product performance criteria respectively for STFC design for block fading channels for all pairs of distinct codewords $\underline{\mathbf{C}}$ and $\hat{\underline{\mathbf{C}}}$ [159]. In order to achieve maximum diversity of $M_r M_b M_t L$, the matrix $\left(\mathbf{D}^n - \hat{\mathbf{D}}^n\right)\mathbf{\Gamma}_n\left(\mathbf{D}^n - \hat{\mathbf{D}}^n\right)^{\mathcal{H}}$ has to be full rank for every pair of different codeword $\mathbf{C}^n$ and $\hat{\mathbf{C}}^n$.

3.4.3 Example of STFC Architecture

The idea of coding across OFDM blocks was first proposed in [165] and later developed in [159] for block fading channels. In these studies, the MIMO channel was assumed constant over multiple OFDM symbols. It was also clearly pointed out that frequency diversity can be achieved by any full diversity SFC and does not necessitate coding across multiple OFDM block. Moreover because of the large number of OFDM tones involved, incurring prohibitive encoding and decoding complexity, no STFC that jointly codes across space, time and frequency as a single entity has been developed to date. Instead, STF coding has been realized by concatenating a channel encoder or frequency encoder with STC through interleaving. A remarkable advantage of concatenating two independent encoders is that the design task is simplified and the complexity greatly reduced. Also the diversity gain and coding gain can be optimized independently.

Several schemes of this nature can be found in the following references [164], [165], [171].

Figure 3.4 shows a schematic diagram of STF coding scheme realized by concatenating a channel encoder with SF encoder.

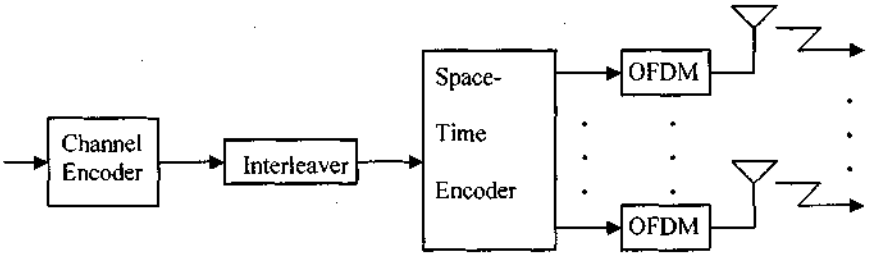

Figure 3.4: STF scheme realized through concatenating a channel encoder with SF encoder.

The channel encoder codes across M_b OFDM blocks which are serial to parallel converted. After interleaving, K source symbols are mapped to M_t OFDM symbols that are transmitted over M_b time instances. A similar scheme has been proposed in [165] where a ST trellis code was used to code across OFDM symbols and STBC to code across OFDM tones, hence STF coding. The STTC used in [165] may be viewed as a repetition code which maps a block of N_c source symbols to $M_b N_c$, hence a code rate of $1/M_b$. Note that techniques such as linear constellation decimation, permutation and rotation may be used for increased time diversity but offer minimal coding gains. For more coding gains, more powerful channel codes such as convolutional codes may be used.

3.5 Simulation Results and Discussion

This subsection presents comparative simulated results for MIMO-OFDM systems. The path gains are modelled as zero-mean and variance $1/(2L)$ per dimension, where L is the total number of multipaths. The space-time block coded OFDM and space-frequency block code (SFBC) follow the system models in Figure 3.1 and Figure 3.2

respectively, while the space-time frequency (STF) system model is as shown in Figure 3.4. The STF coding scheme in Figure 3.4 was proposed in [165]. The AWGN samples are modelled as zero-mean complex random variable with variance $N_0/2$ per dimension. The OFDM tones were set to 128 and cyclic prefix equal to the number of multipaths (or the channel order) in all the simulations, and it was assumed that perfect channel state information is available at the receiver.

For comparison purposes, the effect of cyclic prefix on the overall transmission rate is ignored. Hence the overall transmission rate of the system is based on the MIMO system deployed. The channel characteristics are assumed to be quasi-static, frequency selective Rayleigh fading, with a uniform power profile and equally spaced multipaths on all the subcarriers.

3.5.1 Transmit and Multipath Diversity

Figure 3.5 shows the BER performance for the space-time block coded OFDM under a frequency selective uncorrelated Rayleigh fading channel for one and two transmit antennas. The modulation format is based on BPSK for both one and two transmit antennas. It can be seen that the BER performance improves with increasing number of antennas and multipaths as expected. This is due to increasing transmit diversity gain and frequency diversity gain from the frequency selective nature of the fading channel. This is in agreement with studies carried out in [6] under similar channel characteristics.

3.5.2 Time Correlated Fading

Figure 3.6 shows the BER performance for the space-time block coded OFDM and SFBC both using BPSK under a frequency flat correlated Rayleigh fading channel. The Doppler frequency is normalized to $f_m = f_D N_c T$ in both cases, where f_D is the maximum Doppler frequency. The decision variables for STBC-OFDM are computed over two OFDM blocks i.e. $2N_cT$ for the case of two transmit antennas in the Alamouti scheme. The correlated Rayleigh fading coefficients were generated using the method described in [178].

It can be seen from Figure 3.6 that the BER performance of the SFBC outperforms that of STBC-OFDM when the normalized Doppler frequency is large. However, when the

normalized Doppler frequency is small, there is no significant difference in the BER performance at SNR of up to 25 dB. It is thus reasonable to expect the SFBC to have approximately the same BER performance as the STBC-OFDM when there is no relative motion between the transmitter and the receiver i.e. $f_D = 0$. In such conditions, the channel is said to be time invariant. These results are in agreements with the finding in [151].

3.5.3 Space-Time-Frequency vs. Space-Frequency Coding

Figure 3.7 shows the simulated BER performance for the SFBC and STF coding under a frequency flat Rayleigh fading channel i.e. $L = 1$. The STF coding scheme follows Figure 3.4 and uses the $1/2$ rate repetition code as channel encoder [165]. The SFBC uses BPSK modulation format while STF coding uses QPSK, hence the overall transmission rate is fixed to 1 bit/Hz. It can be seen that the BER performance improves when a channel encoder is concatenated with SFBC, hence STF coding. This is due to diversity gain from the outer repetition code.

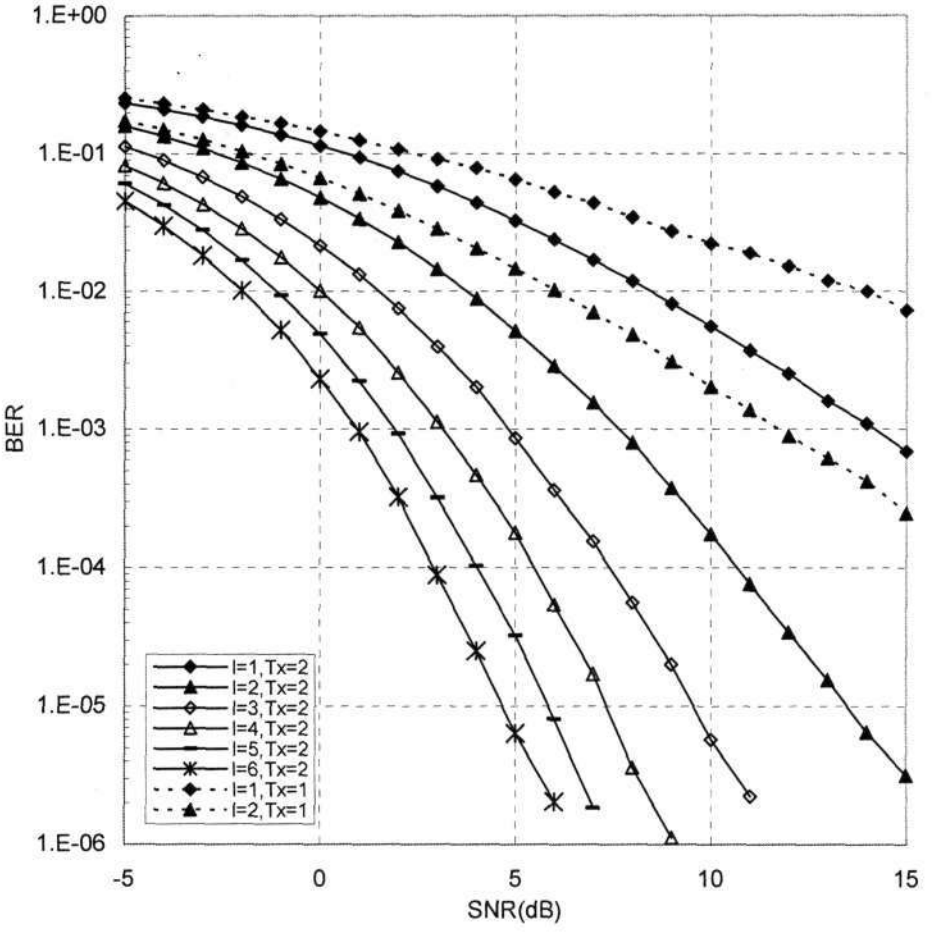

Figure 3.5: BER performance for the space-time block coded OFDM under a frequency selective uncorrelated Rayleigh fading channel for one and two transmit antennas.

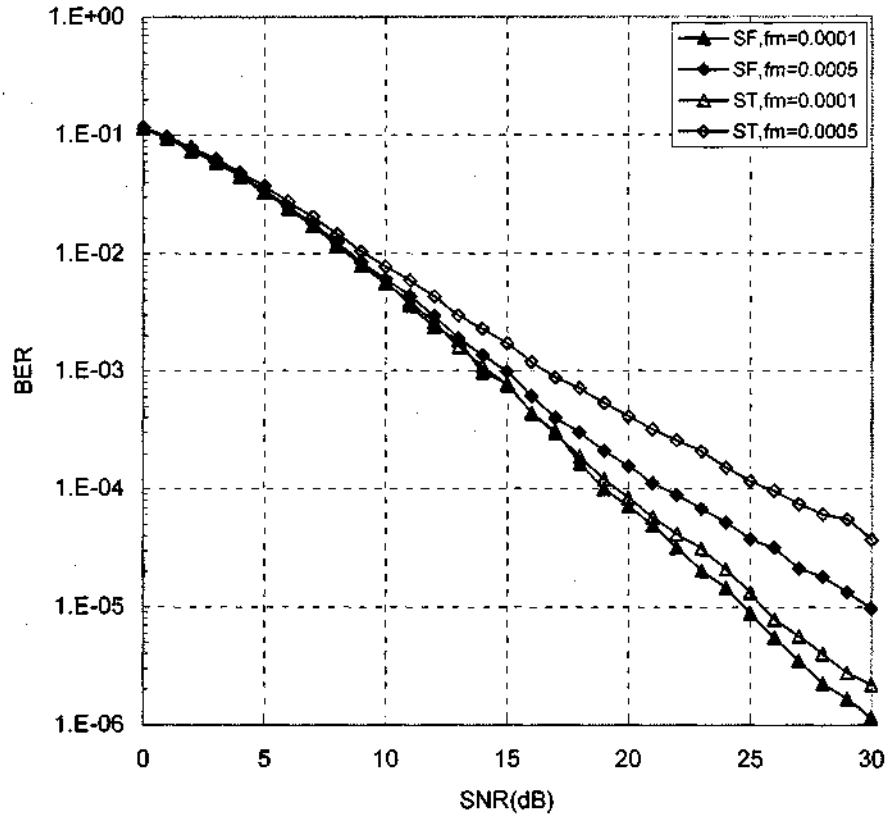

Figure 3.6: BER performance for the space-time block coded OFDM and SFBC under a frequency flat correlated Rayleigh fading channel.

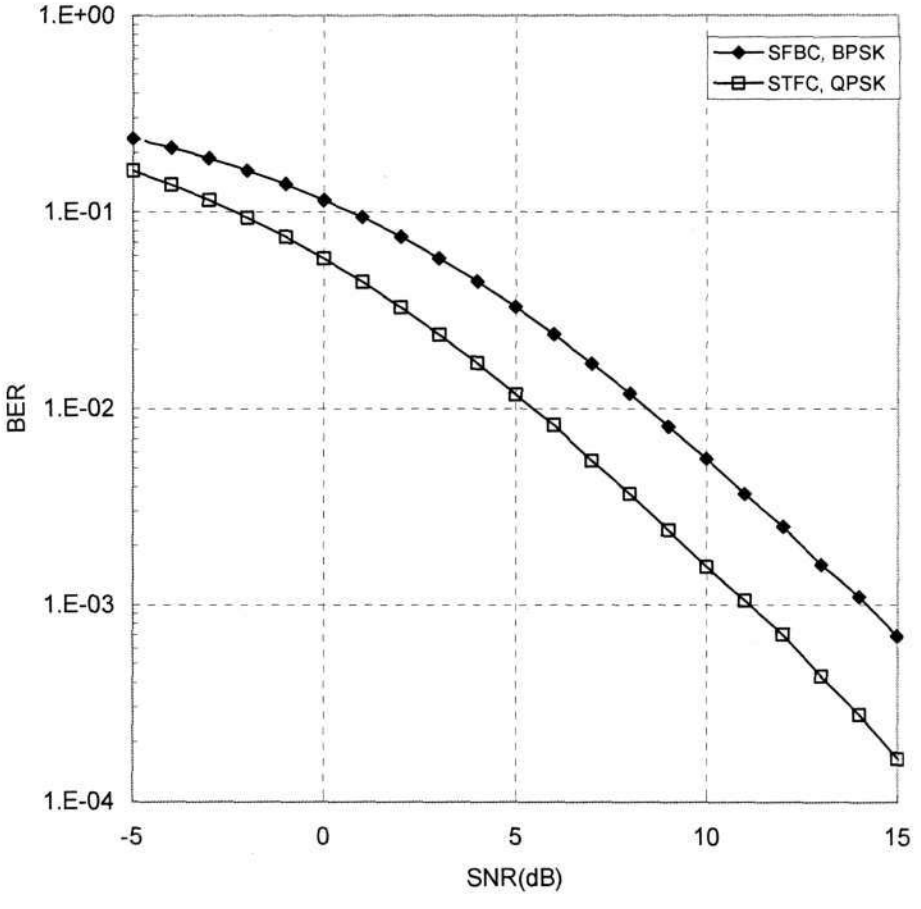

Figure 3.7: BER performance for the SFBC and STF coding under a frequency flat Rayleigh fading channel.

3.6 Conclusion

In this chapter, the performance of STBC-OFDM, SFBC and STF coding was compared through pairwise error probability. It was shown through simulated bit error rate performance that SFBC perform better than space-time block coded OFDM when the normalized Doppler frequency is large. However, when the normalized Doppler frequency is small, there is no significant difference in the BER performance. This is in agreement with the literature since the decision variables for STBC-OFDM are computed over two OFDM blocks and it relies on the symbol period to remain constant for two block period i.e. $2N_cT$ for the case of two transmit antennas, compared to one OFDM block for SFBC i.e. N_cT. Note that there is no frequency diversity gain in using OFDM when the channel characteristics are considered frequency non-selective. Hence, there is no diversity advantage of using STBC as SFBC under frequency flat fading.

CHAPTER 4

REDUNDANT RESIDUE NUMBER SYSTEM CODED SPACE-TIME-FREQUENY MODULATION

4.1 Introduction

The use of OFDM in MIMO systems provides a platform not only for efficient bandwidth transmissions but also for an intriguing signal design. By spreading information across several OFDM tones, transmit and receive antennas, it was shown that a maximum diversity gain of up to a product of temporal diversity, frequency diversity and spatial diversity can be achieved [159], [164]. Most of the proposed space-time-frequency (STF) architectures in the literature maximize frequency diversity predominantly from the frequency selective nature of the fading channel and STF does not guarantee frequency diversity. It was shown that frequency diversity could be achieved without necessarily coding across several OFDM symbols from space-frequency codes (SFC). In [161], [162], full diversity SFC was achieved by use of constellation rotation. A systematic design of full diversity SFC was proposed in [160] by repeating a row of space-time code (STC) matrix L times, where L is equal to the channel selective order. The design of space-time-frequency codes (STFC) that achieves both high data rates and full frequency diversity were addressed in [164].

The use of repetition codes in [160] and similar techniques raises questions as to whether they are more sophisticated codes with better distance properties (of course this may lead to high complexity). Introducing a trellis in the frequency domain

predetermines the transmission path, hence maximizing the frequency gain. Similar to STC, which introduces correlation both in space and time, hence maximizing spatial diversity, STFC ensures joint spatial-spectral diversity by introducing correlation in space, time and frequency in the transmitted signal.

Figure 4.1 illustrates the frequency-time coding design problem of the frequency encoder. The information bit stream to be transmitted enters a frequency encoder, which maps them to a series of parallel symbols that are simultaneously transmitted on several subcarriers. Since the aim of the frequency encoder is to find a mapping from bits to symbols such that the frequency diversity gain is maximized, the choice of a frequency encoder and subcarrier allocation is paramount. The coding is across OFDM tones as opposed to OFDM symbols in most of the STFC in the literature [164].

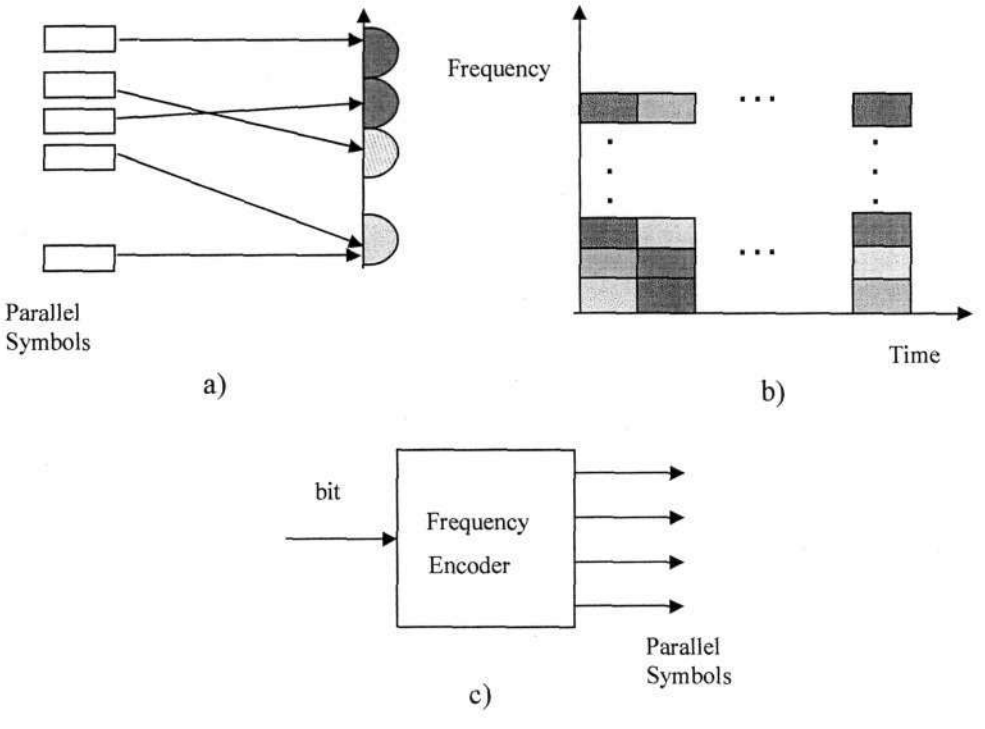

Figure 4.1: Frequency time coding.

Although some STFC designs have addressed this problem in part [159], [165], they are preoccupied with maximizing frequency diversity due to the frequency selective nature of the fading channel. Designing a code that maximizes the frequency diversity due to

multipaths presupposes that the transmitter knows the channel characteristics, which may not be practically possible in some instances. Also because of the large number of OFDM tones involved, it is important to consider a design that maximizes the spatial-spectral diversity and channel coding without incurring prohibitive decoding complexity. One way of achieving that is to concatenate a frequency encoder with space-time (ST) encoder.

In this chapter, a redundant residue number system based STF coding scheme is proposed. The design problem is divided into a STBC and a frequency encoder. The key feature of the proposed STF coding scheme is the frequency encoder. Most STF schemes in the literature use coding across multipaths and OFDM modulation techniques to maximize frequency diversity. The main challenge is the code construction involving a large number of OFDM carriers in a practical system. By dividing the available bandwidth into several non-overlapping subchannels equal to the code length, the proposed scheme codes across a number of subcarriers with STC signalling on each subcarrier. Hence the signal design on each subcarrier is the same as STC and multipath diversity is merely a trivial extension. Besides, any STC design that maximizes diversity can easily exploit the frequency diversity from the selective fading channel. Another advantage of using this scheme is that the frequency encoder is independent of the STC design hence optimizing frequency and space diversities independently.

The rest of this chapter is organized as follows. In Section 4.2 a RRNS based space-time-frequency coding scheme is proposed for block fading channels and its diversity potential investigated. Section 4.3 investigates the proposed RRNS-STF coding scheme over a rapid fading channel followed by numerical results and discussion in Section 4.4. A conclusion is then drawn in Section 4.5.

4.2 Design of RNS-STFC in Block Fading Channels

4.2.1 System Model and Signal Design

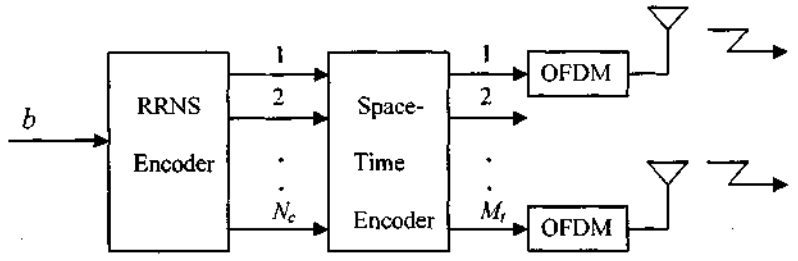

Figure 4.2: Transmitter section of the RRNS-STFC system model

Consider a RRNS coded STF coding scheme with M_t transmit and M_r receive antennas. Figure 4.2 shows the block diagram of the transmitter section. A block of b bits per coding interval enters an outer RRNS(N_c,V) code which systematically encodes them to a set of N_c parallel residues as described in Chapter 2. For systematic RRNS encoding, the b information bits are mapped to V non-redundant residues and $N_c - V$ redundant residues are generated using the base extension (BEX) method (refer to Section 2.3). The residues are each converted to their binary equivalent and a zero bit appended to every b_i bits of the non-redundant residue in order to have the same number of bits on each parallel stream, $b = \sum_{i=1}^{V} b_i$. Recall that redundant residues are each mapped to $b_i = \log_2 m_i + 1$ and non-redundant to $b_i = \log_2 m_i$, hence the moduli should be chosen close to each other for the above condition to hold. Assuming equal number of bits per residue, the code bits on each parallel stream are then mapped to MPSK symbols such that each MPSK symbol has $\tilde{b}$ bits per label.

Suppose there are $b_i = M_t K \tilde{b}$ bits per residue and for every nth time instant, K MPSK symbols on each uth parallel stream enter a STBC encoder. The STBC encoder maps K MPSK symbols on each uth stream onto M_t transmit antennas. After ST coding, a block of N_c STBC matrices, one for each antenna, are OFDM modulated and a cyclic

prefix is appended and transmitted on N_c subcarriers. Hence during the nth time instant, a block of N_c STBC symbols are simultaneously transmitted on N_c subcarriers and M_t transmit antennas. Assuming that the STBC matrix is drawn from a discrete alphabet $S \in A^K$ and that each residue forms M_b STBC matrices, the STF code matrix can be seen as concatenation of $M_b N_c$ STBC matrices defined as

$$\mathbf{C} = \left[\mathbf{C}(0)\mathbf{C}(1)\cdots\mathbf{C}(N_c-1)\right] \in C^{N_c M_b P \times M_t} \tag{4.1}$$

where

$$\mathbf{C}(u) = \begin{bmatrix} c_1^1(u) & c_2^1(u) & \cdots & c_{M_t}^1(u) \\ c_1^2(u) & c_2^2(u) & \cdots & c_{M_t}^2(u) \\ \vdots & \vdots & \ddots & \vdots \\ c_1^{M_b}(u) & c_2^{M_b}(u) & \vdots & c_{M_t}^{M_b}(u) \end{bmatrix} \in C^{M_b P \times M_t}, \tag{4.2}$$

$c_i^n(u) = \left[c_{i,1}^n(u) c_{i,2}^n(u) \cdots c_{i,P}^n(u)\right]$, hence the transmission rate of our RRNS-STF code is equivalent to that of the STBC in(3.2).

$$\overline{\Re}_{STF} = \Re_{STC} = K / P. \tag{4.3}$$

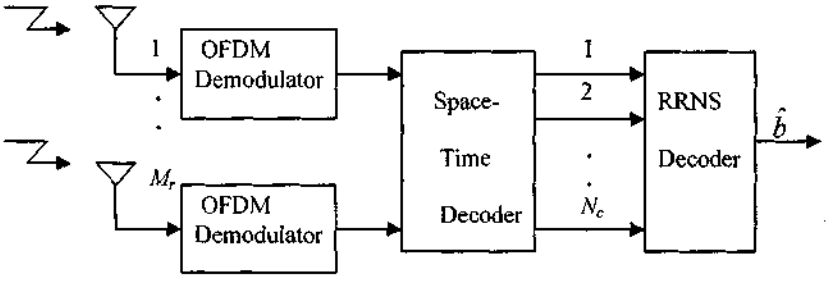

Figure 4.3: Receiver section of the RRNS-STFC system model

Figure 4.3 shows the block diagram of the receiver section of the proposed RRNS-STF coding system model. The received signal is OFDM demodulated and passed on to a space-time decoder. The space-time decoding process transforms the N_c parallel

streams of the received signal into a string of MPSK symbols corresponding to the N_c parallel residues. The MPSK symbols are then converted to binary form, mapped to their corresponding residues and fed to RRNS decoder. The RRNS decoder, in turn decodes the N_c parallel residues to $\hat{b}$ information bits per decoding interval. The received signal is assumed to have perfect timing and synchronization. After cyclic prefix removal and OFDM demodulation, the received symbol on the uth subcarrier during the nth fading block instance is given by

$$\mathbf{Y}^n(u) = \mathbf{C}^n(u)\mathbf{H}^n(u) + \mathbf{Z}^n(u), \tag{4.4}$$

where $\mathbf{H}^n(u)$ and $\mathbf{Z}^n(u)$ are the FFT MIMO channel matrix and AWGN matrix respectively on the uth subcarrier during the nth time instance.

4.2.2 Channel Model

Consider a MIMO-OFDM system propagating through a quasi-static fading channel which experiences frequency selective fading with L independent paths between each pair of transmit and receive antennas. Under this assumption, the path gains for each pair of transmit and receive antennas are constant over one OFDM symbol duration. The path gains are also assumed to be spatially uncorrelated and temporally independent from block to block. The channel impulse response between the ith transmit and the jth receive antennas during the nth time instance is given by

$$h_{i,j}^n(N_cT) = \sum_{l=0}^{L-1} \alpha_{i,j}^n(l)\delta(N_cT - \tau_l), \tag{4.5}$$

where τ_l is the delay of the lth path, $\alpha_{i,j}^n(l)$ is the fading gain of the lth path between the ith transmit and the jth receive antennas during the nth time instance. It is further assumed that all the path gains between any pair of transmit and receive antennas follow a uniform power profile, normalized such that $\sum_{l=0}^{L-1}\left|\alpha_{i,j}^n(l)\right|^2 = 1$, for any given (i, j, l, n). If we define the fading gains between each pair of transmit and receive antennas in vector form as $\mathbf{h}_{i,j}^n = \left[\alpha_{i,j}^n(0)\alpha_{i,j}^n(1)\cdots\alpha_{i,j}^n(L-1)\right]^T$, then the frequency response of the channel matrix on the uth subcarrier in the nth block in (4.4) can be expressed as

$$\mathbf{H}^n(u)=\left[\mathbf{H}_{1,1}^T(u)\cdots\mathbf{H}_{M_t,1}^T(u)\mathbf{H}_{1,2}^T(u)\cdots\mathbf{H}_{M_t,2}^T(u)\cdots\mathbf{H}_{1,M_r}^T\cdots\mathbf{H}_{M_t,M_r}^T(u)\right]^T, \quad (4.6)$$

where $\mathbf{H}_{i,j}^n(u)=\mathbf{W}\mathbf{h}_{i,j}^n$ and

$$\mathbf{W}=\left[e^{-j2\pi u\tau_0/N_c}e^{-j2\pi u\tau_1/N_c}\cdots e^{-j2\pi u\tau_{L-1}/N_c}\right], \quad (4.7)$$

given that N_c is the total number of OFDM tones.

4.2.3 Diversity Criterion

From (4.4), the total received signal can be written as

$$\mathbf{Y}=\mathbf{X}\mathbf{H}+\mathbf{Z}, \quad (4.8)$$

where $\mathbf{Y}\in C^{N_cM_bM_rP}$ is the received vector defined as

$$\mathbf{Y}=\left[\mathbf{Y}^1(0)\mathbf{Y}^2(0)\cdots\mathbf{Y}^{M_b}(0)\mathbf{Y}^1(1)\mathbf{Y}^2(1)\cdots\mathbf{Y}^{M_b}(1)\cdots\mathbf{Y}^{M_b}(N_c-1)\right]^T. \quad (4.9)$$

The transmitted signal matrix $\mathbf{X}\in C^{N_cM_bM_rP\times N_cM_bM_tM_r}$ is defined as,

$$\mathbf{X}=diag\left\{\mathbf{X}(0),\mathbf{X}(1),\cdots\mathbf{X}(N_c-1)\right\}, \quad (4.10)$$

such that $\mathbf{X}(u)=\mathbf{I}_{M_r}\otimes diag\left\{\mathbf{C}^1(u),\mathbf{C}^2(u),\cdots\mathbf{C}^{M_b}(u)\right\}$. The channel vector matrix $\mathbf{H}\in C^{M_tN_cM_bM_r}$ is given by

$$\mathbf{H}=\left[\mathbf{H}^1(0)\mathbf{H}^2(0)\cdots\mathbf{H}^{M_b}(0)\mathbf{H}^1(1)\cdots\mathbf{H}^1(N_c-1)\cdots\mathbf{H}^{M_b}(N_c-1)\right]^T, \quad (4.11)$$

and $\mathbf{Z}\in C^{M_rM_bM_rP}$ denotes the zero mean AWGN vector defined as,

$$\mathbf{Z}=\left[\mathbf{Z}^1(0)\mathbf{Z}^2(0)\cdots\mathbf{Z}^{M_b}(0)\mathbf{Z}^1(1)\cdots\mathbf{Z}^1(N_c-1)\cdots\mathbf{Z}^{M_b}(N_c-1)\right]^T. \quad (4.12)$$

Without redundancy during the RNS coding process, the pairwise error probability of the proposed STF coding scheme between two distinct codewords $\mathbf{X}$ and $\hat{\mathbf{X}}$ derived from $\mathbf{C}$ and $\hat{\mathbf{C}}$ respectively, can be written as [104], [103], [160]

$$P(\mathbf{X},\hat{\mathbf{X}}) \le \binom{2r-1}{r}\left(\prod_{i=1}^{r}\lambda_i\right)^{-1}\left(\frac{\mathrm{SNR}}{M_t}\right)^{-r} \tag{4.13}$$

where r is the rank and $\{\lambda_i\}$ are nonzero eigenvalues of the matrix $(\mathbf{X}-\hat{\mathbf{X}})\mathbf{\Gamma}(\mathbf{X}-\hat{\mathbf{X}})^{\mathcal{H}}$, with $\mathbf{\Gamma} = E\{\mathbf{H}\mathbf{H}^{\mathcal{H}}\}$. From the diversity/rank criterion, the minimum rank of $(\mathbf{X}-\hat{\mathbf{X}})\mathbf{\Gamma}(\mathbf{X}-\hat{\mathbf{X}})^{\mathcal{H}}$ over all distinct codewords $\mathbf{C}$ and $\hat{\mathbf{C}}$ should be as large as possible. Since RNS codes are repetitive in nature, in the absence of redundancy (error correction), $\mathbf{C}^n(u)$ in (4.2) is independent of u, and hence the rank of $(\mathbf{X}-\hat{\mathbf{X}})\mathbf{\Gamma}(\mathbf{X}-\hat{\mathbf{X}})^{\mathcal{H}}$ can be written as

$$\begin{aligned} r &= rank\left[(\mathbf{X}-\hat{\mathbf{X}})\mathbf{\Gamma}(\mathbf{X}-\hat{\mathbf{X}})^{\mathcal{H}}\right] \\ &= rank\left[\mathbf{I}_{N_c}\right] rank\left[\mathbf{I}_{M_r}\right] \sum_{n=1}^{M_b} rank\left[(\mathbf{C}^n-\hat{\mathbf{C}}^n)\mathbf{\Gamma}(\mathbf{C}^n-\hat{\mathbf{C}}^n)^{\mathcal{H}}\right] \\ &= N_c M_r \sum_{n=1}^{M_b} rank\left\{\left[(\mathbf{C}^n-\hat{\mathbf{C}}^n)(\mathbf{C}^n-\hat{\mathbf{C}}^n)^{\mathcal{H}}\right]\circ\mathbf{\Gamma}\right\}, \end{aligned} \tag{4.14}$$

where $\mathbf{\Gamma} = E\left\{\mathbf{H}^n_{i,j}(u)\left(\mathbf{H}^n_{i,j}(u)\right)^{\mathcal{H}}\right\}$ and is independent of u and n. According to the rank inequality, we can define minimum rank of

$$rank\left\{\left[(\mathbf{C}^n-\hat{\mathbf{C}}^n)(\mathbf{C}^n-\hat{\mathbf{C}}^n)^{\mathcal{H}}\right]\circ\mathbf{\Gamma}\right\} \le rank\left[(\mathbf{C}^n-\hat{\mathbf{C}}^n)(\mathbf{C}^n-\hat{\mathbf{C}}^n)^{\mathcal{H}}\right] rank\mathbf{\Gamma}. \tag{4.15}$$

Since the rank of $(\mathbf{C}^n-\hat{\mathbf{C}}^n)(\mathbf{C}^n-\hat{\mathbf{C}}^n)^{\mathcal{H}}$ is at most M_t and the rank of $\mathbf{\Gamma}$ is at most L, the rank of $\left\{\left[(\mathbf{C}^n-\hat{\mathbf{C}}^n)(\mathbf{C}^n-\hat{\mathbf{C}}^n)^{\mathcal{H}}\right]\circ\mathbf{\Gamma}\right\}$ is at most $\min(P, M_t L)$, where P is defined in (3.1). Thus the achievable diversity product using RNS codes without redundancy in STF coding is

$$\min\{N_c M_r M_b P, N_c M_r M_b M_t L\}. \tag{4.16}$$

Since $P = M_t$ for square STBC code matrix, the diversity gain of the RNS-STF coding scheme is $N_c M_b M_r M_t$, a product of OFDM tones (intrinsic frequency diversity) N_c,

time diversity M_b and spatial diversity $M_t M_r$. Since the information to be transmitted is spread over N_c residues, the use of RNS codes offers intrinsic frequency diversity equal to the number of OFDM tones. This frequency diversity is due to the repetitive nature of RNS codes and is independent of the frequency selective nature of the fading channel. Frequency diversity due to multipath can be further exploited by techniques such as constellation rotation [162], repetition [160] and permutation [164], [96]. Hence the RNS-STF coding scheme offers a potential frequency diversity gain of up to $N_c L$.

4.2.4 Diversity Concept and Coding Gain

With redundancy/error correction, the frequency diversity of RRNS-STF coding scheme is limited to the Hamming distance $d_{\min}$ and the channel order, hence the pairwise error probability (codeword error) in (4.13) may be written as [27], [28], [38], [39]

$$P(\mathbf{X}, \hat{\mathbf{X}}) \leq \sum_{u=t+1}^{N_c} \binom{N_c}{u} \left(1 - P_u\right)^{N_c - u} \left(P_u\right)^u , \tag{4.17}$$

where $t = \left(d_{\min} - 1\right)/2$ is the error correction capability and P_u is the probability of the uth residue/subcarrier symbol in error, given by [104]

$$P_u \leq \binom{2M_t M_r M_b - 1}{M_t M_r M_b} \left(\prod_{i=1}^{M_t M_r M_b} \lambda_i \right)^{-1} \left(\frac{\mathrm{SNR}}{M_t} \right)^{-M_t M_r M_b} . \tag{4.18}$$

Assume that the number of transmit and receive antennas together with the time diversity components are kept constant. Note that the asymptotic decay $\left(\mathrm{SNR}/M_t\right)^{-M_t M_r M_b}$ in (4.18) is only valid for all eigenvalues $\lambda_i > 0$. Even then many of the eigenvalues may be so small that they are of no relevance at reasonable SNR. Hence the decay may be weak and therefore increasing the Hamming distance of the RRNS code higher than the relevant number of eigenvalues may not significantly increase the steepness of the error curves. It is therefore important to consider the frequency diversity degree of the RRNS-STF coding scheme in two dimensions; frequency diversity due to the error event given by the Hamming distance and the diversity order of the channel influenced by the relevant eigenvalues. In some applications where the

channel and the RRNS code fail to provide full diversity, they may still provide a coding gain given by

$$G_{RNS}\left(\mathbf{X},\hat{\mathbf{X}}\right)=10\log(\Re_{RNS}d_{\min})\ \text{dB}, \tag{4.19}$$

where $\Re_{RNS}$ is the rate of the RRNS code. Since the coding gain is responsible for the shift of the error rate curve to the left, if the shift is big enough, the RRNS-STF coded system may need a lower SNR at any given bit error rate. Hence the use of RNS codes in STF coding offers an intrinsic frequency diversity component that has not been considered so far in the literature. Note however that the number of nearest neighbours and the number of different error coefficients also play an important part in the BER performance. Increasing the Hamming distance leads to increased number of nearest neighbours, hence a large error coefficient which may negate the diversity gain on the overall bit error rate performance of the system.

4.2.5 Transmission Rate of the RRNS-STFC

Although one may argue that introducing redundancy in the OFDM tones may reduce the bandwidth, the overall performance improvement and the overall code rate of the system may tell a different story. As was stated in (4.3) the transmission rate of the proposed STF coding scheme in this chapter is equal to that of the inner STCB (STTC may also be used). By choosing the frequency encoder with a high code rate such as RRNS codes and a high modulation format for the inner STBC, one can compensate for the loss in bandwidth efficiency due to redundancy.

4.3 Performance of RRNS coded STFC in Fast Fading Channels

4.3.1 Time and Frequency Selective Fading

The channel model is an important parameter in the design of any communication system. In the preceding section and in Chapter 3, the MIMO channel was modelled as a frequency selective multipath fading channel with wide-sense stationary uncorrelated scattering for a given block (quasi-static fading). However, due to high data rates, high mobility and transmit diversity using multiple antennas, the above condition may not hold for a wireless MIMO channel. One also needs to incorporate spatial characteristics

of the channel on top of classical understanding of fading and Doppler spread such as angle of arrival, time delay spread and adaptive array geometry. Several studies have been devoted to channel modelling in MIMO systems and its effect on the channel capacity and bit error rate performance [175], [176], [174].

Consider a fast fading frequency selective MIMO channel where the fade gain varies from one STC code symbol to another. The fade gain from one STC symbol may be considered time invariant i.e. flat fading or time variant i.e. time selective fading. Whereas a frequency selective channel provides multipath diversity, a time selective channel provides Doppler diversity that might be exploited through the use of a Rake receiver [39]. We use Clarke's two-dimensional isotropic scattering model where the angle of arrival is uniformly distributed over $[0, 2\pi]$ to incorporate the spatial element of the channel [174]. The received signal statistics on the uth subcarrier during the nth time instant are defined the same way as in (4.4) except the channel characteristics $\mathbf{H}^n(u)$. To study the received signal statistics and the correlation properties on their envelope as a function of frequency, time, antenna separation and angle of arrival, we model spatial-temporal time and frequency selective fading channel impulse response as

$$h_{i,j}^n(T,t) = \sum_{l}^{L} \mathbf{E}_t(\varphi_l)\alpha_{i,j}^n(l,t)\partial(T - l/K\Delta_f)\mathbf{E}_r(\varphi_l), \tag{4.20}$$

for the ith transmit and the jth receive antenna elements on the nth block. In (4.20) above, ϕ_l denotes the angle of arrival for the lth nonzero tap, whose delay is $l/K\Delta_f$, given that $\Delta_f = 1/N_cT$ is the subcarrier spacing, and $\alpha_{i,j}^n(l,t)$ is the complex fading coefficient. $\mathbf{E}_t(\varphi_l)$ and $\mathbf{E}_r(\varphi_l)$ are the array gains at the transmitter and receiver respectively defined as a function of the antenna geometry and angle of arrival, $\mathbf{E}_g(\varphi_l) = \exp\left[-j2\pi\Delta(i-1)\cos\varphi_l/\lambda\right]$, where Δ is the antenna separation. Assuming a uniform angle of arrival and adequate antenna separation, the array gain can be set to unity i.e. $\mathbf{E}_t(\varphi_l) = 1$ and $\mathbf{E}_r(\varphi_l) = 1$. L is the total number of resolvable paths (channel order). A detailed study of MIMO channels and their statistical models is not covered in this thesis but may be found in [175], [176] and the references therein. If we consider our STFC codeword to be time limited over M_bN_cT hence a bandwidth $1/M_bN_cT$, following a particular lth path of the ith and the jth antenna pair's random process, the

Fourier transform of the time response for the complex amplitude can be expressed as [175]

$$\alpha_{i,j}^{n}(l,t)=\sum_{q=-f_D M_b N_c T}^{f_D M_b N_c T}\beta_{i,j}^{n}(u,l,q)e^{j2\pi tq/(M_b N_c T)}, \tag{4.21}$$

given that $\beta_{i,j}^{n}(u,l,q)$ is the independent circularly symmetric complex Gaussian random variable (follows a Rayleigh distribution) and f_D is the Doppler frequency . We can then express the channel response of the nth time slot and the uth subcarrier as

$$\begin{aligned}\mathbf{H}_{i,j}^{n}(u)&=\sum_{l}^{L}\alpha_{i,j}^{n}(l,uT)e^{-j2\pi ul/N_c}\\&=\mathbf{h}_{i,j}^{n}\boldsymbol{\omega}_u,\end{aligned} \tag{4.22}$$

where $\mathbf{h}_{i,j}^{n}=\left[\alpha_{i,j}^{n}(0,uT)\alpha_{i,j}^{n}(1,uT)\cdots\alpha_{i,j}^{n}(L-1,uT)\right]^{\mathcal{H}}$ is the L sized vector of all time responses such that

$$\alpha_{i,j}^{n}(l,uT)=\sum_{q=-f_D M_b N_c T}^{f_D M_b N_c T}\beta_{i,j}^{n}(u,l,q)e^{j2\pi qu/(M_b N_c)}, \tag{4.23}$$

while $\boldsymbol{\omega}_u=\left[e^{0}e^{-j2\pi u/N_c}\cdots e^{-j2\pi u(L-1)/N_c}\right]^{T}$ contains the corresponding FFT coefficients.

It can be seen from (4.22) that there is discrete-time and frequency complex exponential bases, justifying extrinsic diversity gains. This is due to the time (Doppler) and frequency selective nature of the fading channel. For the uncorrelated fading channel, both time and frequency selectivity have the same effect, i.e. improve the performance of the system if collected over several taps. Hence in this thesis, we shall consider only a frequency selective channel with L diversity/channel, in which equation (4.23) becomes

$$\alpha_{i,j}^{n}(l,uT)=\beta_{i,j}^{n}(u,l)e^{j2\pi u/N_c}. \tag{4.24}$$

4.3.2 The Effect of Time Correlation

In most OFDM systems, the cyclic prefix is assumed large enough so that the effect of ISI is limited to the cyclic prefix which is discarded at the receiver. The effects of spatial correlation is well investigated and covered in [175], [176] and the references therein. Therefore we concentrate on the effect of time correlation in this subsection.

Assuming that the fading process remains constant over M_t consecutive symbol intervals, and that there is no spatial or spectral correlation, the zero mean complex Gaussian variables based on Jakes' model [174] for $\hat{T} = M_t N_c T$ symbols apart in a frequency selective time correlated fading channel is given by

$$\begin{aligned}
\hat{\Gamma}_u &= E\left\{\mathbf{H}_{i,j}^{(n+\kappa)\hat{T}}(u)\left(\mathbf{H}_{i,j}^{(n\hat{T})}(u)\right)^{\mathcal{H}}\right\} \\
&= E\left\{\sum_{l=0}^{L-1}\alpha_{i,j}^{(n+\kappa)\hat{T}}(l,u)e^{-j2\pi lu/N_c}\left(\sum_{q=0}^{L-1}\alpha_{i,j}^{(n\hat{T})}(q,u)e^{-j2\pi qu/N_c}\right)^{*}\right\} \\
&= E\left\{\sum_{l=0}^{L-1}\alpha_{i,j}^{(n+\kappa)\hat{T}}(l,u)\left(\alpha_{i,j}^{(n\hat{T})}(l,u)\right)^{*}\right\} \\
&= J_0\left(2\pi\kappa f_D\hat{T}\right)\sum_{l=0}^{L-1}\sigma_u^2(l).
\end{aligned} \tag{4.25}$$

where $\hat{\Gamma}_u$ denotes the autocorrelation function on the uth subcarrier and $\sigma_u^2(l)$ is the power profile on the lth path and the uth subcarrier. Note that $\hat{\Gamma}_u$ and $\sigma_u^2(l)$ are independent of u. We assume a uniform power profile on all the subcarriers, i.e. $\sum_{l=0}^{L-1}\sigma_u^2(l)=1$. Focusing on the maximum achievable diversity gain of the proposed RRNS-STF coding scheme under time correlation, the sum of ranks in (4.14) for a fast fading channel can be written as

$$r \le M_r\sum_{u=1}^{N_c} rank\left\{\left[\left(\mathbf{C}(u)-\hat{\mathbf{C}}(u)\right)\left(\mathbf{C}(u)-\hat{\mathbf{C}}(u)\right)^{\mathcal{H}}\right]\circ\boldsymbol{\Gamma}_u\right\}, \tag{4.26}$$

given $\mathbf{C}(u)$ is defined in (4.1) and $\boldsymbol{\Gamma}_u$ is a correlation matrix whose elements are defined in (4.25). The rank of $\left(\mathbf{C}(u)-\hat{\mathbf{C}}(u)\right)\left(\mathbf{C}(u)-\hat{\mathbf{C}}(u)\right)^{\mathcal{H}}$ is at most PM_b and the

rank of Γ_u is at most L, hence the rank of our scheme under fast fading frequency selective channel conditions is

$$r \le \min\left(M_r N_c P M_b, M_r N_c M_t L\right). \tag{4.27}$$

Considering that $L << M_b$ and $P \ge M_t$ in practice, the maximum achievable diversity gain for a fast fading time correlated frequency selective channel is

$$r \le M_r N_c M_t L. \tag{4.28}$$

Note that time correlation only affects the time diversity component of the proposed RRNS-STF coded system. The performance may be improved through bit/symbol interleaving.

4.3.3 Analytical Model

Consider a STF coding MIMO system with N_c OFDM tones, M_t transmit and M_r receive antennas propagating through a frequency selective fast Rayleigh fading channel. The system model is as discussed in Section 4.2.1. Assuming perfect channel state information, after removing the cyclic prefix and OFDM demodulation, the received signal on the uth subcarrier during the nth time instance is given by

$$\mathbf{Y}^n(u) = \mathbf{C}_n(u)\mathbf{H}_n(u) + \mathbf{Z}_n(u), \tag{4.29}$$

where the transmitted signal matrix $\mathbf{C}_n(u) \in C^{M_r P \times M_t}$ is defined in (4.2), the received vector matrix $\mathbf{Y}_n(u) \in C^{M_r P}$, and AWGN vector matrix $\mathbf{Z}_n(u) \in C^{M_r P}$ are as defined as

$$\begin{aligned} \mathbf{Y}_n(u) &= \left[y_1^n(u) y_2^n(u) \cdots y_{M_r}^n(u) \right]^T, \\ \mathbf{Z}_n(u) &= \left[z_1^n(u) z_2^n(u) \cdots z_{M_r}^n(u) \right]^T. \end{aligned} \tag{4.30}$$

The channel vector matrix $\mathbf{H}_n(u) \in C^{M_t N_c M_b M_r}$ is defined as in (4.6) except for the channel coefficients corresponding to the ith transmit and the jth receive antenna during the nth time instant on the uth subcarrier defined as $\mathbf{H}_{i,j}^n(u) = \mathbf{W}\mathbf{h}_{i,j}^n$, differ in

$\mathbf{h}_{i,j}^{n} = \left[\alpha_{i,j}^{n}(u,0)\alpha_{i,j}^{n}(u,1)\cdots\alpha_{i,j}^{n}(u,L-1)\right]^{T}$. The PEP of decoding a $\hat{\mathbf{C}}_n(u)$ given that the codeword $\mathbf{C}_n(u)$ was transmitted can be expressed as [39], [104],

$$\begin{aligned} P\left(\mathbf{C}_n(u),\hat{\mathbf{C}}_n(u)\right) &= P\left(\left\|\mathbf{Y}_n(u)-\mathbf{C}_n(u)\right\|^2 > \left\|\mathbf{Y}_n(u)-\hat{\mathbf{C}}_n(u)\right\|^2\right) \\ &= P\left(\mathrm{Re}\left\{tr\left[\mathbf{Y}_n^{\mathcal{H}}(u)\left(\mathbf{C}_n(u)-\hat{\mathbf{C}}_n(u)\right)\mathbf{H}_n(u)\right]\right\}\right). \end{aligned} \tag{4.31}$$

Hence the average PEP can be written as

$$P\left(\mathbf{C}_n(u),\hat{\mathbf{C}}_n(u)\right) = \int_{-\infty}^{0} P_{\mathbf{g}^n(u)}(x)dx, \tag{4.32}$$

where $\mathbf{g}_n(u) = \mathrm{Re}\left\{tr\left[\mathbf{Y}_n^{\mathcal{H}}(u)\left(\mathbf{C}_n(u)-\hat{\mathbf{C}}_n(u)\right)\mathbf{H}_n(u)\right]\right\}$ and $P_{\mathbf{g}^n(u)}(x)$ denotes the pdf of $\mathbf{g}_n(u)$ at x. Note that $\mathbf{g}_n(u)$ can be written in quadratic form of the correlated complex Gaussian random variables, i.e. $\mathbf{g}_n(u) = \tilde{\mathbf{g}}_u^{\mathcal{H}}\mathbf{Q}_u^n\tilde{\mathbf{g}}_u$, $\tilde{\mathbf{g}}_u = \left[\mathbf{Y}_u(u)\mathbf{H}_u(u)\right]^T$ and

$$\mathbf{Q}_u^n = \begin{bmatrix} \mathbf{0} & \mathbf{I}_{M_r}\otimes\left(\mathbf{C}_n(u)-\hat{\mathbf{C}}_n(u)\right)^{\mathcal{H}} \\ \mathbf{I}_{M_r}\otimes\left(\mathbf{C}_n(u)-\hat{\mathbf{C}}_n(u)\right) & \mathbf{0} \end{bmatrix}. \tag{4.33}$$

Consider a residue symbol on the uth subcarrier spanning M_b matrices per residue, its pdf can therefore be written from its characteristic function as [39]

$$P_{\mathrm{G}(u)}(x) = \frac{1}{2\pi}\int_{-\infty}^{\infty}\Phi_{\mathrm{G}(u)}(s)\exp(-sx)ds, \tag{4.34}$$

where $\mathbf{G}_u = \tilde{\mathbf{G}}_u^{\mathcal{H}}\mathbf{Q}_u\tilde{\mathbf{G}}_u$, given that $\tilde{\mathbf{G}}_u = \left[\tilde{\mathbf{g}}_1(u)\tilde{\mathbf{g}}_2(u)\cdots\tilde{\mathbf{g}}_{M_b}\right]$,

$$\mathbf{Q}_u = \begin{bmatrix} \mathbf{0}_{M_b} & \mathbf{C}^{\mathcal{H}}(u)\mathbf{I}_{M_b} \\ \mathbf{C}(u)\mathbf{I}_{M_b} & \mathbf{0}_{M_b} \end{bmatrix}, \tag{4.35}$$

given that $\mathbf{0}_{M_b}$ is a $M_b \times M_b$ zero matrix and $\mathbf{C}(u) = \left[\mathbf{C}_1(u)\mathbf{C}_2(u)\cdots\mathbf{C}_{M_b}(u)\right]$ whose elements are defined as $\mathbf{C}_n(u) = \mathbf{I}_{M_r}\otimes\left(\mathbf{C}_n(u)-\hat{\mathbf{C}}_n(u)\right)$. Assuming a frequency flat

independent fading channel i.e. $L=1$ with no correlation and a uniform power profile, the characteristic function $\Phi_{G(u)}(s)$ can be expressed as

$$\Phi_{G(u)}(s)=\left|\mathbf{I}_{2M_rM_rM_b}-s\boldsymbol{\Phi}_u\mathbf{Q}_u\right|^{-1}, \tag{4.36}$$

where $\boldsymbol{\Phi}_u$ is the covariance matrix on the uth subcarrier defined as

$$\boldsymbol{\Phi}_u=\left(\begin{bmatrix}\sigma^2+N_0 & \sigma^2\\ \sigma^2 & \sigma^2\end{bmatrix}\otimes\mathbf{I}_{M_b}\right)\otimes\mathbf{I}_{M_r}, \tag{4.37}$$

for σ^2 and N_0 are variances of complex channel and AWGN during the nth time interval on the uth subcarrier. Note that the Hermitian Gaussian quadratic form $\mathbf{G}_u=\tilde{\mathbf{G}}_u^{\mathcal{H}}\mathbf{Q}_u\tilde{\mathbf{G}}_u$ can be diagonalized by an orthogonal transformation into [177]

$$\tilde{\mathbf{G}}_u^{\mathcal{H}}\mathbf{Q}_u\tilde{\mathbf{G}}_u=\sum_{i=1}^{2M_rM_rM_b}\lambda_i\left|\mathcal{V}_i\right|^2, \tag{4.38}$$

where λ_i are egeinvalues of the correlation matrix $\boldsymbol{\Phi}_u\mathbf{Q}_u$ and $\mathcal{V}_i$ are independent zero-mean, unit variance Gaussian random variables. Using the alternative form of the complimentary error function [179]

$$erfc(x)=\frac{2}{\pi}\int_0^{\infty}\frac{e^{-x^2(t^2+1)}}{t^2+1}dt \quad \text{for } x>0, \tag{4.39}$$

the average PEP of the symbol residue on the uth subcarrier can be written as

$$P\left(\mathbf{C}(u),\hat{\mathbf{C}}(u)\right)=\int_0^{\infty}Q\left(\sqrt{2\mathcal{V}}\right)P(\mathcal{V})d\mathcal{V}, \tag{4.40}$$

which yields

$$
\begin{aligned}
P\left(\mathbf{C}(u),\hat{\mathbf{C}}(u)\right) &= \frac{1}{\pi}\int_0^{\infty}\int_0^{\infty}\frac{e^{-\mathcal{V}^2(t^2+1)}}{t^2+1}P(\mathcal{V})\,d\mathcal{V}dt \\
&= \frac{1}{\pi}\int_0^{\infty}\frac{\Phi_{\mathbf{G}(u)}(s)\big|_{s=-(t^2+1)}}{t^2+1}dt \\
&= \frac{1}{\pi}\int_0^{\infty}\frac{1}{\left(t^2+1\right)\prod_{i=1}^{2M_tM_b}\left(1+\lambda_{i,u}(1+t^2)\right)^{M_r}}dt.
\end{aligned}
\tag{4.41}
$$

The integral in (4.41) can be solved using the numerical methods such as the Gauss-Chebyshev quadrature to give [104], [107], [108], [109], [110], [111], [112], [172], [179]

$$
P\left(\mathbf{C}(u),\hat{\mathbf{C}}(u)\right) = \frac{1}{2n}\sum_{j=1}^{n}\prod_{i=1}^{2M_tM_b}\left(1+\lambda_{i,u,j}\right)^{-M_r} + R_n, \tag{4.42}
$$

where $\lambda_{i,u,j} = \lambda_{i,u}\sec^2\left[\left(2j-1\right)\pi/4n\right]$ and n is a small positive integer. As n increases, the remainder term R_n becomes negligible. The probability of decoding codeword $\hat{\mathbf{X}}$ given that $\mathbf{X}$ was transmitted $P(\mathbf{X},\hat{\mathbf{X}})$ can be calculated from (4.17) by substituting $P_u = P\left(\mathbf{C}(u),\hat{\mathbf{C}}(u)\right)$.

4.3.3.1 Remarks

Firstly, note that when there is no time correlation, the channel fades independently and the covariance matrix $\mathbf{\Phi}_u\mathbf{Q}_u$ is full rank. Hence from (4.37) and the dimensions of the covariance matrix $\mathbf{\Phi}_u\mathbf{Q}_u$, the maximum achievable diversity advantage is $2M_rM_tM_b$. This implies that both the STFC and the complex channel are full rank. However, if the channel is time correlated, the covariance matrix in (4.37) becomes

$$
\mathbf{\Phi}_u = \begin{bmatrix}
\zeta_{0,0}(u) & \zeta_{0,1}(u) & \cdots & \zeta_{0,M_b-1}(u) \\
\zeta_{1,0}(u) & \zeta_{1,1}(u) & \cdots & \zeta_{1,M_b-1}(u) \\
\vdots & \vdots & \ddots & \vdots \\
\zeta_{M_b-1,0}(u) & \zeta_{M_b-1,1}(u) & \cdots & \zeta_{M_b-1,M_b-1}(u)
\end{bmatrix} \otimes \mathbf{I}_{M_r}, \tag{4.43}
$$

for $\zeta_{i,j}(u) = E\left\{\mathbf{g}_i(u)(u)\mathbf{g}_j^{\mathcal{H}}(u)\right\}$ defined as

$$\zeta_{i,j}(u)=\begin{bmatrix} E\{\mathbf{Y}_i(u)\mathbf{Y}_j^{\mathcal{H}}(u)\} & E\{\mathbf{Y}_i(u)\mathbf{H}_j^{\mathcal{H}}(u)\} \\ E\{\mathbf{H}_i(u)\mathbf{Y}_j^{\mathcal{H}}(u)\} & E\{\mathbf{H}_i(u)\mathbf{H}_j^{\mathcal{H}}(u)\} \end{bmatrix}. \tag{4.44}$$

Therefore maximum achievable diversity advantage is dependent on the rank of the matrix $\mathbf{\Phi}_u\mathbf{Q}_u$, which reflects the relative motion between the transmitter and the receiver. Note however that when the channel is heavily correlated i.e. $f_DT >> 0$, the correlation matrix in (4.43) tends to (4.37), which is the correlation matrix for the independent fading channel. Hence, the performance improves with increasing f_DT. This is consistent with the literature [142], where it was shown that for coherent reception, the multisampling receiver benefits from the implicit time diversity of the fast fading channel.

Secondly, note that in the presence of multipaths i.e. $L>1$, each path is assumed to fade independently and hence the autocorrelation of the lth path assuming Jakes' model can be defined as $E\left\{\alpha_{\tau_1\hat{T}}(u,l_1)\alpha^*_{\tau_2\hat{T}}(u,l_2)\right\}=\sigma_u^2(l)$ for $l_1=l_2$ and zero otherwise, where $\hat{T}=M_tN_cT$. For comparison purposes, it is assumed that the total received energy for frequency selective fading channel is equal to the received energy for flat fading channel, i.e. $\sum_{l=1}^{L}\sigma^2(l)=\sigma^2$, where L is the channel odder. Using the same approach as for frequency flat fading, the characteristic function in (4.36) can be expressed as the product of the channel order

$$\Phi_{G(u)}(s)=\prod_{l=1}^{L}\left|\mathbf{I}_{2M_tM_rM_b}-s\mathbf{\Phi}_{u,l}\mathbf{Q}_u\right|^{-1}, \tag{4.45}$$

where $\mathbf{\Phi}_{u,l}$ is the covariance matrix on the lth path defined as in (4.37) except for the variance $\sigma^2(l)=E\left\{\alpha_i(u,l)\alpha_j^*(u,l)\right\}$. Assuming independent fading on each subcarrier, then frequency selective fading leads to additional frequency diversity advantage. Similarly, the codeword error probability for a frequency selective fading channel can be derived using methods for a flat fading channel.

4.4 Numerical Results and Discussion

In this subsection, numerical results for the proposed space-time-frequency coding at the receiver are presented and discussed. By keeping the transmit diversity order fixed, we investigate the effect of time and frequency diversity for the proposed RRNS-STF coding scheme. The analytical model is as discussed in Section 4.3.3 with the transmitter and the receiver models based on Figure 4.2 and Figure 4.3 respectively. The RRNS encoder is used as the frequency encoder and the Alamouti [88] two transmit antennas space-time block structure used for space-time encoding (encoder). Systematic RRNS coding is used with a zero bit appended on each non-redundant residue equivalent bits in order to have equal number of bits on each parallel stream. The moduli for eight subcarriers $m_1 = 229$, $m_2 = 233$, $m_3 = 239$, $m_4 = 241$, $m_5 = 247$, $m_6 = 251$, $m_7 = 253$, $m_8 = 255$ were taken from [33]. Note that there are eight bits per residue/subcarrier. The measured pairwise error probability (PEP) is presented as a function of SNR (E_b/N_o) in dB and is computed from (4.17).

Figure 4.4 shows the PEP performance comparison of the proposed RRNS coded with the uncoded (i.e. no frequency encoder) and repetition coded space-time frequency (STF) coding scheme under frequency flat Rayleigh fading. For fair comparison, the overall transmission rate of each system should be equal. The uncoded system uses BPSK space-time encoder, hence 1 bit/Hz while the repetition coded and RRNS coded STF both use QPSK space-time encoder. For RRNS(8,6), hence $6/8$ code rate with $t = 1$ error correction capability, the overall transmission rate is $3/2$ bits/Hz, while for RRNS(8,4), hence $4/8$ code rate with $t = 2$ error correction capability, the overall transmission rate is 1 bits/Hz. Note that since 8 bits moduli, hence 8 bit/residues are used, the time diversity component $M_b = 2$. The repetition coded STF coding scheme follows STF system model proposed in [165]. The $1/2$ rate repetition outer encoder is concatenated with the inner two transmit QPSK Alamouti STBC, hence the overall transmission rate is 1 bit/Hz.

It can be seen from Figure 4.4 that the PEP performance improves on application of the outer encoder i.e. for the repetition and RRNS code. This is due to diversity gain offered by the repetition code and the inherent repetitive nature of RRNS codes. However, the PEP performance curves of the proposed RRNS-STF scheme are much steeper than that

of the repetition code. This is due to both the repetitive nature of RRNS codes and coding across residues (which is equivalent to coding across OFDM tones), which maximizes the frequency diversity gain as reflected by the curve's shift to left as we move from $t=1$ to $t=2$ error correction capabilities. Note that when there is no multipath, the proposed STF coding scheme in [165] only achieves two dimensional diversity gain i.e. spatial and temporal diversities. There is no frequency diversity advantage/gain for the uncoded or repetition coded STF coding scheme under frequency flat fading. The STF coding scheme proposed in [164] can be categorized as uncoded STF in the absence of multipaths.

Figure 4.5 shows the PEP performance for the proposed RRNS coded STF coding scheme under frequency flat Rayleigh fading with and without time correlation. The RRNS(8,6) code is used along with QPSK Alamouti's two transmit STBC, hence a code rate of $6/8$, $M_b=2$ and $t=1$ error correction capability. It can be seen that the independent fading channel (i.e. no time correlation) performs better than rapidly fading channel as expected. However, at relatively high mobility (reflected by a high normalized Doppler frequency $f_m=f_DT$) the PEP performance improves tremendously, becoming comparable to the independent fading channel. This is because for coherent reception, the multisampling receiver (i.e. $M_b>1$ per residue/subcarrier) benefits from the implicit time diversity of the fast fading channel. This is consistent with the literature [142].

Figure 4.6 shows the PEP performance for the proposed RRNS coded STF coding scheme under frequency selective Rayleigh fading. The RRNS(8,6) code is used along with QPSK Alomouti's two transmit STBC, hence a code rate of $6/8$, $M_b=2$ and $t=1$ error correction capability. It can be seen in Figure 4.6 that the PEP performance improves with increasing multipaths as expected.

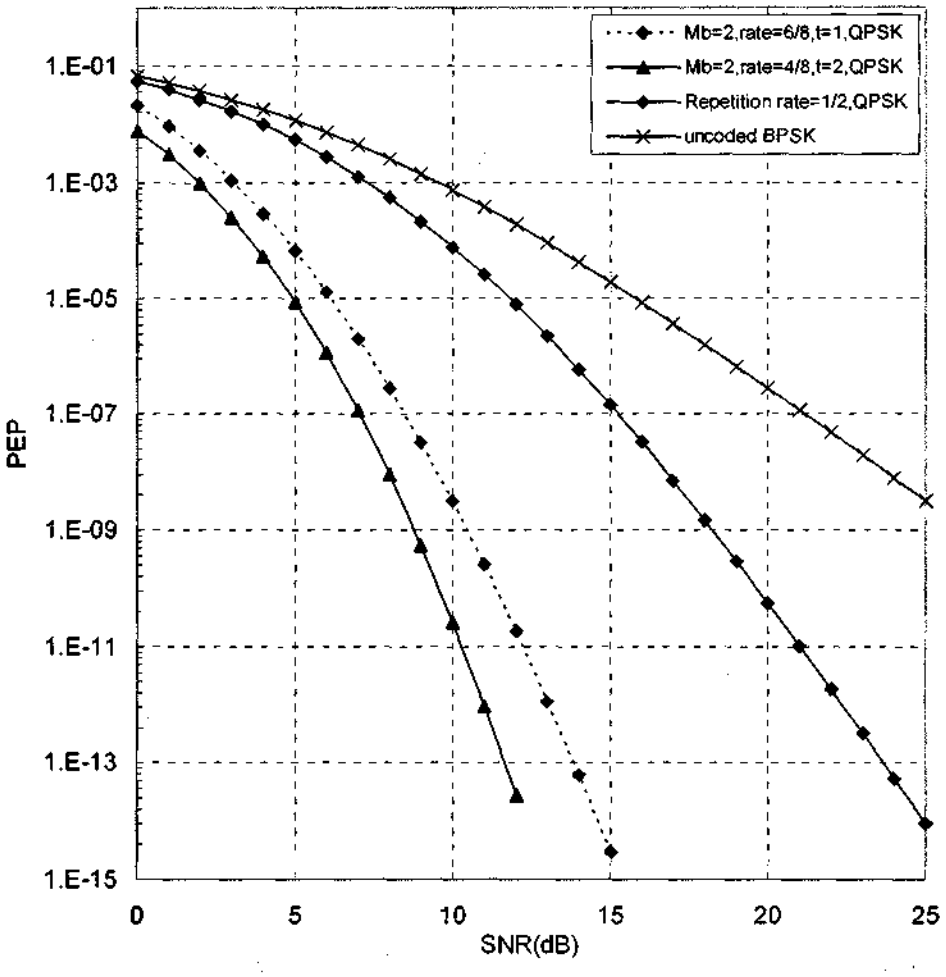

Figure 4.4: PEP performance comparison of the proposed RRNS coded with the uncoded and repetitive STF coding systems.

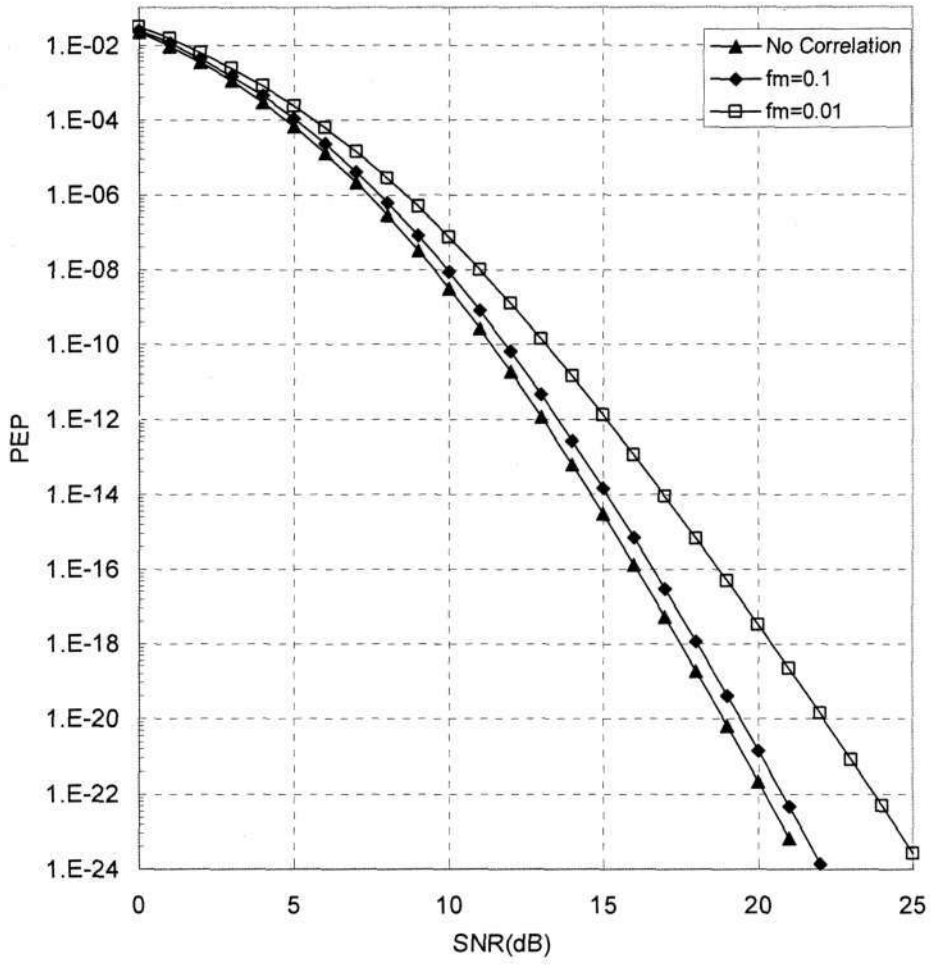

Figure 4.5: Numerical PEP performance for the proposed RRNS-STF coding scheme under a rapidly frequency flat fading channel with error correction capability t.

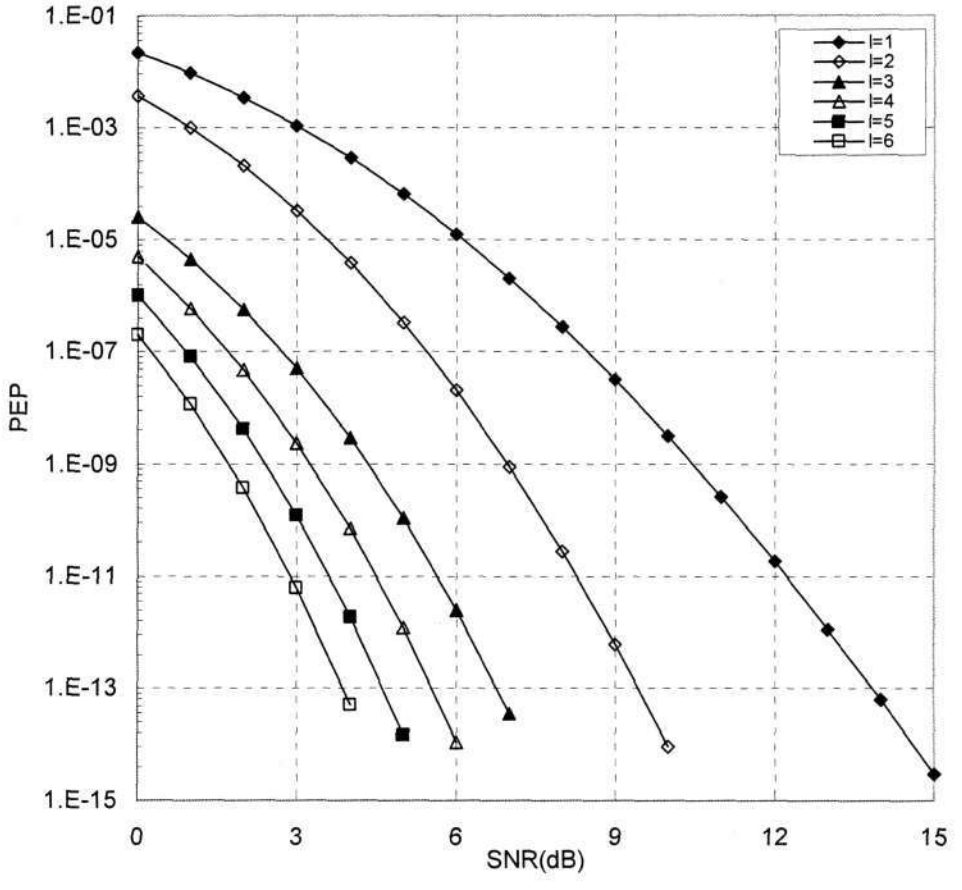

Figure 4.6: PEP performance of the proposed RRNS-STF coding scheme under frequency selective fading.

4.5 Conclusion

In this chapter, a RRNS based space-time-frequency coding scheme was proposed. The key feature of the proposed STF coding scheme is the frequency encoder. Most STF schemes in the literature use coding across multipaths and OFDM modulation techniques to maximize frequency diversity. The main challenge is the code construction involving a large number of OFDM carriers in a practical system. By dividing the available bandwidth into several non-overlapping subchannels equal to the code length, the proposed scheme codes across a number of subcarriers with space-time signalling on each subcarrier. Hence the signal design on each subcarrier is the same as that of space-time codes and can be easily extended to frequency selective fading.

The proposed space-time-frequency code design can achieve full rate and diversity gain of $M_t M_r M_b N_c$ over quasi-static fading channels. The diversity order incorporates the number of subcarriers (OFDM tones) previously not considered in the design of already existing space-time-frequency architecture. Hence the proposed STF coding scheme can achieve up to a maximum diversity gain of $M_t M_r M_b N_c L$.

CHAPTER 5

RRNS CODED DIFFERENTIAL STF CODING IN RAPID FADING CHANNELS

5.1 Introduction

The gain of multiple-input multiple-output orthogonal frequency division multiplexing (MIMO-OFDM) comes at the expense of increased receiver complexity. Furthermore, most of the proposed space-time-frequency coding schemes assume frequency selective block fading channels which is not an ideal assumption for broadband wireless communications. Relatively high mobility in broadband wireless communication systems may result in high Doppler frequency, hence time selective (rapid) fading. Rapidly changing channel characteristics impedes the channel estimation process and may result in incorrect estimates of the channel coefficients.

To circumvent the need for a tedious estimation process in wireless multiple-input multiple-output (MIMO) systems, we resort to noncoherent differential modulation (DM). However, conventional differential modulation (CDM) suffers a 3 dB penalty compared to coherent detection. Multi-symbol differential modulation (MSDM) for M-ary phase shift keying (MPSK) was proposed to improve the performance of CDM [64], [65], [67], [68]. MSDM was extended to space-time block codes (STBC) [122], [123], [124], [125]. In multi-symbol differential STBC, the complexity increases with increasing observation period i.e. $N > 2$ and the number of antennas. A less complex but suboptimal decision feedback differential modulation (DFDM) scheme was

proposed for a single antenna [69], [70], [71] and has been extended to STBC [126], [127], [128], [129], [130]. It was shown that increasing diversity can eliminate the flooring effect [127], [128]. However, to maximize the coding gain, low rate convolutional codes were used, hence reducing the overall rate of the system. In [84] and Chapter 2, redundant residue number system codes were used in place of convolutional codes and shown to achieve higher data rates with minimal complexity.

In this chapter, a redundant residue number system coded iterative noncoherent differential space-time-frequency (DSTF) modulation scheme is proposed. This is an extension of the work done in [84] from a single antenna to MIMO systems. To enhance the features of RNS codes, i.e. the mutual exclusive nature of residues, each parallel stream of residue is mapped onto a separate subcarrier per coding interval. Hence, the RNS code is used as a frequency encoder. By dividing the available bandwidth into several non-overlapping subchannels equal to the code length, the proposed scheme codes across a number of subcarriers with differential STBC signalling on each subcarrier. This has some similarities to subcarrier grouping proposed in [159] and [164], but differs in the code construction, frequency encoder and decoding strategy. Since the frequency encoder is independent of the space-time code (STC) design, the proposed DSTF scheme is easy to construct and is not limited to STBC (can be extended to space-time trellis codes). Bit-interleaving is employed on each subcarrier to break the error dependency of the channel and provide time diversity. Since the same information is transmitted over several residues/carriers, the proposed scheme offers frequency diversity irrespective of the frequency selective fading nature of the wideband channel. It is shown through analytical expressions and simulation results that the proposed scheme can maximize diversity gains over space, time and frequency domains.

In the second part of this chapter, a soft-input soft-output decision feedback differential modulation (SISO-DFDM) is proposed. This is an extension of the work that was done in [169] for multiple antennas. In these studies, iterative DFDM system feeding back only hard decisions was employed. It was noted that although there is an improvement in the differential demodulation process, not much coding gain was realized through iterative decoding. The system performance was mainly dependent on the number of test patterns. This is because in iterative DFDM, passing only hard decisions limits the advantages of iterative decoding. The DFDM decoding metric is modified to

incorporate both soft information and the hard decisions from the channel decoder (RRNS). Results show that significant coding gains can be achieved by passing soft information. The decoding process is not limited to the proposed scheme but can be used in any iterative DFDM system with a channel encoder e.g. convolutional codes. Note that for $N = 2$, the proposed system reduces to conventional iterative decoding, opposed to a single pass in the iterative DFDM system proposed in [127], [128].

The rest of this chapter is organized as follows, Section 5.2 presents the system model of the proposed differential STF coding scheme followed by the decision metric in Section 5.3. A hard decision iterative decoding process for differential STF coding is discussed in Section 5.4. The characterization and the performance of the proposed scheme is presented in Section 5.5, followed by the results for the hard decision differential STF coding in Section 5.6. A soft-input soft-output decision feedback differential STF coding is presented in Section 5.7 followed by its results in Section 5.8, and a conclusion is drawn in Section 5.9.

5.2 System Model

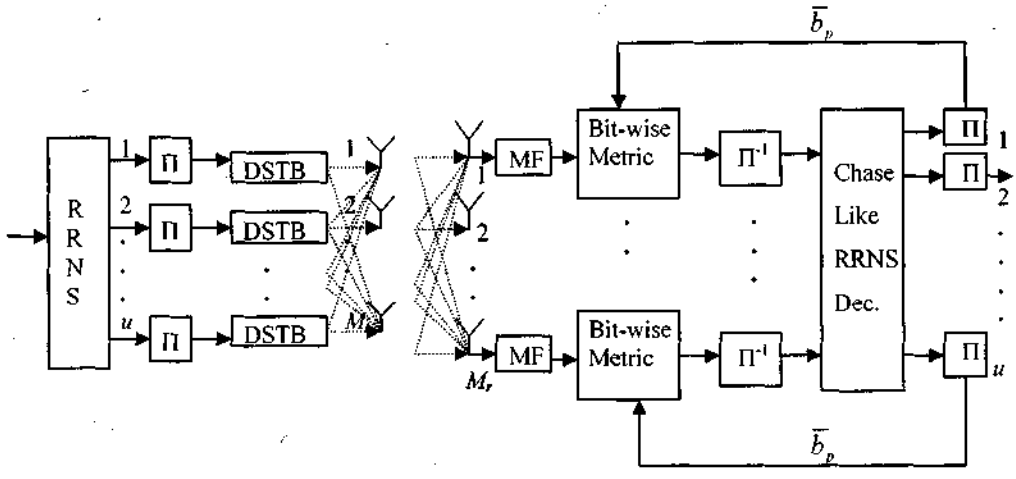

a) Transmitter b) Receiver

Figure 5.1: Transmitter and receiver block diagrams for RRNS coded differential space-time-frequency modulation.

Figure 5.1 depicts a baseband DSTF coding scheme with M_t transmit and M_r receive antennas. Figure 5.1(a) shows the block diagram of the transmitter section. A block of b information bits enter an outer RRNS(u,n) code per coding interval. The outer RRNS(u,n) code systematically encodes to a set of u parallel residues as described in Chapter 2. In systematic RRNS encoding, the information bits are grouped such that $b_i = \log_2 m_i$ and $b = \sum_{i=1}^{n} b_i$ for $i = 1, 2, \cdots, n$, are mapped to non-redundant residues and redundant residues are generated using the base extension (BEX) method. The redundant residues are each mapped to $b_i = \log_2 m_i + 1$ for $2^{b_i} > m_i$. The residues on each parallel stream for a given frame are converted to their binary equivalent and a zero bit appended on every b_i bits of the non-redundant residues in order to have the same number of bits on each parallel stream, hence a code rate of n/u. Each parallel stream is bit-interleaved and mapped to MPSK symbols that are fed to a differential STBC[1]. The output from each differential encoder is mapped to a separate subcarrier and transmitted over M_t antennas as shown in Figure 5.1(a). The differential code matrix on the uth subcarrier and the kth symbol matrix interval is given by

$$\mathbf{S}_u[k] = \mathbf{V}_u[k]\mathbf{S}_u[k-1], \tag{5.1}$$

where $\mathbf{V}_u[k]$ and $\mathbf{S}_u[k]$ are $M_t \times M_t$ unitary information and code matrix respectively such that $\mathbf{V}_u[k]\mathbf{V}_u^{\mathcal{H}}[k] = \mathbf{I}_{M_t}$ and $\mathbf{S}_u[k]\mathbf{S}_u^{\mathcal{H}}[k] = \mathbf{I}_{M_t}$. Superscript $\mathcal{H}$ denotes the transpose conjugate and $\mathbf{I}_{M_t}$ is an $M_t \times M_t$ identity matrix.

The received signal is passed through a bank of matched filters (MF) followed by a decision feedback differential STBC decoder based on bit metric computation as illustrated in Figure 5.1(b). The decoding process will be discussed in Section 5.3 and 5.4. The message matrix is obtained by multiplying the conjugate transpose of the previous code matrix,

$$\mathbf{V}_u[k] = \mathbf{S}_u[k]\mathbf{S}_u^{\mathcal{H}}[k-1] = \mathbf{V}_u[k]\mathbf{S}_u[k-1]\mathbf{S}_u^{\mathcal{H}}[k-1]. \tag{5.2}$$

---

[1] Space-time trellis codes can also be used in which case the differential process would be carried out on MPSK symbol.

The received signal on the uth subcarrier, vth receive and μth transmit antennas in the $\tilde{k} = M_t k + \mu$ symbol interval is

$$r_{u,v}[\tilde{k}] = \sum_{\mu=1}^{N_t} s_{u,\mu}[\tilde{k}] h_{u,\mu,v}[\tilde{k}] + n_{u,v}[\tilde{k}], \tag{5.3}$$

where $n_{u,v}[\tilde{k}]$ is the zero mean complex additive white Gaussian noise (AWGN) at the vth receive antenna with $N_0/2$ per dimension and $h_{u,\mu,v}[\tilde{k}]$ is the fading gain between transmit antenna μth and receive antenna vth on the uth subcarrier. Assuming the fading process remains constant over M_t consecutive symbol intervals and that there is no spatial or spectral correlation, the autocorrelation between two zero mean complex Gaussian random variables M_t symbols apart is [174]

$$\varphi_h(\tau) = E\left\{h_{u,v,\mu}[k] h^*_{u,v,\mu}[k + M_t]\right\} = \sigma_h^2 J_0\left(2M_t \pi f_D T\right), \tag{5.4}$$

where $E\{\cdot\}$ denotes the expectation, $*$ is the complex conjugate, $f_D T$ is the normalized Doppler frequency and σ_h^2 is the normalizing constant equal to unity. Equation (5.3) can be rewritten in matrix form as

$$\mathbf{R}_u[k] = \mathbf{S}_u[k]\mathbf{H}_u[k] + \mathbf{N}_u[k], \tag{5.5}$$

where the $M_t \times M_r$ matrices $\mathbf{R}_u[k]$ and $\mathbf{N}_u[k]$ are the receive and AWGN matrix respectively on the uth subcarrier during the kth symbol matrix interval. The continuous fading process $\mathbf{H}_u[k]$ is an $M_t \times M_r$ matrix. For MSDM, the observation interval consists of N block matrix symbols. Hence the received matrix per subcarrier $\mathbf{R}_{u,k}$ in the kth symbol interval defined as function of N is

$$\mathbf{R}_{u,k} = \mathbf{S}_{u,k}\mathbf{H}_{u,k} + \mathbf{N}_{u,k}, \tag{5.6}$$

where

$$
\begin{aligned}
\mathbf{R}_{u,k} &= \left[\mathbf{R}_u[k]\mathbf{R}_u[k-1]\cdots\mathbf{R}_u[k-N+1]\right]^T, \\
\mathbf{H}_{u,k} &= \left[\mathbf{H}_u[k]\mathbf{H}_u[k-1]\cdots\mathbf{H}_u[k-N+1]\right]^T, \\
\mathbf{N}_{u,k} &= \left[\mathbf{N}_u[k]\mathbf{N}_u[k-1]\cdots\mathbf{N}_u[k-N+1]\right]^T, \\
\mathbf{S}_{u,k} &= diag\{\mathbf{S}_u[k],\mathbf{S}_u[k-1],\cdots,\mathbf{S}_u[k-N+1]\}.
\end{aligned}
\tag{5.7}
$$

5.3 Decision Metric

Starting from the MSDM stated in [124] we adjust the equations to reflect the frequency term. The received vector matrix on the uth subcarrier $\mathbf{R}_{u,k}$ conditioned on the transmitted vector matrix $\mathbf{V}_{u,k} = \mathbf{V}_u[k]\mathbf{V}_u[k-1]...\mathbf{V}_u[k-N+2]$ is a complex-valued zero mean multivariate Gaussian random matrix with a probability density function (pdf) given by

$$
P(\mathbf{R}_{u,k} / \mathbf{V}_{u,k}) = \frac{\exp\left\{-tr(\mathbf{R}_{u,k}^{\mathcal{H}}\mathbf{\Lambda}_{u,k}^{-1}\mathbf{R}_{u,k})\right\}}{\pi^{M_t N}\left|\mathbf{\Lambda}_{u,k}\right|^{M_r}},
\tag{5.8}
$$

where $|\bullet|$ and $tr(\bullet)$ denotes the determinant and the trace of a matrix respectively, $\mathbf{\Lambda}_{u,k}$ is the conditional covariance matrix defined as $\mathbf{\Lambda}_{u,k} = E\{\mathbf{R}_{u,k}\mathbf{R}_{u,k}^{\mathcal{H}} / \mathbf{V}_{u,k}\}$. Assuming continuous flat fading, $\mathbf{\Lambda}_{u,k}$ can be expressed in terms of the fading correlation and AWGN as

$$
\begin{aligned}
\Lambda_{u,k} &= E\left\{\left(\mathbf{S}_{u,k}\mathbf{H}_{u,k} + \mathbf{N}_{u,k}\right)\left(\mathbf{S}_{u,k}\mathbf{H}_{u,k} + \mathbf{N}_{u,k}\right)^{\mathcal{H}}\right\} \\
&= M_r\left(\mathbf{S}_{u,k}\mathbf{\Gamma}_h^{u,k}\mathbf{S}_{u,k}^{\mathcal{H}} + N_0\mathbf{I}_{NM_t}\right)
\end{aligned}
\tag{5.9}
$$

where $\mathbf{\Gamma}_h^{u,k}$ is the fading correlation matrix whose coefficients are given by (5.4) and can be expressed as

$$
\begin{aligned}
\mathbf{\Gamma}_h^{u,k} &= \begin{bmatrix}
\varphi_h[0] & \varphi_h[M_t] & \cdots & \varphi_h[M_t(N-1)] \\
\varphi_h[-M_t] & \varphi_h[0] & \vdots & \varphi_h[M_t(N-2)] \\
\vdots & \vdots & \ddots & \vdots \\
\varphi_h[-M_t(N-1)] & \varphi_h[-M_t(N-2)] & \cdots & \varphi_h[0]
\end{bmatrix} \otimes \mathbf{I}_{M_t} \\
&= \bar{\mathbf{\Gamma}}_h \otimes \mathbf{I}_{M_t},
\end{aligned}
\tag{5.10}
$$

where $\otimes$ denotes the Kronecker product. Given the unitary and orthogonallity properties of $\mathbf{S}_{u,k}$ the covariance matrix in (5.9) can be expressed as

$$\Lambda_{u,k} = M_r \left\{ \mathbf{S}_{u,k} \left(\mathbf{\Gamma}_h^{u,k} + N_0 \mathbf{I}_{NM_r} \right) \mathbf{S}_{u,k}^{\mathcal{H}} \right\}, \tag{5.11}$$

and is independent of the transmitted message sequence. It is assumed that the carriers are adequately spaced and independent of each other. A uniform power profile is also assumed among the subcarriers. Hence the u and k subscripts on $\Lambda_{u,k}$ and superscripts on $\mathbf{\Gamma}_h^{u,k}$ can be dropped, i.e. $\Lambda_{u,k} = \Lambda$ and $\mathbf{\Gamma}_h^{u,k} = \mathbf{\Gamma}_h$. Using the rules of the Kronecker product [177] and applying the orthogonallity property of $\mathbf{S}_{u,k}$, the inverse of the correlation matrix Λ in (5.11) can then be calculated as follows,

$$\begin{aligned} \Lambda^{-1} &= \frac{1}{M_r} \left\{ \mathbf{S}_{u,k} \left(\left(\tilde{\mathbf{\Gamma}}_h + N_0 \mathbf{I}_N \right) \otimes \mathbf{I}_{M_r} \right)^{-1} \mathbf{S}_{u,k}^{\mathcal{H}} \right\} \\ &= \frac{1}{M_r} \left\{ \mathbf{S}_{u,k} \left(\left(\tilde{\mathbf{\Gamma}}_h + N_0 \mathbf{I}_N \right)^{-1} \otimes \mathbf{I}_{M_r} \right) \mathbf{S}_{u,k}^{\mathcal{H}} \right\} \\ &= \frac{1}{M_r} \left\{ \mathbf{S}_{u,k} \left(\mathbf{T} \otimes \mathbf{I}_{M_r} \right) \mathbf{S}_{u,k}^{\mathcal{H}} \right\}, \end{aligned} \tag{5.12}$$

Where $\tilde{\mathbf{\Gamma}}_h$ is defined in (5.10) and

$$\mathbf{T} = \left(\tilde{\mathbf{\Gamma}}_h + N_0 \mathbf{I}_N \right)^{-1} = \begin{bmatrix} t_{00} & t_{01} & \cdots & t_{0N-1} \\ t_{10} & t_{11} & \cdots & t_{1N-1} \\ \vdots & \vdots & \ddots & \vdots \\ t_{N-10} & t_{N-11} & \cdots & t_{N-1N-1} \end{bmatrix}. \tag{5.13}$$

Substituting (5.12) in (5.8), expanding the exponential term and ignoring constant terms, the conditional pdf can be rewritten as

$$P(\mathbf{R}_{u,k} / \mathbf{V}_{u,k}) = \exp\left[\mathrm{Re}\left\{ tr\left(\sum_{i=1}^{N-1} \sum_{j=0}^{N-1} t_{ij} \mathbf{R}_u^{\mathcal{H}}[k-i] \mathbf{S}_u[k-i] \mathbf{S}_u^{\mathcal{H}}[k-j] \mathbf{R}_u[k-j] \right) \right\} \right], \tag{5.14}$$

where t_{ij} are elements of the inverse of the correlation matrix defined in (5.13). Expanding (5.14) further, the pdf can be written as

$$P(\mathbf{R}_{u,k}/\mathbf{V}_{u,k}) = \exp\left[\operatorname{Re}\left\{tr\left(\sum_{i=0}^{N-1} t_{ii}\mathbf{R}_u^{\mathcal{H}}[k-i]\mathbf{S}_u[k-i]\mathbf{S}_u^{\mathcal{H}}[k-i]\mathbf{R}_u[k-i]\right)\right\}\right.$$
$$\left. +2\operatorname{Re}\left\{tr\left(\sum_{i=1}^{N-1}\sum_{j=0}^{i-1} t_{ij}\mathbf{R}_u^{\mathcal{H}}[k-i]\mathbf{S}_u[k-i]\mathbf{S}_u^{\mathcal{H}}[k-j]\mathbf{R}_u[k-j]\right)\right\}\right] \quad (5.15)$$

Note that the first term in (5.15) is a constant and independent of the transmitted sequence, hence the pdf reduces to

$$P(\mathbf{R}_{u,k}/\mathbf{V}_{u,k}) \approx \exp\left[2\operatorname{Re}\left\{tr\left(\sum_{i=1}^{N-1}\sum_{j=0}^{i-1} t_{ij}\mathbf{R}_u^{\mathcal{H}}[k-i]\mathbf{S}_u[k-i]\mathbf{S}_u^{\mathcal{H}}[k-j]\mathbf{R}_u[k-j]\right)\right\}\right]. \quad (5.16)$$

Applying the unitary property and replacing $\mathbf{S}_u[k-i]\mathbf{S}_u^{\mathcal{H}}[k-j]$ as in (5.2), the pdf in (5.16) can be rewritten as

$$P(\mathbf{R}_{u,k}/\mathbf{V}_{u,k}) \approx \exp\left[2\operatorname{Re}\left\{tr\left(\sum_{i=1}^{N-1}\sum_{j=0}^{i-1} t_{ij}\mathbf{R}_u^{\mathcal{H}}[k-i]\mathbf{R}_u[k-j]\prod_{l=j}^{i-1}\mathbf{V}_u[k-l]\right)\right\}\right]. \quad (5.17)$$

As in [127], [128], the decision feedback differential pdf on each subcarrier conditioned on the candidate symbol $\mathbf{V}_u[k]$ (not on the entire N observation symbols) is derived from (5.17) by feeding back $N-1$ past decision i.e. $\{\mathbf{V}_u[k-l]\}$, with previously detected symbols $\{\tilde{\mathbf{V}}_u[k-l]\}$ except for the kth matrix symbol. Hence the DFDM pdf conditioned on the candidate symbol on the uth subcarrier is given by

$$P(\mathbf{R}_{u,k}/\mathbf{V}_u[k]) \approx \exp\left[2\operatorname{Re}\left\{tr\left(\mathbf{R}_u^{\mathcal{H}}[k]\mathbf{V}_u[k]\sum_{i=1}^{N-1} t_{0i}\mathbf{R}_u[k-i]\prod_{j=1}^{i-1}\tilde{\mathbf{V}}_u[k-j]\right)\right\}\right], \quad (5.18)$$

where $\tilde{\mathbf{V}}_u[k-j]$ are the hard decision matrix symbols from previous detection. The bit metric for the kth matrix symbol interval can be calculated from (5.18) by averaging over the STBC constellation whose symbol metrics have $b \in \{0,1\}$ in the ρth bit position as

$$\lambda_b^{u,k}[\rho] = \log \sum_{\mathbf{V}_{u,k} \in \mathcal{A}_b^{\rho}} P(\mathbf{R}_{u,k}/\mathbf{V}_u[k]). \quad (5.19)$$

Thus the bit log-likelihood-ratio (LLR) metric for the kth STBC label in the ρth bit position and uth subcarrier is given by

$$\tilde{\lambda}_{\rho}^{u,k} = \lambda_{0}^{u,k}[\rho] - \lambda_{1}^{u,k}[\rho]. \tag{5.20}$$

5.4 Hard Decision Iterative Decision Feedback Differential STFC

The iterative decoding process for the hard decision Chase like RRNS decoder in this differential STF coding scheme follows that described in Section 2.4.3 except for the emphasis on the parallel structure. The decision feedback differential metric is also calculated based on differential STBC matrix.

For every decoding interval, the soft information generated according to (5.20) is sent to a Chase like RRNS decoder. Through the use of the Chase algorithm as described in Section 2.4.3, a codeword is then decoded as the transmitted message bits for a given frame. The decoded codeword is mapped to non-redundant residues and redundant residues are generated based on BEX methods. The residues are then converted to their binary equivalent and bit-interleaving carried on each parallel stream. After bit-interleaving, the bits on each parallel stream are mapped to MPSK symbols, differentially coded by STBC and fed back to the DFDM decoder for a new metric computation as shown in Figure 5.1(b). The entire process is repeated for the desired number of iterations before making the final decision on the possible transmitted codeword.

For the first iteration, there are no previous decisions available and conventional differential modulation is used as in [127], [128]. For further iterations, re-modulated fed back matrix symbols from previous iterations are used to calculate the bit LLR values for $N > 2$ observation periods as described in equations (5.18), (5.19), and (5.20).

5.5 Performance Analysis

Since the logarithmic function is monotonically increasing, maximizing $P(\mathbf{R}_{u,k} / \mathbf{V}_u[k])$ over $\mathbf{V}_u[k]$ in (5.18) is equivalent to maximizing $\log\left(P(\mathbf{R}_{u,k} / \mathbf{V}_u[k])\right)$ over $\mathbf{V}_u[k]$.

Hence the decision metric $\hat{V}$ for detecting $\mathbf{V}_u[k]$ is obtained by maximizing (5.18) over a STBC signal constellation A,

$$\hat{V} = \max_{\mathbf{V}_u[k]\in A} \mathrm{Re}\left\{ tr\left[\mathbf{R}_u^{\mathcal{H}}[k]\mathbf{V}_u[k]\sum_{i=1}^{N-1} t_{0i}\mathbf{R}_u[k-i]\prod_{j=1}^{i-1}\tilde{\mathbf{V}}_u[k-j]\right]\right\}. \tag{5.21}$$

Assuming independent subcarrier, genie-aided feedback, the pairwise error probability (PEP) of detecting $\tilde{\mathbf{V}}_u[k]$ given that $\mathbf{V}_u[k]$ was transmitted is

$$P\left(\mathbf{V}_u[k], \tilde{\mathbf{V}}_u[k]\right) = P\left(\mathrm{Re}\, tr\left\{\mathbf{X}_{u,k}\left(\mathbf{V}_u[k]-\tilde{\mathbf{V}}_u[k]\right)\mathbf{Y}_{u,k}\right\}\right) \tag{5.22}$$

where

$$\begin{aligned}
&\mathbf{X}_{u,k} = \mathbf{H}_u[k] + \mathbf{S}_u^{\mathcal{H}}[k]\mathbf{N}_u[k],\\
&\mathbf{Y}_{u,k} = \sum_{i=1}^{N-1} t_{0i}\left(\mathbf{H}_u[k-i] + \mathbf{S}_u^{\mathcal{H}}[k-i]\mathbf{N}_u[k-i]\right),\\
&\mathbf{X}_{u,k} = \left[x_{0,0}^u x_{1,0}^u \cdots x_{M_t-1,0}^u \cdots x_{M_t-1,M_r-1}^u\right]^T,\\
&\mathbf{Y}_{u,k} = \left[y_{0,0}^u y_{1,0}^u \cdots y_{N_t-1,0}^u \cdots y_{M_t-1,M_r-1}^u\right]^T,\\
&x_{v,\mu}^u = h_{u,\mu,v}[M_t k] + s_{u,v}[M_t k]n_{u,\mu}[M_t k],\\
&y_{v,\mu}^u = \sum_{i=1}^{N-1} t_{0,i}\left(h_{u,\mu,v}[M_t(k-i)] + s_{u,v}[M_t(k-i)]n_{u,\mu}[M_t(k-i)]\right).
\end{aligned} \tag{5.23}$$

Let $\mathbf{g}_{u,k} = \left[\mathbf{X}_{u,k}^T \mathbf{Y}_{u,k}^T\right]^T$ be a vector matrix of two zero mean Gaussian random variables on the uth subcarrier and the kth symbol matrix defined in (5.22). The PEP in Hermitian Gaussian quadratic form for the uth subcarrier (or residue) spanning K symbol matrices per residue can be expressed as [39], [129], [130]

$$P\left(\mathbf{V}_u, \tilde{\mathbf{V}}_u\right) = P\left(\mathrm{Re}\left[tr\left\{\mathbf{G}_u^{\mathcal{H}}\mathbf{L}_u\mathbf{G}_u\right\}\right]\right), \tag{5.24}$$

such that $\mathbf{G}_u = \left[\mathbf{g}_{u,1}, \mathbf{g}_{u,2}, \cdots, \mathbf{g}_{u,K}\right]^T$,

$$\mathbf{L}_u = \begin{bmatrix} \mathbf{O}_K & \mathbf{I}_K\mathbf{C}_u^{\mathcal{H}} \\ \mathbf{I}_K\mathbf{C}_u & \mathbf{O}_K \end{bmatrix}, \tag{5.25}$$

where $\mathbf{O}_K$ is a $K \times K$ zero matrix, $\mathbf{C}_u = [\mathbf{C}_{u,1}\mathbf{C}_{u,2}\cdots\mathbf{C}_{u,K}]^T$ whose elements are defined as $\mathbf{C}_{u,k} = \mathbf{I}_{M_r} \otimes \left(\mathbf{V}_u[k] - \bar{\mathbf{V}}_u[k]\right)$. Through eigendecomposition, the characteristic function can be expressed as [128]

$$\Phi_{(\mathbf{V}_u,\bar{\mathbf{V}}_u)}(s) = E\left\{\exp\left(G_u^{\mathcal{H}}\mathbf{L}_u G_u\right)\right\} = \frac{1}{\det\left(\mathbf{I}_{2M_rM_tK} + s\boldsymbol{\Phi}_u\mathbf{L}_u\right)}, \tag{5.26}$$

where the correlation matrix $\boldsymbol{\Phi}_u = E\left\{\mathbf{G}_u^{\mathcal{H}}\mathbf{G}_u\right\}$ is defined as

$$\boldsymbol{\Phi}_u = \begin{bmatrix} \zeta_{0,0}(u) & \zeta_{0,1}(u) & \cdots & \zeta_{0,K-1}(u) \\ \zeta_{1,0}(u) & \zeta_{1,1}(u) & \cdots & \zeta_{1,K-1}(u) \\ \vdots & \vdots & \ddots & \vdots \\ \zeta_{K-1,0}(u) & \zeta_{K-1,1}(u) & \cdots & \zeta_{K-1,K-1}(u) \end{bmatrix} \otimes \mathbf{I}_{M_r}, \tag{5.27}$$

for

$$\zeta_{i,j}(u) = E\left\{g_{u,i}g_{u,j}\right\} = \begin{bmatrix} E\{\mathbf{X}_{u,i}\mathbf{X}_{u,j}\} & E\{\mathbf{X}_{u,i}\mathbf{Y}_{u,j}\} \\ E\{\mathbf{Y}_{u,i}\mathbf{X}_{u,j}\} & E\{\mathbf{Y}_{u,i}\mathbf{Y}_{u,j}\} \end{bmatrix}. \tag{5.28}$$

Note that for perfect channel state information, the coefficients in (5.28) of the correlation matrix in (5.27) reduce to

$$\zeta_{i,j}(u) = E\left\{g_{u,i}g_{u,j}\right\} = \begin{bmatrix} E\{\mathbf{X}_{u,i}\mathbf{X}_{u,j}\} & 0 \\ 0 & 0 \end{bmatrix} = E\{\mathbf{X}_{u,i}\mathbf{X}_{u,j}\}. \tag{5.29}$$

The pdf of a function can be calculated from its characteristic function as [39]

$$f(x) = \frac{1}{2\pi}\int_{-\infty}^{\infty}\Phi_x(s)\exp(-sx)ds. \tag{5.30}$$

Thus the PEP in (5.24) can be directly calculated from its characteristic function in (5.26) and expressed in terms of eigenvalues $\chi_{u\mu}^k$ as

$$P(\mathbf{V}_u,\bar{\mathbf{V}}_u) = \frac{1}{2\pi}\int_{-\infty}^{\infty}\int_{0}^{\infty}e^{-s(\mathbf{V}_u,\bar{\mathbf{V}}_u)}d(\mathbf{V}_u,\bar{\mathbf{V}}_u)\prod_{k=1}^{2K}\prod_{\mu=1}^{M_r}\left(1+s\chi_{u\mu}^k\right)^{-M_r}ds. \tag{5.31}$$

But

$$\int_0^{\infty} e^{-s(\mathbf{V}_u,\bar{\mathbf{V}}_u)} d(\mathbf{V}_u,\bar{\mathbf{V}}_u) = -\frac{1}{s}, \tag{5.32}$$

Hence the PEP in (5.31) reduces to

$$P(\mathbf{V}_u,\bar{\mathbf{V}}_u) = \frac{-1}{2\pi}\int_{-\infty}^{\infty} s^{-1}\left(\prod_{k=1}^{2K}\prod_{\mu=1}^{M_t}\left(1+s\chi_{u\mu}^{k}\right)^{-M_r}\right)ds. \tag{5.33}$$

Letting $s = c + jw$ and extracting the real part, the integral in (5.33) can be rewritten as

$$P(\mathbf{V}_u,\bar{\mathbf{V}}_u) = \frac{c}{2\pi}\int_{c-j\infty}^{c+j\infty}\frac{1}{c^2+\omega^2}\prod_{k=1}^{2K}\prod_{\mu=1}^{M_t}\left(1+(c^2+\omega^2)\chi_{u\mu}^{k}\right)^{-M_r}d\omega. \tag{5.34}$$

A closed form expression for PEP is obtained by solving the one dimensional integral in (5.34) using numerical integration methods such as the Gauss-Chebyshev quadrature along the region of convergence [172], [107], [104], [108], [109], [110], [111], [112]. Let $\omega = c\tan(\theta)$, then (5.34) can be expressed as

$$P(\mathbf{V}_u,\bar{\mathbf{V}}_u) = \frac{1}{\pi}\int_0^{\pi/2}\prod_{k=1}^{2K}\prod_{\mu=1}^{M_t}\left(1+c^2\sec^2(\theta)\chi_{u\mu}^{k}\right)^{-M_r}d\theta. \tag{5.35}$$

An upper bound on PEP can be obtained from (5.35) by setting $\theta = \pi/2$ [103]. Note that if M_t and M_r are kept constant, the correlation matrix $\mathbf{\Phi}_u$ in (5.27) is independent of u but dependent on K symbol matrices. Since the same information is transmitted over several subcarriers, RNS coding offers frequency diversity, independent of the frequency selective nature of the fading channels. Without error correction, assuming equal egeinvalues from carrier to carrier which is often the case when signal matrices are drawn from orthogonal design, the total PEP (probability of symbol error P_s) is given by

$$P_s = \frac{1}{\pi}\int_0^{\pi/2}\prod_{k=1}^{2K}\prod_{\mu=1}^{M_t}\left(1+c^2\sec^2(\theta)\chi_{u\mu}^{k}\right)^{-M_rU}d\theta, \tag{5.36}$$

where U is the total number of residues/subcarriers. It can be seen from (5.36) that the total PEP is maximized by increasing K and u. Maximizing u maximizes the inherent frequency diversity of the RNS codes while K maximizes the product of the eigenvalues

linked to the code length of the STC code, a design criteria for STC in fast fading channels [86]. Alternatively K can be seen as the temporal component in STF [159]. Introducing redundancy across subcarriers limits the frequency diversity to the Hamming distance ($d_{\min}$) in the proposed DSTF coding scheme. It is well known that under certain conditions STBC guarantees M_t transmit diversity [89], [90], [88], hence the proposed scheme can achieve a maximum diversity order of KM_tM_rU (derived in Chapter 4). For K = 1, U = 1, the proposed DSTF signal model reduces to differential STBC, similar to [128]. The advantage of using this scheme is that the frequency encoder is independent of the STC design hence maximizing frequency and space diversity independently. The frequency encoder is concatenated through a bit-interleaver to a STC code and iterative decoding is used to maximize the time diversity.

It was shown in [53] that the performance of generalized minimum distance decoding is dominated by errors at the algebraic decoding stage. Assuming ideal bit-interleaving and independent subcarriers with a uniform power profile, the maximum likelihood upper bound on the BER (P_b) for RRNS code is obtained in a similar manner to that of a Reed Solomon code [38], [39], [27], [28] as

$$P_b \le \frac{2^{mK-1}}{U(2^{mK}-1)} \sum_{u=t+1}^{U} u \binom{U}{u} P_{de}^{u}, \tag{5.37}$$

where t is the error correction capability of the RRNS code, U is the total number of residues, mK is the number of bits per residue and P_{de}^{u} is the probability that the received residue sequence has u erroneous residues, given by [39]

$$P_{de}^{u} = \left(1 - P(\mathbf{V}_u, \bar{\mathbf{V}}_u)\right)^{U-u} \left(P(\mathbf{V}_u, \bar{\mathbf{V}}_u)\right)^{u}. \tag{5.38}$$

5.6 Results for Hard Decision Iterative differential STFC

In this section simulation and numerical results for the proposed hard decision iterative differential STF coding are presented and discussed. The simulation model is as shown in Figure 5.1. A random interlevear is applied on each subcarier and bits mapped to QPSK symbols using Gray labelling. The differential encoder on each subcarrier

follows the Alamouti $M_t = 2$ and $M_r = 1$ signal model [88]. Thus the received matrix in is given by [115]

$$R_u[k] = \begin{bmatrix} r_u[2k] \\ r_u[2k+1] \end{bmatrix} = \begin{bmatrix} s_u[2k] & s_u[2k+1] \\ s_u^*[2k+1] & s_u^*[2k] \end{bmatrix} \begin{bmatrix} h_u[2k] \\ h_u[2k+1] \end{bmatrix} + \begin{bmatrix} n_u[2k] \\ n_u[2k+1] \end{bmatrix}, \quad (5.39)$$

where all the elements of the matrices are defined in (5.3). The differential code matrix $\mathbf{S}_u[k]$ is defined as in (5.1). The information matrix $\mathbf{V}_u[k]$ and the initial differential code matrix $\mathbf{S}_u[0]$ are defined as

$$\mathbf{S}_u[0] = \begin{bmatrix} 1/\sqrt{2} & 1/\sqrt{2} \\ -1/\sqrt{2} & 1/\sqrt{2} \end{bmatrix}, \quad \mathbf{V}_u[k] = \begin{bmatrix} a_{2k} & a_{2k+1} \\ -a_{2k+1}^* & a_{2k}^* \end{bmatrix},$$

where

$$a \in A = \left\{ \frac{e^{j2\pi m/M}}{\sqrt{2}}, m = 0, 1, \cdots, M-1 \right\}.$$

Time correlated flat fading Rayleigh coefficients are generated based on Jake's model [174] for a normalized Doppler frequency $f_D T = 0.02$. Systematic RRNS coding is used for all simulations and a zero bit appended on each non-redundant residue equivalent bits. Moduli $m_1 = 229$, $m_2 = 233$, $m_3 = 239$, $m_4 = 241$, $m_5 = 247$, $m_6 = 251$, $m_7 = 253$, $m_8 = 255$ are taken from [33]. Since the RRNS code has 8 moduli, the 8 parallel residue streams for DSTF were mapped to 8 subcarriers. The numerical BER is computed from (5.37).

Figure 5.2 shows numerical and simulated BER performance for DFDM with $N = 5$ observation periods, two iterations, $m_1, m_2, m_3, m_4, m_5, m_6$ non-redundant and m_7, m_8 redundant moduli. Hence RRNS(8,6) code rate of $3/4$, error capability $t = 1$ and minimum distance $d_{\min} = 3$. It can be seen that increasing the test patterns from 2^0 to 2^{10} improves the performance of the Chase like RRNS decoder bringing the simulation in close proximity with the upper bound on the BER. This is due to increasing number of valid codewords, which increases with increasing the number of test patterns. This leads to increased coding gain hence the BER performance improvement. However,

increasing the number of test patterns amounts to increasing the Hamming distance between the received codeword and error patterns. This leads to increased Hamming weight, hence poorer BER performance at low SNR observed with increasing test pattern. Note that although iterative decoding is used, hard decisions are fed back to the decision feedback differential STBC metric computer. Hence the BER performance is predominantiy limited by the number of test patterns. To achieve comparable simulation results to the analysis, many test patterns are used. Even then, there's still a discrepancy mainly due to the suboptimal nature of the DFDM decoding process compared to the maximum likelihood analytical bound.

Figure 5.3 shows numerical BER performance for the DSTF coding for CDM (i.e. $N=2$) with K varying symbol matrices per residue, varying rate and t. Since QPSK mapping was used for the two transmit antenna Alamouti scheme, the number of bits per residue is $4K$. It can be seen that for a fixed error correction capability $t=1$, increasing K improves the BER performance. The information per residue is spread over K symbol matrices during the STBC signal processing. This is equivalent to increasing the effective code length hence maximizing the product gain for STF on each subcarrier. It can be seen that the curve for RRNS(12,10) code is steeper than that of RRNS(8,6) which in turn is steeper than that of RRNS(4,2) code. This is because increasing the number of parallel paths (subcarriers) increases the inherent repetitive nature of RNS codes, hence increasing frequency diversity. As can be seen from the above mentioned curves, this leads to superior BER performance at high SNR and is consistent with the results in [33]. It can also be seen from Figure 5.3 that BER performance improves tremendously with increasing K and t for a fixed rate of $1/2$. This is due to a combination of increasing product gain (K), parallel paths (U) and error correction capability t, hence maximizing the time and frequency diversities for a given fixed number of transmit antennas. The increasing coding gains play a predominant part as is reflected by shift in the curves.

Figure 5.4 shows the numerical BER performance of the proposed scheme with increasing observation N. It can be seen that the BER performance improves with increasing observation as expected, reducing the performance gap between coherent and CDM. However there is no significant performance improvement from $N=5$ to $N=10$. This is mainly due to the suboptimal nature of DFDM decoding process.

Figure 5.5 shows the simulated BER performance for the proposed DSTF, differential QPSK and differential STBC with $N = 2$ observations. The test patterns are set to 2^4 and a RRNS(8,6) channel encoder used in all the threes systems, hence a rate of $3/4$. The simulation model for a single antenna differential QPSK follows [84] and differential STBC is similar to DSTF except that all the residues are serially transmitted on a single carrier. For $N > 2$ symbol observations, the number of iteration is set to 2. It can be seen from Figure 5.5 that the BER performance improves not only with increasing observations N but also with increasing number of transmit antenna M_t as expected. However, the performance for DSTF scheme improves more rapidly than that of differential STBC. This is due to parallel transmission of residues which enhances their mutual exclusive property. Serially transmitted bit-interleaved differential STBC modulation spreads errors across parallel residues (per coding interval) in contrast to bit-interleaving carried out on each independent parallel stream in the proposed DSTF. This destroys the mutually exclusive property of residues in fading channels resulting in poorer BER performance of differential STBC than the proposed DSTF.

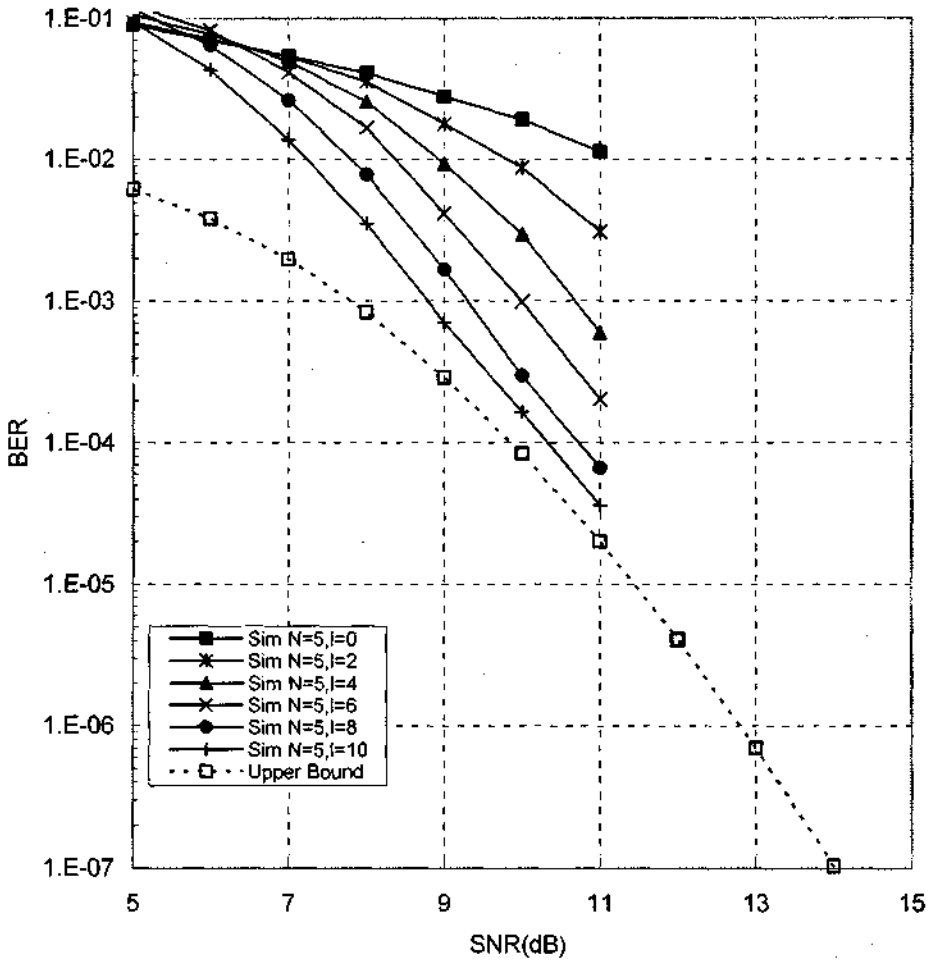

Figure 5.2: Simulated and numerical BER performance for decision feedback differential modulation with $N = 5$, two iterations.

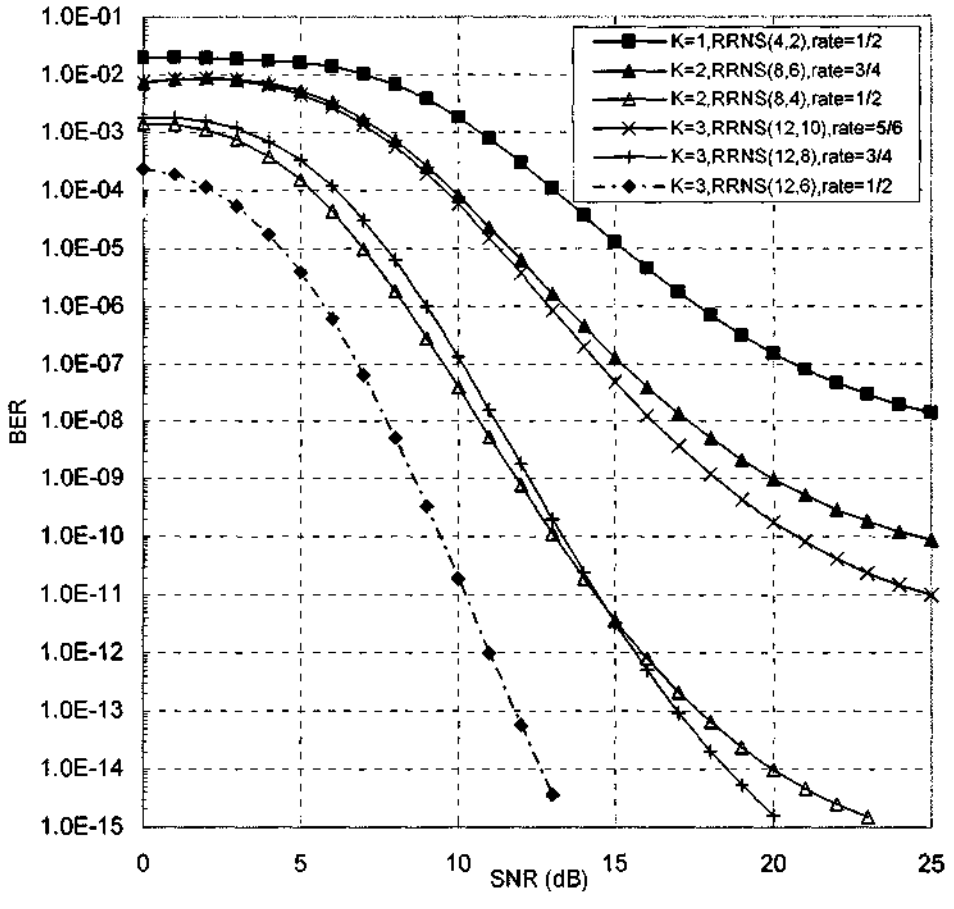

Figure 5.3: Numerical BER performance for the conventional differential STF coding i.e. $N = 2$ with varying symbol matrices per residue, rate and error correction capability t.

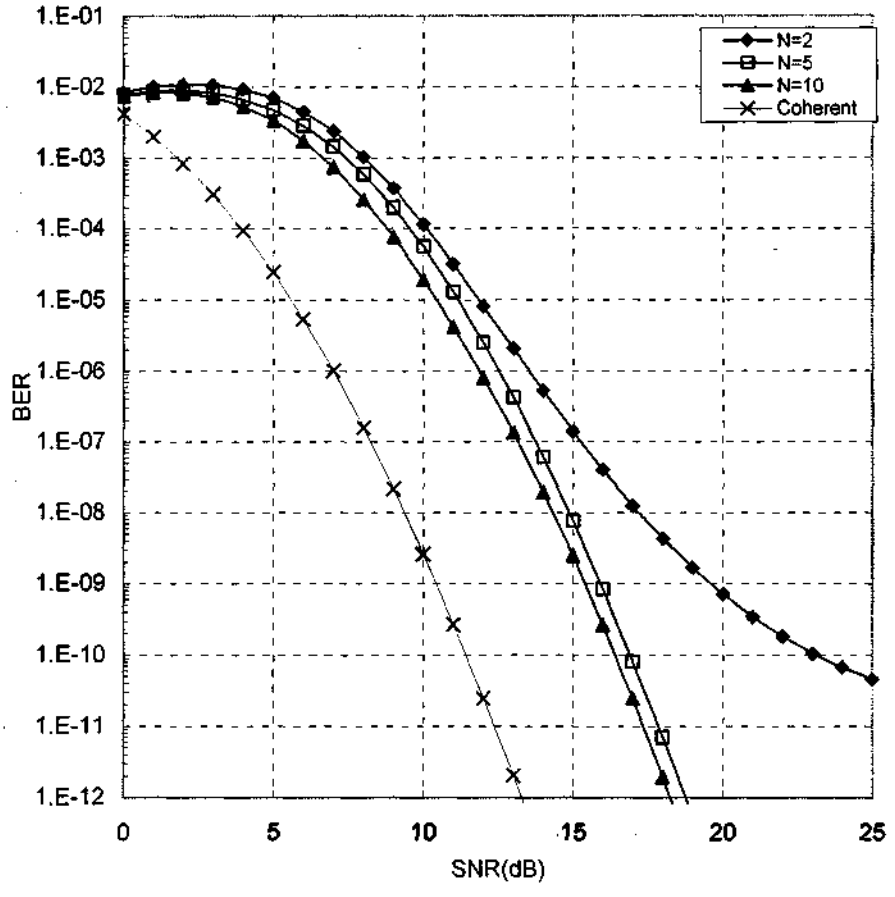

Figure 5.4: Analytical BER performance for the proposed decision feedback differential STF coding with increasing observations N.

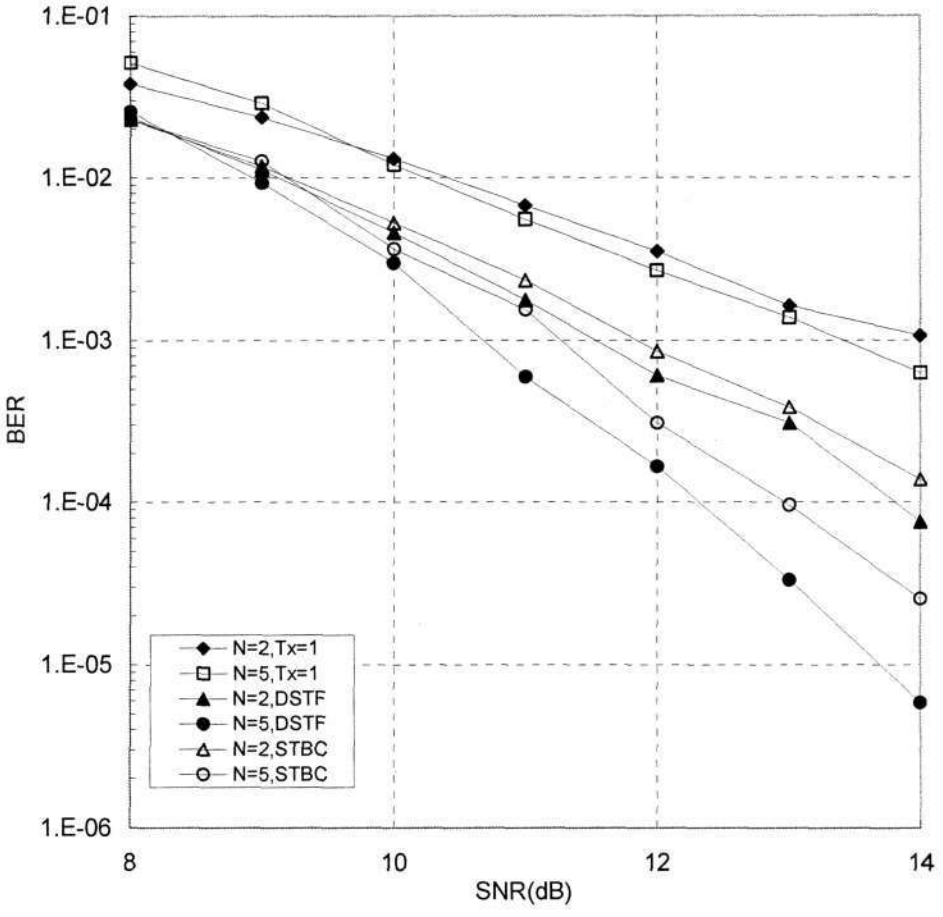

Figure 5.5: Simulated BER performance for differential STF coding, single antenna differential MPSK and differential STBC with $N = 2$ observations.

5.7 Soft-Input Soft-Output Decision Feedback Differential STFC

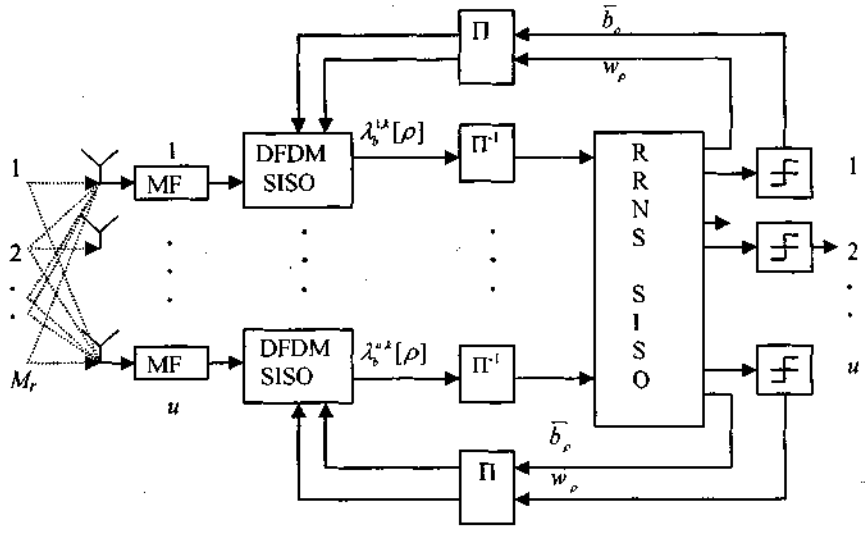

Figure 5.6 Receiver block diagram for a SISO decision feedback differential STFC

The system model for SISO decision feedback differential STF coding scheme follows that of Section 5.2 except for the decoder. The receiver section of the block diagram in Figure 5.1(b) is replaced with Figure 5.6. At the receiver, the received signal is passed through a bank of matched filters (MF) followed by a decision feedback differential STBC soft-input soft-output (SISO) decoder as illustrated in Figure 5.6.

The basic structure of the iterative receiver which consists of two stages SISO decoders is shown in Figure 5.6. The first stage is the soft-output of the differential STBC demodulator based on the DFDM. It takes the soft-input from the channel (received signal matrix over N observation periods), the hard decisions and the a priori information from the channel decoder. Using these inputs, the DFDM SISO computes the a posteriori log-likelihood ratios (LLR) which are deinterleaved and passed onto the second stage of the receiver.

The second stage of the receiver comprises of RRNS SISO decoder. It takes the deinterleaved soft-output from the DFDM SISO as its only soft-input. The RRNS SISO decoder then computes a new set of a posteriori LLR values as the soft-output. It is from

this soft-output that the extrinsic information is calculated and fed back to the DFDM SISO as the a priori information together with decoded bits as hard decisions. The whole process is then repeated for a specified number of iterations after which a final decision on the decoded bits is made. Note that there is no direct received signal from the channel to the input of the RRNS SISO decoder as in the case of block turbo codes [45], [46], [37]; instead the DFDM metric is adjusted to include the a priori information.

For the first iteration, there are no previous decisions available so the SISO uses the decoding process for CDM i.e. $N = 2$. For further iterations, re-modulated fed back matrix symbols and the extrinsic information from previous iterations are used to calculate the bit log-likelihood ratios for $N > 2$ observation periods as in (5.46). It is also worth noting that iterative decoding can still be carried out for the case of $N = 2$, as opposed to a single pass in iterative DFDM proposed in [72], [128], [84]. This is because in the aforementioned references, iterative decoding is geared towards improving the performance of DFDM. Therefore when $N = 2$, there is no feedback hence no iteration.

5.7.1 Soft-Input Soft-Output for STBC

The a posteriori code bit LLR for a decision feedback differential demodulator is derived in this subsection. Substituting (5.19) into (5.20), the LLR of the code bit in the ρth position of the $\mathbf{V}_u[k]$ label on the uth subcarrier can be expressed as

$$\lambda_b^{u,k}[\rho] = \log \frac{\sum_{\mathbf{V}_u[k] \in A_{b=1}^{\rho}} P(\mathbf{R}_{u,k} / \mathbf{V}_u[k])}{\sum_{\mathbf{V}_u[k] \in A_{b=1}^{\rho}} P(\mathbf{R}_{u,k} / \mathbf{V}_u[k]))}, \tag{5.40}$$

where A_b^{ρ} is the subset of all symbols $\mathbf{V}_u[k] \in A_b^{\rho}$ whose labels have value b in the ρth position. For m bits in each label, the conditional probability in (5.40) can be expanded as follows

$$\begin{aligned} P(\mathbf{R}_{u,k} / \mathbf{V}_u[k]) &= P(\mathbf{R}_{u,k} / b_1, \ldots, b_{\rho}, \ldots, b_m) \\ &= P\left(\mathbf{R}_{u,k}, b_1, \ldots, b_{\rho-1}, b_{\rho+1}, \ldots, b_m / b_{\rho}\right) / \prod_{i \neq \rho} P(b_i). \end{aligned} \tag{5.41}$$

It is well known that the a posteriori log-likelihood ratio (LLR) of the code bit $b_\rho \in \{+1,-1\}$ at the output of the decision-feedback differential demodulator is given by

$$\lambda_b^{u,k}[\rho] = \log \frac{P(b_\rho = +1/\mathbf{R}_{u,k})}{P(b_\rho = -1/\mathbf{R}_{u,k})}. \tag{5.42}$$

Applying the Bayes' rule, (5.42) can be written as

$$\lambda_b^{u,k}[\rho] = \log \frac{P(\mathbf{R}_{u,k}/b_\rho = +1)}{P(\mathbf{R}_{u,k}/b_\rho = -1)} + \log \frac{P(b_\rho = +1)}{P(b_\rho = -1)}, \tag{5.43}$$

where

$$P(b_\rho) = \frac{1}{2}\left[1 + b_\rho \tanh\left(w_\rho/2\right)\right], \tag{5.44}$$

and w_ρ is the normalized extrinsic information from the channel decoder. It can easily be seen that the first term in (5.43) is the extrinsic information about the code bit and the second term, the a priori information. Substituting (5.41) in (5.43) yields,

$$\lambda_b^{u,k}[\rho] = \log \frac{\sum_{\mathbf{V}_u[k] \in A_{b=+1}^{\rho}} P\left(\mathbf{R}_{u,k}, b_1, \ldots, b_{\rho-1}, b_{\rho+1}, \ldots, b_m / b_\rho\right) / \prod_{i \neq \rho} P(b_i)}{\sum_{\mathbf{V}_u[k] \in A_{b=-1}^{\rho}} P\left(\mathbf{R}_{u,k}, b_1, \ldots, b_{\rho-1}, b_{\rho+1}, \ldots, b_m / b_\rho\right) / \prod_{i \neq \rho} P(b_i)} + \log \frac{P(b_\rho = +1)}{P(b_\rho = -1)}. \tag{5.45}$$

Substituting (5.18) into (5.45), the soft-output of the DFDM decoder can be written as

$$\lambda_b^{u,k}[\rho] = \frac{\sum_{\mathbf{V}_u[k] \in A_{b=+1}^{\rho}} \exp\left[2\,\mathrm{Re}\left\{tr\left(\mathbf{R}_u^{\eta}[k]\mathbf{V}_u[k]\sum_{i=1}^{N-1} t_{0i}\mathbf{R}_u[k-i]\prod_{j=1}^{i-1}\tilde{\mathbf{V}}_u[k-j]\right)\right\}\right]\prod_{i \neq \rho} P(b_i)}{\sum_{\mathbf{V}_u[k] \in A_{b=-1}^{\rho}} \exp\left[2\,\mathrm{Re}\left\{tr\left(\mathbf{R}_u^{\eta}[k]\mathbf{V}_u[k]\sum_{i=1}^{N-1} t_{0i}\mathbf{R}_u[k-i]\prod_{j=1}^{i-1}\tilde{\mathbf{V}}_u[k-j]\right)\right\}\right]\prod_{i \neq \rho} P(b_i)}$$
$$+ \log \frac{P(b_\rho = +1)}{P(b_\rho = -1)}. \tag{5.46}$$

The soft-output is then deinterleved and passed on to the channel decoder (RRNS-SISO) as the soft-input as illustrated in Figure 5.6.

5.7.2 Soft-Input Soft-Output Channel Decoder

The RRNS SISO is used as the channel decoder. The soft decision decoding algorithm is based on that of linear block turbo codes [45], [46], [37]. The hard decision decoding algorithm is as described in Section 2.3.2. The Chase algorithm was discussed in Section 2.4.3 and is repeated here for clarity.

The deinterleaved soft-output from the first stage SISO module on each parallel stream is normalized and fed to the RRNS SISO as soft-input. A hard decision $z_{\tilde{\rho}}$ associated to the soft information $y_\rho = \tilde{\lambda}_\rho^{u,k} N_0/2$ is made [47], which yields a binary sequence $\mathbf{Z} = [z_1 z_2 ... z_m .... z_{mK} ... z_{mKu}]$ per coding interval. Note that the deinterleaved LLR values computed in (5.46) are used by the RRNS SISO channel decoder as if they were observations from BPSK modulation over an AWGN channel. The confidence values $|y_\rho|$ are then sent to the Chase algorithm which generates a set of 2^l error patterns according to l least reliable confidence values $|y_\rho|$. The error patterns are each added to $\mathbf{Z}$ by modulo two additions to produce a new sequence $\mathbf{Z}'$ which is mapped to u residues respectively and sent to the hard decision RRNS decoder. At the output of the RRNS hard decision decoder, a set of valid codewords is searched and the codeword with the minimum metric decoded as the candidate codeword $\mathbf{C}$ according to

$$\hat{v}_i = \left\| \mathbf{Y} - \bar{\mathbf{Z}}^i \right\|^2. \tag{5.47}$$

In (5.47), $\bar{\mathbf{Z}}^i$ is the ith codeword at the output of the hard decision decoder and $\|\cdot\|$ denotes the norm. The algorithm is then extended to find a competing (or discarded) codeword $\mathbf{D}$ which decodes to $b_\rho \neq \hat{b}_\rho$ and has a minimum Euclidean distance compared to the other codewords which decode to $b_{\tilde{\rho}} \neq \hat{b}_{\tilde{\rho}}$. The soft-output is then calculated as [46]

$$\bar{y}_\rho = b_\rho \left[\frac{\|\mathbf{Y} - \mathbf{D}\|^2 - \|\mathbf{Y} - \mathbf{C}\|^2}{4} \right]. \tag{5.48}$$

Thus normalized extrinsic information w_ρ in the ρ th position can be obtained by

$$w_\rho = \overline{y}_\rho - y_\rho . \tag{5.49}$$

If there is no such discarded codeword that decodes to $b_\rho \neq \hat{b}_\rho$ in the ρ th position, the extrinsic information is estimated as in [46] and [32] as

$$w_\rho \approx \beta \times b_\rho , \tag{5.50}$$

where β is a normalizing coefficient. The extrinsic information corresponding to a bit in each residue is fed back as the a priori information to the DFDM SISO. For each iteration, a hard decision on the transmitted bit is made based on (5.48). The decoded codeword is mapped to non-redundant residues as described in Section II. Redundant residues are generated through BEX method and the whole process is repeated for the entire frame. The residues on each parallel stream are then converted to their binary equivalent, bit-interleaved and fed back to the DFDM SISO as hard decisions.

In order to find the most likely candidate codeword and successfully calculate the soft-output, a high number of least reliable positions l hence a large number of test patterns is required. If no valid codeword is found, **Z** is then decoded as the transmitted codeword and the extrinsic information set to zero for a given coding interval. Note that the proposed scheme passes on both soft information and hard decisions to the DFDM decoding process.

5.8 SISO Decision Feedback Differential STFC Results

In this section simulation and numerical results are presented and discussed. The transmitter section for the simulation model is based on Figure 5.1(a) and soft-input soft-output decoder/receiver is as described in Section 5.7 and illustrated by Figure 5.6. A random bit-interleaver is applied on each subcarrier and bits are mapped to QPSK symbols using Gray labeling. The differential STBC on each subcarrier follows the Alamouti $M_t = 2$ and $M_r = 1$ signal model [88]. Time correlated flat fading Rayleigh coefficients are generated based on Jake's model [174] for a normalized Doppler frequency $f_D T = 0.02$. Systematic RRNS coding is used for all simulations and a zero bit appended on each non-redundant residue equivalent bits. Moduli $m_1 = 229$, $m_2 = 233$, $m_3 = 239$, $m_4 = 241$, $m_5 = 247$, $m_6 = 251$, $m_7 = 253$, $m_8 = 255$ are taken

from [33]. Unless otherwise stated the RRNS(8,4) code is used, hence $t = 2$ error correction capability and 8 parallel residue streams for DSTF are mapped to 8 subcarriers. The maximum likelihood upper bound on the BER is computed from (5.37) . Simulation results for the SISO DFDM are indicated as S_o and hard decision as H_d respectively. The number of test patterns is indicated by l least reliable positions while "*it*" stands for iteration.

Figure 5.7 shows the simulated and numerical BER performance of the SISO and hard decision iterative DFDM for the proposed DSTF coding scheme for $N = 2$ observations with increasing test patterns and number of iterations. It can be seen that for $l = 2$ at $it = 1$, the SISO and hard DFDM have the same BER performance. However the BER performance of the SISO DFDM system can be improved further by increasing the number of iterations as illustrated by the curve *So*, $l = 2$, $it = 4$. It can also be seen from Figure 5.7 that the simulated BER performance tremendously improves with increasing test patterns and number of iterations, becoming comparable to the maximum likelihood based analytical results.

Figure 5.8 shows the simulated BER performance of the SISO and hard decision iterative DFDM for the proposed DSTF coding scheme for $N = 5$ observations with increasing number of iterations at a fixed test patterns $l = 2$. It can be seen that for $l = 2$, $it = 2$, the BER performance improves by almost 1 dB at high SNR from the hard DFDM to the soft DFDM proposed DSTF scheme. No significant performance improvement for the hard DFDM scheme is realized by increasing the number of iterations from $it = 2$, to $it = 4$. This is mainly because feeding back hard decision limits the coding gains that should be achieved through iterative decoding process. Hence the BER performance of hard decision iterative DFDM is predominantly dependent on the number of test patterns and the error correction capability of the code. However for the SISO DFDM, the BER performance improves tremendously with increasing number of iterations as expected.

Figure 5.9 shows the simulated and numerical BER performance of the SISO DFDM for the proposed DSTF coding scheme for $N = 5$ observations. The simulated results are fixed to $it = 6$ with increasing test patterns. It can be seen that as the number of test patterns increases, the BER performance of the simulated results approach the bounds.

Figure 5.10 shows the simulated BER performance of the SISO DFDM for the proposed DSTF coding scheme for $N = 2$ and $N = 5$ observations at $l = 4$ with increasing iterations. It can be seen that the BER performance improves with increasing observation periods i.e. $N > 2$ as expected. However the performance of $N = 5$ improves more rapidly than that of $N = 2$ with increasing iterations. This is because of the increased number of observations and passing not only hard decision but also soft information to the iterative DFDM decoding process.

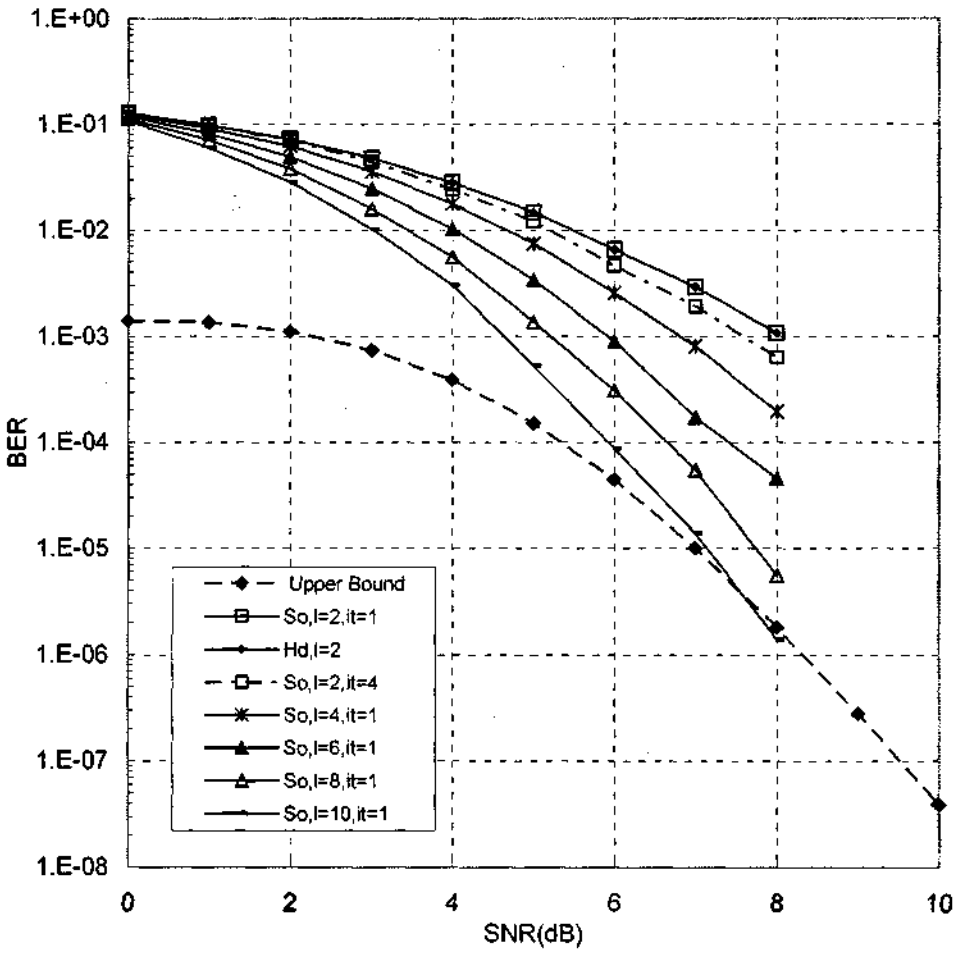

Figure 5.7: Simulated and numerical BER performance of the SISO and hard decision iterative DFDM for the proposed DSTF coding scheme for $N = 2$.

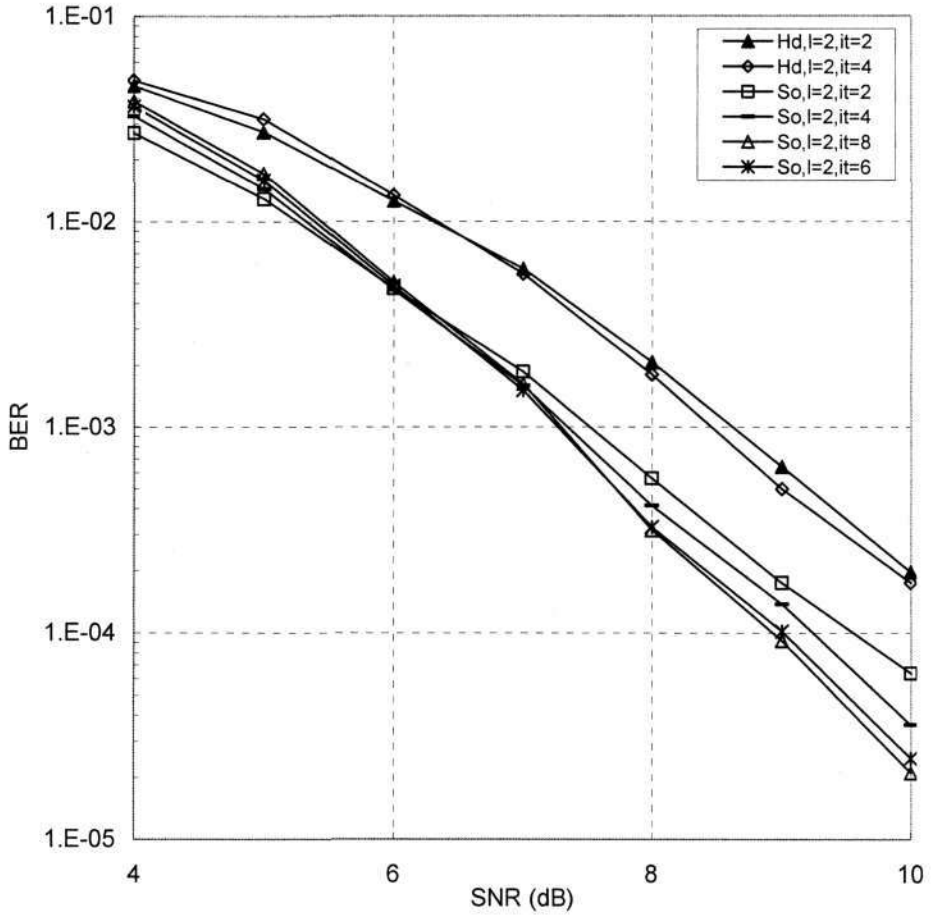

Figure 5.8: Simulated BER performance of the SISO and hard decision iterative DFDM for the proposed DSTF coding scheme for $N = 5$ observations with increasing number of iterations at a fixed test patterns $l = 2$.

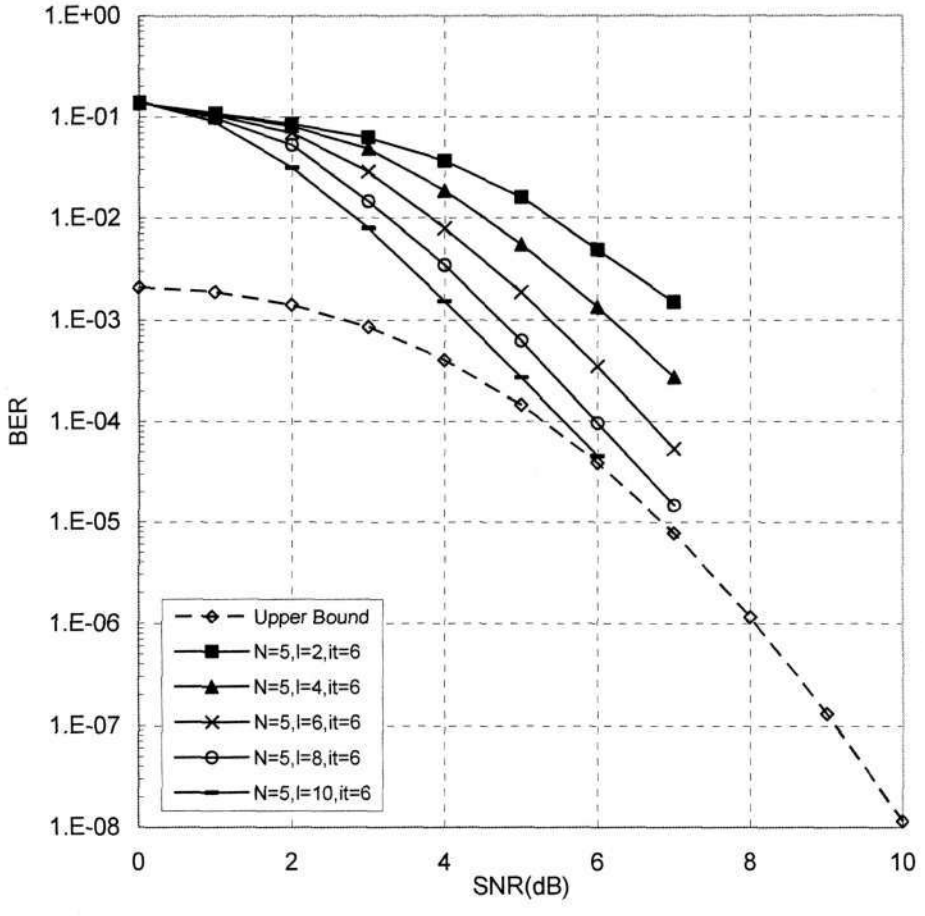

Figure 5.9: Simulated and numerical BER performance of the SISO DFDM for the proposed DSTF coding scheme for $N = 5$ observations.

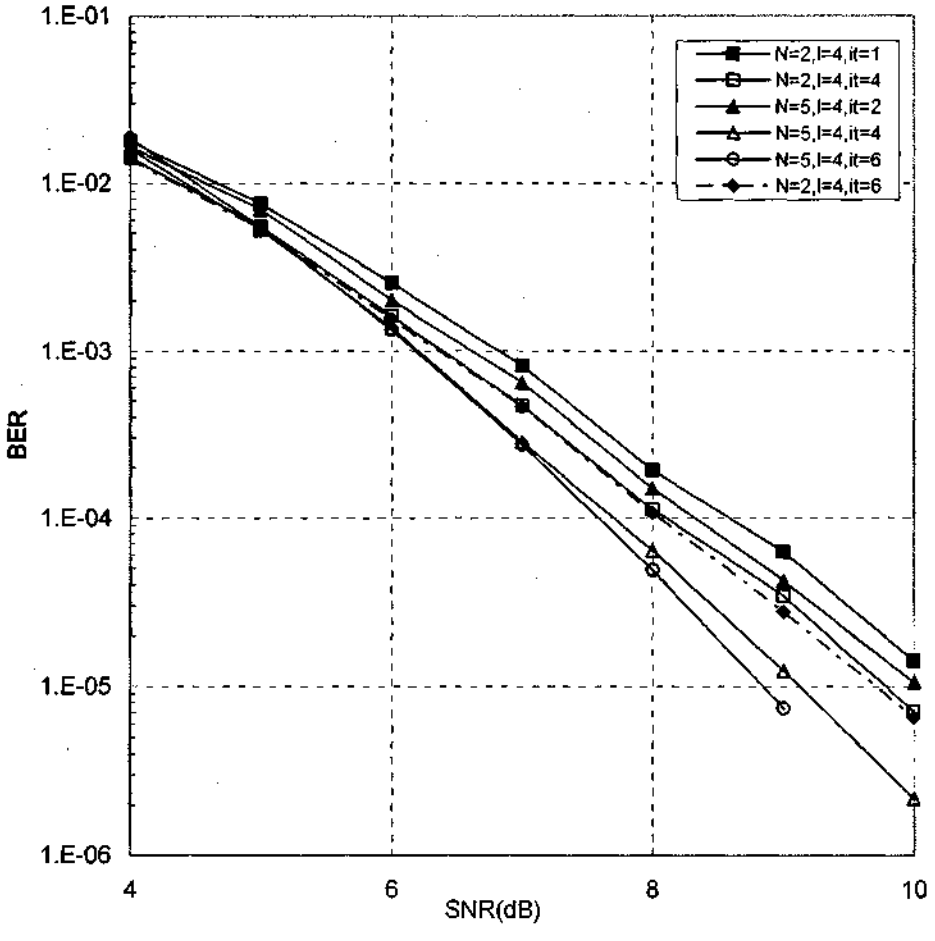

Figure 5.10: Simulated BER performance of the SISO DFDM for the proposed DSTF coding scheme for $N = 2$ and $N = 5$ observations at $l = 4$ with increasing iterations.

5.9 Conclusion

In this chapter, the hard decision and soft-input soft-output DFDM schemes for a STF modulation systems were presented. The a posteriori bit LLR values for both hard and SISO DFDM were derived. The PEP and BER expressions were also derived. Analytical and simulation results are in agreement, validating the analysis.

It was shown that the BER performance improves with increasing observation periods i.e. $N > 2$. The BER performance of hard decision iterative DFDM is predominantly dependent on the number of test patterns. However for the SISO DFDM, the BER performance improves not only with increasing number of test patterns but also with increasing iterations. In SISO DFDM, the BER performance for high observation periods improves more rapidly with increasing iterations.

It was shown that RNS codes offer extrinsic frequency diversity and parallel transmission enhances residue features. Furthermore, coding across subcarriers maximizes the frequency diversity gain. It was also shown that increasing symbol matrices per residue improves the performance of the proposed DSTF system, maximizing time diversity. Since STBC signalling is used, the proposed scheme under certain constraints guarantees transmit diversity equal to the number of transmit antennas, while maximizing the time and frequency diversities.

The use of SISO DFDM instead of hard DFDM maximizes the coding gain realized through iterative decoding process which plays a predominant role in the decoding process.

The proposed scheme can be deployed in existing standards which require high speed data rates such wireless LAN, wideband CDMA to mention but a few.

CHAPTER 6

CONCLUSION

6.1 Summary

This thesis deals with the design of a technique for combining channel coding, frequency diversity and spatial diversity into a bandwidth efficient communication scheme, and characterizing the performance of such a system in a wireless broadband environment.

Firstly, this thesis discusses achieving temporal diversity through employing error correcting coding combined with interleaving. Turbo-like serial concatenation of a standard outer channel encoder to an inner code was realized by deploying noncoherent differential MPSK modulation as the inner code. An iterative decision feedback differential modulation approach to joint decoding and demodulation process was discussed, whereby soft information is exchanged from the demodulator to the decoder, and hard decisions from the decoder to the demodulator. Redundant residue number system (RRNS) coding was proposed to be used as the channel encoder. It was shown that RRNS codes can offer better or similar bit error rate performance in bit-interleaved coded modulation schemes than the traditionally used convolutional codes, at minimal complexity and high data rates.

The rapidly growing need for fast and reliable transmission over a wireless channel motivates the development of communication systems that can support high data rates at low complexity. Combining OFDM with multiple-input multiple-output (MIMO)

systems to form MIMO-OFDM not only reduces the complexity by eliminating the need for equalization but also provides large channel capacity and a high diversity potential. The wireless broadband channel characterized by multipaths is transformed into a series of frequency flat fading subchannels, which through appropriate signal design can result in additional diversity advantage. The signal design and the diversity potential of the MIMO systems namely space-time coded OFDM, space-frequency and space-time-frequency coding schemes were presented and discussed. By concatenating a channel encoder with MIMO-OFDM in what is known as space-time-frequency coding, it was shown that the performance is greatly improved mainly due to a combination of spatial, temporal and spectral diversity gain.

In this thesis, the use of residue number system as the frequency encoder in space-time-frequency coding scheme was proposed. Most space-time-frequency (STF) coding schemes in the literature use coding across multipaths and OFDM modulation techniques to maximize frequency diversity. There is no additional diversity advantage in using such schemes under frequency flat fading channel characteristics. It was shown that RNS codes' repetitive nature can be exploited to offer additional intrinsic frequency diversity advantage, and coding maximizes the diversity gain. In the proposed STF coding scheme, the available bandwidth is divided into several non-overlapping subchannels equal to the code length with space-time signalling on each subcarrier. The signal design on each subcarrier is the same as that of space-time codes and multipath diversity is merely a trivial extension. Hence, spatial diversity and frequency diversity can be optimized/maximized independently. It was shown that the proposed STF coding scheme has potential diversity gain equal to the product of spatial diversity $M_t M_r$, temporal diversity M_b, number of OFDM tones N_c and channel order L.

Two differential STF coding schemes were presented and discussed. One deals with hard decision metric for decision feedback differential STF coding. This is an extension of RNS coded differential modulation from a single antenna system to a STF coded MIMO system proposed in Chapter 4. The second differential STF coding scheme deals with soft decision decoding for bit-interleaved decision-feedback differential modulation. The hard and soft decision metric for decision feedback differential STF modulation bit metrics were derived and the performance characterized. It is was shown that increasing diversity can reduce or eliminate the flooring effect in conventional

differential detection and significant coding gains can be achieved by passing not only hard decisions but also soft information in iterative decision feedback differential modulation. The soft-input soft-output decoding process is not limited to RRNS coded scheme but can be used in any iterative decision feedback differential modulation system with channel encoder e.g. convolutional codes.

6.2 Future work

It was observed that the current soft decoding algorithms for RRNS codes are suboptimal in nature. These algorithms can be improved in several ways. The implementation of the optimal trellis based decoding algorithms to RRNS codes needs to be investigated.

Further studies need to be carried out in search of a joint space-time-frequency code analogous to space-time codes that can maximize spatial, temporal and frequency diversity gain as a single entity.

BIBLIOGRAPHY

[1] C.E. Shannon, "A mathematical theory of communications," *Bell Systems Technical Journal*, 1948.

[2] G.J. Foschini, M. Gans, "On the limits of wireless communication in a fading environment when using multiple antennas," *Wireless Personal Commun.*, vol. 6, pp. 311-335, Mar. 1998.

[3] E. Telatar, "Capacity of multi-antenna Gaussian channels," *AT&T Technical Report Bell Lab.*, Jun. 1995.

[4] T. Marzettz, B. Hochwald, "Capacity of a mobile multiple-antenna communication link in Rayleigh flat fading," *IEEE Trans. Inform. Theory*, vol. 45, pp. 139-157, Jan. 1999.

[5] D. Gesbert, M. Shafi, D. Shiu, P.J. Smith, A. Naguib, "From theory to practice: An overview of MIMO space-time coded wireless systems," *IEEE J. Selected Areas in commun.*, vol. 21, pp. 281-301, Apr. 2003.

[6] E.G. Larsson, P. Stoica, *Space-Time Block Coding for Wireless Communications*, Cambridge University Press, 2003.

[7] H. Jafarkhani, *Space-Time Coding: Theory and Practice*, Cambridge University Press, 2005.

[8] L.j. Cimini Jr., "Analysis and simulation of digital mobile channel using orthogonal frequency division multiplexing," *IEEE Trans. Commun.*, vol. 33, pp. 665-675, Jul. 1985.

[9] B.P. Crow, I. Widjada, J.G. Kim, P.T. Sakai, "IEEE 802.11 wireless local area network," *IEEE Commun. Magazine*, vol. 35, pp. 116-126, Sept. 1997.

[10] L. Philippe, B. Ditrich, B. Christophe, F. Laurence, "WiMAX, making ubiquitous high-speed data services a reality," *Alcatel Strategy White Paper*, http://www.alcatel.com/pulications.

[11] R. Nee, R. Prasad, *OFDM for Wireless Multimedia Communications*, Artech House, 2000.

[12] D.C. Jones, "Frequency domain echo cancellation for discrete multitone asymmetric digital subscriber line transceivers," *IEEE Trans. Commun.*, vol. 43, pp. 1663-1672, Feb./Mar./Apr. 1995.

[13] T.S Rappaport, A. Annamalai, R.M. Buehrer, W.H. Tranter, "Wireless communications: Past events and future perspective," *IEEE Commun. Magazine*, 50th Anniversary Issue, pp. 148-161, May 2002.

[14] E. Beglieri, J. Proakis, S. Shamai, "Fading channels: Information theoretic and communications aspects," *IEEE Trans. Inform. Theory*, vol. 44, pp. 2619-2692, Oct. 1998.

[15] D.M Mandelbaum, "On a class of arithmetic codes and a decoding algorithm," *IEEE Trans. Inform. Theory*, pp. 85-88, Jan. 1976.

[16] R.S. Katti, "A new residue arithmetic error correction scheme," *IEEE Trans. Computers*, vol. 45, pp. 13-19, Jan. 1996.

[17] L.L. Yang, L. Hanzo, "Redundant residue number system based on error correction codes," in *Proc. IEEE VTC'01 Fall*, pp. 1472-1476, Oct. 2001.

[18] H. Krishna, K.Y. Lin, J.D. Sun, "A coding theory approach to error control in redundant residue number systems-Part I: Theory and single error correction," *IEEE Trans. Circuits Systems*, vol. 39, pp. 8-17, Jan. 1992.

[19] J.D. Sun, H. Krishna, "A coding theory approach to error control in redundant residue number systems- Part II: multiple error detection and correction," *IEEE Trans. Circuits Systems*, vol. 39, pp. 18-34, Jan. 1992.

[20] H. Krishna, J.D. Sun, "On theory and fast algorithms for error correction in residue number system product codes," *IEEE Trans. Computers*, vol. 42, pp. 840-853, Jul. 1993.

[21] L.L. Yang, L. Hanzo, "Minimum-distance decoding of redundant residue number system codes," in *Proc. IEEE ICC'01*, pp. 2975-2979, Jun. 2001.

[22] M.A. Soderstrand, W.K. Jenkins, G.A. Jullien, F.J. Taylor, *Modern Applications of Residue Number System Arithmetic to Digital Signal Processing*, IEEE Press: New York, 1986.

[23] A.S. Madhukumar, F. Chin, "Performance studies of a residue number system based CDMA system over burst communication channels," *Wireless Personal Commun.*, vol. 22, pp. 89-102, Jul. 2002.

[24] L. Yang, L. Hanzo, "Residue number system arithmetic assisted m-ary modulation," *IEEE Commun. Letters*, vol. 3, pp. 28-30, Feb. 1999.

[25] L. Yang, L. Hanzo. "Residue number system based multiple code DS-CDMA systems," in *Proc. VTC'99 Spring*, pp. 1450-1454, May 1999.

[26] O. Goldreich, D. Ron, M. Sudan, "Chinese remaindering with errors," *IEEE Trans. Inform. Theory*, vol. 46, pp 1330-1338, Jul. 2000.

[27] L.L. Yang, L. Hanzo, "A residue number system based parallel communication scheme using orthogonal signalling- Part I: System Outline," *IEEE Trans. Veh. Technol.*, vol. 51, pp. 1534-1546, Nov. 2002.

[28] L.L. Yang, L. Hanzo, "A residue number system based parallel communication scheme using orthogonal signalling- Part II: Multipath fading channels," *IEEE Trans. Veh. Technol.*, vol. 51, pp. 1547-1559, Nov. 2002.

[29] T.H. Liew, L. Yang, L. Hanzo, "Systematic redundant residue number system codes: Analytical upper bound and iterative decoding performance over AWGN and Rayleigh channels," *IEEE Trans. Commun.*, vol. 54, pp. 1006-1016, Jun. 2006.

[30] T. Keller, T.H. Liew, L. Hanzo, "Adaptive rate redundant residue number system coded multicarrier modulation," *IEEE J. Selected Areas Commun.*, vol. 18, pp. 2292-2300, Nov. 2000.

[31] T.H. Liew, L.L. Yang, L. Hanzo, "Soft-decision redundant residue number system based error correction coding," in *Proc. IEEE VTC'99 Fall*, pp. 2546-2550, Sept. 1999.

[32] T.H. Liew, L.L. Yang, L. Hanzo, "Iterative decoding of redundant residue number system codes," in *Proc. IEEE VTC'00 Fall*, pp. 576-580, May 2000.

[33] L. Hanzo, T.H. Liew, B.L. Yeap, *Turbo Coding, Turbo Equalization and Space-Time Coding for Transmission over Wireless Channels*, L. Hanzo, T.H. Liew, B.L. Yeap , 2002.

[34] C. Berrou, A. Glavieux, P. Thitimajishima, "Near Shannon limit error correcting coding and decoding: Turbo codes," in *Proc. IEEE ICC'93*, pp. 106-1070, May 1993.

[35] C. Berrou, A. Glavieux, "Near Shannon limit error correcting coding and decoding: Turbo codes," *IEEE Trans. Commun.*, vol. 44, pp. 1261-1271, Oct. 1996.

[36] L. R. Bahl, J. Cocke, F. Jelinek, J. Raviv, "Optimum decoding for linear codes for minimizing symbol error rate," *IEEE Trans. Inform. Theory*, vol. 20, pp. 284-287, Mar. 1974.

[37] R. H. Morelos-Zaragoza, *The Art of Error Correcting Coding*, John Wiley & Sons, 2002.

[38] S. Lin, D. J. Costello, *Error Control Coding*, 2nd ed., Pearson Prentice Hall, 2004.

[39] J.G. Proakis, *Digital Communications*, 4th ed., McGraw-Hill, 2001.

[40] S. Benedetto, D. Divsalar, G. Montorsi, F. Pollara, "A soft-in soft-out APP module for iterative decoding of concatenated codes," *IEEE Commun. Letters*, vol. 1, pp. 22-24, Jan. 1997.

[41] S. Benedetto, D. Divsalar, G. Montorsi, F. Pollara, "Serial concatenation of interleaved codes: Performance analysis, design, and iterative decoding," *IEEE Trans. Inform. Theory*, vol. 44, pp. 909926, May 1998.

[42] R. Kotter, "Fast generalized minimum-distance decoding of algebraic geometry and Reed-Solomon codes," *IEEE Trans. Inform. Theory*, vol. 42, pp. 721-738, May 1996.

[43] M. P. C. Fossorier, S. Lin, "Chase type and GMD coset decoding," *IEEE Trans. Commun.*, vol. 48, pp. 345-350, Mar. 2000.

[44] H. Tang, Y. Liu, M. Fossorier, S. Lin, "On combining Chase-2 and GMD decoding algorithms for nonbinary block codes," *IEEE Commun. Letters*, vol. 50, pp. 209-211, May. 2001.

[45] R. M. Pyndiah, "Near-optimum decoding of product codes: block turbo codes," *IEEE Trans. Commun.*, vol. 46, pp. 1003-1010, Aug. 1998.

[46] O. Aitsa, R. Pyndiah, "Performance of Reed-Solomon block turbo code," in *Proc. IEEE GLOBECOM'96*, pp.121-128, Nov. 1996.

[47] A. Picart, R. Pyndiah, "Adapted iterative decoding of product codes," in *Proc. IEEE GLOBECOM'99*, pp. 2357-2362, Dec. 1999.

[48] P. A. Martin, D. P. Taylor, "Distance based adaptive scaling in sub-optimal iterative decoding," *IEEE Trans. Commun.*, vol. 50, pp. 869-871, Jun. 2002.

[49] Z. Chi, L. Song, K. K. Parhi, "On the performance/complexity tradeoff in block turbo decoder design," *IEEE Trans. Commun.*, vol. 52, pp. 173-175, Feb. 2004.

[50] M. K. Cheng, P. H. Siegel, "Iterative soft-decision Reed-Solomon decoding on partial response channels," in *Proc. IEEE GLOBECOM'03*, pp. 1588-1592, Dec. 2003.

[51] J. Jiang, K. R. Narayanan, "Iterative soft decoding of Reed-Solomon codes," *IEEE Commun. Letters*, vol. 8, pp. 244-246, Apr. 2004.

[52] R. Koetter, A. Vardy, "Algebraic soft-decision decoding of Reed-Solomon codes," *IEEE Trans. Inform. Theory*, vol. 49, pp. 2809-2825, Nov. 2003.

[53] D. Agrawal and A. Vardy, "Generalized minimum distance decoding in the Euclidian space: Performance analysis," *IEEE Trans. Inform. Theory*, vol. 46, pp 60-83, Jan. 2000.

[54] M. P. C. Fossorier, S. Lin, "Error performance analysis for reliability based decoding algorthms," *IEEE Trans. Inform. Theory*, vol. 48, pp 287-293, Jan. 2002.

[55] E. Zehavi, "8-PSK Trellis codes for a Rayleigh channel," *IEEE Trans. Commun.*, vol. 40, pp. 873-884, May 1992.

[56] G. Caire, G. Taricco, E. Biglieri, "Bit-interleaved coded modulation," *IEEE Trans. Inform. Theory*, vol. 44, pp. 927-946, May 1998.

[57] X. Li, J.A. Ritcey, "Trellis-coded modulation with bit interleaving and iterative decoding," *IEEE J. Selected Areas Commun.*, vol. 17, pp. 715-723, Apr. 1999.

[58] F. Simoens, H. Wymeersch, H. Bruneel, M. Moeneclaey, "Multi-dimensional mapping for bit-interleaved coded modulation with BPSK/QPSK signalling," *IEEE Commun. Letters*, vol. 9, pp. 453-455, May 2005.

[59] F. Schreckenbach, N. Gortz, J. Hagenauer, G. Bauch, "Optimization of symbol mappings for bit-interleaved coded modulation with iterative decoding," *IEEE Commun. Letters*, vol. 7, pp. 593-595, Dec. 2003.

[60] N. Fajar, H. Ogiwara, "Performance evaluated method of bit-interleaved turbo trellis-coded modulation and its optimization," *IEICE Trans. Fundamentals*, vol. E87-A, pp. 1583-1590, Jun. 2004.

[61] J.J. Boutros, F. Boixadera, C. Lamy, "Bit-interleaved coded modulation for multiple-input multiple-output channel," in *Proc. IEEE ISSSTA'00*, pp. 123-126, Sep. 2000.

[62] J. Hagenaur, P. Hoeher, "A viterbi algorithm with soft-decision output and its applications," in *Proc. IEEE GLOBECOM'89*, pp. 1680-1686, Nov. 1989.

[63] J. Hagenaur, E. Offer, L. Papke, "Iterative decoding of binary block and convolutional codes," *IEEE Trans. Inform. Theory*, vol. 42, pp. 429-445, Mar. 1996.

[64] X. Ma, G.B. Georgios, B. Lu, "Block differential encoding for rapid fading channels," *IEEE Trans. Commun.*, vol. 52, pp. 416-425, Mar. 2004.

[65] D. Divsalar, M.P. Simon, "Multiple-symbol differential detection of MPSK," *IEEE Trans. Commun.*, vol. 38, pp. 300-308, Mar. 1990.

[66] D. Divsalar, M.P. Simon, "Maximum-likelihood differential detection of uncoded and trellis coded phase amplitude modulation over AWGN and fading channel metrics and performance," *IEEE Trans. Commun.*, vol. 42, pp. 76-89, Jan. 1994.

[67] F. Edbauer, "Bit error rate of binary and quaternary DPSK signals with multiple differential feedback detection," *IEEE Trans. Commun.*, vol. 40, pp. 457-460, Mar. 1992.

[68] M.K. Simon, M. Alouini, "Multiple symbol differential detection with diversity reception," in *Proc. IEEE GLOBECOM'00*, pp. 985-989, Nov. 2000.

[69] F. Adachi, M. Sawahashi, "Decision feedback multiple-symbol differential detection for M-ary DPSK," *Electronic Letters*, vol. 29, pp. 1385-1387, Jul. 1993.

[70] R. Scober, W.H. Gestacker, J.B. Huber, "Decision feedback differential detection of MDPSK for flat Rayleigh fading channel," *IEEE Trans. Commun.*, vol. 47, pp. 1025-1035, Jul. 1999.

[71] L.H.J. Lampe, R. Schober, "Decision -feedback differential demodulation of bit-interleaved coded MDPSK for flat Rayleigh fading channels," in *Proc. IEEE GLOBECOM'00*, pp. 965-969, Nov. 2000.

[72] L.H.J. Lampe, R. Schober, "Iterative decision-feedback differential demodulation of bit-interleaved coded MDPSK for flat Rayleigh fading channels," *IEEE Trans. Commun.*, vol. 49, pp. 1176-1184, Jul. 2001.

[73] P. Hoeher, J. Lodge, "Turbo DPSK: iterative differential PSK demodulation and channel decoding," *IEEE Trans. Commun.*, vol. 47, pp. 837-843, Jun. 1999.

[74] K.R. Narayan, G.L. Stuber, "A serial concatenation approach to iterative demodulation and decoding," *IEEE Trans. Commun.*, vol. 47, pp. 956-96, Jul. 1999.

[75] I.D. Marsland, P.T. Mathiopoulos, "On the performance of iterative noncoherent detection of coded M-PSK signals," *IEEE Trans. Commun.*, vol. 48, pp. 588-596, Apr. 2000.

[76] D. Raphaeli, "Noncoherent coded modulation," *IEEE Trans. Commun.*, vol. 44, pp. 172-183, Sept. 1996.

[77] G. Colavolpe, R. Raheli, "Noncoherent sequence detection," *IEEE Trans. Commun.*, vol. 47, pp. 1376-1385, Sept. 1999.

[78] G. Colavolpe, G. Ferrari, R. Raheli, "Noncoherent iterative (turbo) decoding," *IEEE Trans. Commun.*, vol. 48, pp. 1488-1498, Sept. 2000.

[79] G. Colavolpe, R. Raheli, "Theoretical analysis and performance limits of noncoherent sequential detection of coded PSK," *IEEE Trans. Inform. Theory*, vol. 46, pp. 1483-1494, Jul. 2000.

[80] I. D. Marsland, P.T. Mathioploulos, "Multiple differential detection of parallel concatenated convolutional (turbo) codes in correlated fast Rayleigh fading," *IEEE J. Selected Area Commun.*, vol. 16, pp. 265-275, Feb. 1998.

[81] P. Vanichchanut, C. Sritiapetch, S. Nakpeerayuth, L. Wuttisittikulkij, "APP demodulator for turbo coded multiple symbol differential detection under correlated Rayleigh fading channels," in *Proc. IEEE GLOBECOM'04*, CD-ROM , Dec. 2004.

[82] C. Chung, F. Hwang, "Diversity codes for differential phase modulation in a correlated Rayleigh fading channel," *IEEE Trans. Commun.*, vol. 49, pp. 1154-1157, Jul. 2001.

[83] Y. Ma, T.J. Lim, "Bit error probability for MDPSK and NCFSK over arbitrary Rician fading channels," *IEEE J. Selected Areas Commun.*, vol. 18, Nov. 2000.

[84] R.N. Akol, F. Takawira, "Performance of coded residual arithmetic differential MPSK modulation," in *Proc. IEEE WCNC'06*, pp. 1927-1932, Apr. 2006.

[85] J.C. Geuy, M.P. Fitz, M.R. Bell, W.Y. Kuo, "Signal design for transmit diversity wireless communication systems over Rayleigh fading channels," in *Proc. IEEE VTC'96 Spring*, pp. 136-140, Apr./ May 1996.

[86] V. Tarokh, N. Seshadri, A.R. Calderbank, "Space-time-codes for high data rate wireless communication: Performance criterion and code construction," *IEEE Trans. Inform. Theory*, vol. 44, pp. 744-765, Mar. 1998.

[87] A.F. Naguib, N. Seshadri, AR. Calderbank, "Increasing data rate over wireless channels," *IEEE Signal Process. Magazine*, vol. 48, pp. 76-92, May 2000.

[88] S. Alamouti, "A simple transmitter diversity scheme for wireless communications," *IEEE J. Selected Areas Commun.*, vol. 16, pp. 1451-1459, Mar. 1998.

[89] V. Tarokh, H. Jafarkhani, A.R. Calderbank, "Space-time block codes from orthogonal designs," *IEEE Trans. Inform. Theory*, vol. 45, pp. 1456-1467, Jul. 1999.

[90] W. Su, X. Xia, "On space-time block codes from complex orthogonal designs," *Wireless Personal Commun.*, vol. 25, pp. 1-26, Apr. 2003.

[91] W. Su, X. Xia, "Signal constellations for quasi-orthogonal space-time block codes with full diversity," *IEEE Trans. Inform. Theory*, vol. 50, pp. 2331-2347, Oct. 2004.

[92] O. Tirkkonen, A. Hottinen, "Square-matrix embeddable space-time block codes for complex signal constellations," *IEEE Trans. Inform. Theory*, vol. 48, pp. 384-395, Feb. 2002.

[93] N. Hassanpour, H. Jafarkhani, "A class of full diversity space-time codes," in *Proc. IEEE GLOBECOM'03*, pp. 3336-3340, Dec. 2003.

[94] G. Han, "Generalized PSK in space-time coding," *IEEE Trans. Commun.*, vol. 53, pp.790-801, May 2005.

[95] S. Li, X. Tao, W. Wang, P. Zhang, C. Han, "Generalized delay diversity code: A simple and powerful space-time coding scheme," in *Proc. IEEE ICCT'00*, pp. 1697-1703, 2000.

[96] M. Tao, R.S. Cheng, "Space code design in delay diversity transmission for PSK modulation," in *Proc. IEEE VTC'02 Fall*, pp. 444-448, Sept. 2002.

[97] J. Tan, G.L. Stuber, "Multicarrier delay diversity modulation," in *Proc. GLOBECO'03*, pp. 1633-1637, Dec. 2003.

[98] R. Vaze, V. Shashindhar, B.S. Rajan, "A high-rate generalized coded delay diversity scheme and its diversity-multiplexing tradeoff," in *Proc. IEEE ICC'05*, pp. 448-452, May. 2005.

[99] J. H. Winters, "The diversity gain of transmit diversity in wireless systems with Rayleigh fading," *IEEE Trans. Veh. Technol.*, vol. 47, pp. 119-123, Feb. 1998.

[100] Q. Yan, R.S. Blum, "Robust space-time block coding for rapid fading channels," in *Proc. IEEE GLOBECOM'01*, pp. 460-464, Nov. 2001.

[101] Y. Xin, Z. Wang, G.B. Giannakis, "Space-time constellation-rotating codes maximizing diversity and coding gains," in *Proc. IEEE GLOBECOM'01*, pp. 455-459, Nov. 2001.

[102] Y. Xin, Z. Wang, G.B. Giannakis, "Space-time diversity systems based on linear constellation precoding," *IEEE Trans. Wireless Commun.*, vol 2, pp. 294-309, Mar.2003.

[103] H. Lu, Y. Wang, P.V. Vijay, K.M. Chugg, "Remarks on space-time codes including a new lower bound and an improved code," *IEEE Trans. Inform. Theory*, vol. 49, pp. 2752-2757, Oct. 2003.

[104] S. Siwamogsatham, M.P. Fitz, J.H. Grimm, "A new view of performance analysis of transmit diversity schemes in correlated Rayleigh fading," *IEEE Trans. Inform. Theory*, vol. 48, pp.950-956, Apr. 2002.

[105] W. Su, Z. Sofar, K.J.R. Liu, "Diversity analysis of space-time modulation over time-correlated Rayleigh fading channels," *IEEE Trans. Inform. Theory*, vol. 50, pp.1832-1839, Aug. 2004.

[106] Y. Huang, J.A. Ritcey, "Tighter bounds for iteratively decoded bit-interleaved space-time coded modulation," *IEEE Commun. Letters*, vol. 8, pp. 153-155, Mar. 2004.

[107] G. Taricco, E. Biglieri, "Exact pairwise probability of space-time codes," *IEEE Trans. Inform. Theory*, vol. 48, pp.510-513, Feb. 2002.

[108] C.B. Peel, A.L. Swindlehurst, "Effective SNR for space-time modulation over a time-varying Rician channel," *IEEE Trans. Commun.*, vol. 52, pp. 17-23, Jan. 2004.

[109] H. Shah, A. Hedayat, A. Nosratinia, "Performance of concatenated channel codes and orthogonal space-time block codes," *IEEE Trans. Wireless Commun.*, vol. 5, pp. 1406-1414, Jun. 2006.

[110] M. Byun, B. G. Lee, "New bounds of pairwise error probability for space-time codes in Rayleigh fading channels," in *Proc. IEEE WCNC'02*, pp. 17-21, Mar. 2002.

[111] H. Shin, J.H. Lee, "Upper bound on the error probability for space-time codes in fast fading channels," in *Proc. IEEE VTC'02 Fall*, pp. 243-246, Sept. 2002.

[112] R. Li, P.Y. Kam, "New tight bounds on the pairwise error probability for unitary space-time modulation," *IEEE Commun. Letters*, vol. 9, pp. 289-291, Apr. 2005.

[113] Y. Li, J. Moon, "Performance of bit-interleaved space-time coding for OFDM in block fading channels," in *Proc. IEEE VTC'04*, 2004.

[114] G. Ganesan, P. Stoica, "Differential modulation using space-time block codes," *IEEE Signal Process. Letters*, vol. 9, pp. 57-60, Feb. 2002.

[115] V. Tarokh, H. Jafarkhani, "A differential detection scheme for transmit diversity," *IEEE J. Selected Areas Commun.*, vol. 18, pp. 1169-1174, Jul. 2000.

[116] B.L. Highes, "Differential space-time modulation," *IEEE Trans. Inform. Theory*, vol. 46, pp. 2567-2578, Nov. 2000.

[117] B.M. Hochwald, T.L. Marzetta, "Unitary space-time modulation for multiple-antenna communications in Rayleigh flat fading," *IEEE Trans. Inform. Theory*, vol. 46, pp. 543-564, Mar. 2000.

[118] B.M. Hochwald, W. Sweldens, "Differential unitary space-time modulation," *IEEE Trans. Commun.*, vol. 48, pp.2041-2052, Dec. 2000.

[119] X. Liang, X. Xia, "Unitary signal constellations for differential space-time modulation with two transmit antennas: Parametric codes, optimal designs and bounds," *IEEE Trans. Inform. Theory*, vol. 48, pp. 2291-2322, Aug. 2002.

[120] W. Zhao, G. Leus, G.B. Giannakis, "Algebraic design of unitary space-time constellations," in *Proc. IEEE ICC'03*, pp. 3180-3184, May 2003.

[121] B. Hassibi, B.M. Hochwald, "Cayley differential unitary space-time codes," *IEEE Trans. Inform. Theory*, vol. 48, pp. 1485-1503, Jun. 2002.

[122] C. Gao, A.M. Haimovich, "Multiple-symbol differential detection for space-time block codes," in *Proc. CISS'02*, CD-ROM, Mar. 2002.

[123] B. Bhukania, P. Schniter, "Multiple-symbol detection of differential unitary space-time modulation in fast-fading channels with known correlation," in *Proc. CISS'02*, CD-ROM, Mar. 2002.

[124] R. Schober, L.H.J. Lampe, "Noncoherent receivers for differential space-time modulation," *IEEE Trans. Commun.*, vol. 50, pp. 768-777, May 2002.

[125] R. Schober, L.H.J. Lampe, "Differential modulation diversity," *IEEE Trans. Veh. Technol.*, vol.51, pp. 1431-1444, Nov. 2002.

[126] Y. Liu, X. Wang, "Multiple-symbol decision-feedback space-time differential decoding in fading channels," *EURASIP Journal on Applied Signal Process.*, pp. 297-304, Mar. 2002.

[127] L.H.J. Lampe, R. Schober, "Bit-interleaved coded differential space-time modulation," in *Proc. IEEE ICC'02*, pp. 1434-1438, May 2002.

[128] L.H.J. Lampe, R. Schober, "Bit-interleaved coded differential space-time modulation," *IEEE Trans Commun.*, vol. 50, pp. 1429-1439, Sept. 2002.

[129] C. Ling, H. Li, A.C. Kot, "On decision-feedback detection of differential space-time modulation in continuous fading," *IEEE Trans. Commun.*, vol. 52, pp. 1613-1617, Oct. 2004.

[130] B. Bhukania, P. Schniter, "On robustness of decision-feedback detection of DPSK and differential unitary space-time modulation in Rayleigh-fading channels," *IEEE Trans. Wireless Commun.*, vol. 3, pp. 1481-1489, Sept. 2004.

[131] W. Zhao, G. Leus, G.B. Giannakis, "Orthogonal design of unitary constellation for uncoded and trellis-coded noncoherent space-time systems," *IEEE Trans. Inform. Theory*, vol. 50, pp. 1319-1327, Jun. 2004.

[132] M.L. McCloud, M. Brehler, M.K. Varanasi, "Signal design and convolutional coding for noncoherent space-time communications on the block-Rayleigh-fading channel," *IEEE Trans. Inform. Theory*, vol. 48, pp.1186-1194, May 2002.

[133] F. Alesiani, A. Tarable, "Differential space-time CDMA with turbo decoding," in *Proc. IEEE GLOBECOM'03*, pp. 616-620, Dec. 2003.

[134] M. Tao, R.S. Cheng, "Trellis coded differential unitary space-time modulation over flat fading channels," *IEEE Trans. Commun.*, vol. 51, pp. 587-596, Apr. 2003.

[135] I. Bahceci, T.M. Duman, "Combined turbo coding and space-time modulation," *IEEE Trans. Commun.*, vol. 50, pp. 1244-1249, Aug. 2002.

[136] S.K. Jayaweera, H.V. Poor, "Turbo (iterative) decoding of a unitary space-time code with a convolutional code," in *Proc. IEEE VTC'02 Spring*, pp. 1020-1024, May 2002.

[137] K.J. Han, J.H. Lee, "Iterative differential space-time block code with low complexity," in *Proc. IEEE VTC'02 Spring*, pp. 1322-1325, May 2002.

[138] A. Nallanathan, L.P. Yan, "Turbo differential space-time block codes with iterative demodulation and decoding," in *Proc. IEEE ICC'05*, pp. 1891-1895, May 2005.

[139] C. Ling, H. Li, A.C. Kot, "Noncoherent sequence detection of differential space-time modulation," *IEEE Trans. Inform. Theory*, vol. 49, pp. 2727-2734, Oct 2003.

[140] D.P. Liu, Q.T. Zhang, Q. Chen, "Structures and performance of noncoherent receivers for unitary space-time modulation on correlated fast-fading channels," *IEEE Trans. Veh. Technol.*, vol. 53, pp. 1116-1125, Jul. 2004.

[141] C. Gao, A.M. Haimovich, "BER analysis of MPSK space-time block codes with differential detection," *IEEE Commun. Letters*, vol. 7, pp. 314-316, Jul. 2003.

[142] C. Ling, K.H. Li, A.C. Kot, Q.T. Zhang, "Multisampling decision-feedback linear prediction receivers for differential space-time modulation over Rayleigh fast-fading channels," *IEEE Trans. Commun.*, vol. 51, pp. 1214-1223, Jul. 2003.

[143] M. Brehler, M.K. Varanasi, "Asymptotic error probability analysis of quadratic receivers in Rayleigh-fading with applications to a unified analysis of coherent and noncoherent space-time receivers," *IEEE Trans. Inform. Theory*, vol. 47, pp. 2383-2399, Sept. 2001.

[144] G. Bauch, "Differential modulation and cyclic delay diversity in orthogonal frequency-division multiplexing," *IEEE Trans. Commun.*, vol. 54, pp. 798-801, May 2006.

[145] Y. Li, J.C. Chuang, N.R. Sollenberger, "Transmit diversity for OFDM systems and its impact on high-rate data wireless networks," *IEEE J. Selected Areas Commun.*, vol. 17, pp. 1233-1243, Jul. 1999.

[146] R.S. Blum, Y. Li, J.H. Winters, Q. Yan, "Improved space-time coding for MIMO-OFDM wireless communications," *IEEE Trans. Commun.*, vol. 49, pp.1873-1878, Nov. 2001.

[147] B. Lu, X. Wang, K.R. Narayanan, "LDPC-based space-time coded OFDM systems over correlated fading channels: Performance analysis and receiver design," *IEEE Trans Commun.*, vol. 50, pp. 74-88, Jan. 2002.

[148] X. Zhuang, F.W. Vook, "Performance of trellis coded OFDM with antenna diversity," in *Proc. IEEE GLOBECOM'01*, pp. 3106-3110, Nov. 2001.

[149] D. Agrawal, V. Tarok, A. Naguib, N. Seshadri, "Space-time coded OFDM for high data-rate wireless communication over wideband channels," in *Proc. IEEE VTC'98 Spring*, pp. 2232-2236, May 1998.

[150] D. Tujkovic, M. Juntti, M. Latva-aho, "Space-frequency turbo coded OFDM," in *Proc IEEE GLOBECOM'01*, pp. 876-800, Nov. 2001.

[151] K.F. Lee, D.B. Williams, "A space-frequency transmitter diversity technique for OFDM systems," in *proc. IEEE GLOBECOM'00*, pp. 1473-1477, Nov. 2000.

[152] Z. Hong, B.L. Hughes, "Robust space-time codes for broadband OFDM systems," in *Proc. IEEE WCNC'02*, pp. 105-108, Mar. 2002.

[153] H. Blolcskei, A.j. Paulraj, "Space-frequency coded broadband OFDM systems," in *Proc IEEE. WCNC'00*, pp. 1-6, Apr. 2000.

[154] H. Blolcskei, A.j. Paulraj, "Space-frequency coded MIMO-OFDM with variable multiplexing-diversity tradeoff," *In Proc. IEEE ICC'03*, pp. 2837-2841, May 2003.

[155] L. Sho, S. Roy, S. Sandhu, "Rate-one space frequency block codes with maximum diversity gain for MIMO-OFDM." In *Proc. IEEE GLOBECOM'03*, pp. 809-813, Dec. 2003.

[156] A. Huebner, F. Schuehlein, M. Bossert, E. Costa, H. Haas, "A simple space-frequency coding scheme with cyclic delay diversity for OFDM," in *Proc. IEE EPMCC'03*, pp. 106-110, Apr. 2003.

[157] H. Sampath, R. Narasimhan, "A simple scalable space-frequency coding scheme for MIMO-OFDM," in *Proc. IEEE VTC'04 Fall*, pp. 640-644, Sept. 2004.

[158] W. Zhang, X. Xia, P.C. Ching, "A design of high-rate space-frequency codes for MIMO-OFDM systems," in *Proc. IEEE GLBECOM'04*, pp. 209-213, Dec. 2004.

[159] Z. Liu, Y. Xin, G.B. Giannakis, "Space-time-frequency coded OFDM over frequency-selective fading Channels," *IEEE Trans. Signal Process.*, vol. 50, pp. 2465-2476, Oct. 2002.

[160] W. Su, Z. Safar, M. Olfat, K.J.R. Liu, "Obtaining full-diversity space-frequency codes from space-time codes via mapping," *IEEE Trans. Signal Process.*, vol. 51, pp. 2905-2916, Nov. 2003.

[161] Y. Chen, E. Aktas, U. Tureli, "Optimal space–frequency group codes for MIMO-OFDM system," *IEEE Trans. Commun.*, vol. 54, pp. 553-562, Mar. 2006.

[162] W. Su, Z. Sofar, K.J. Ray Liu, "Full-rate full-diversity space-frequency codes with optimum coding advantage," *IEEE Trans. Inform. Theory*, vol. 51, pp. 229-249, Jan. 2005.

[163] Ma, G. Leus, G.B. Giannakis, "Space-time-Doppler block coding for correlated time-selective fading channels," *IEEE Trans. Signal Process.*, vol. 53, pp. 2167-2181, Jun. 2005.

[164] H. Li, "Differential space-time modulation over frequency-selective channels," *IEEE Trans. Signal Process.*, vol. 53, pp. 2228-2242, Jun. 2005.

[165] Y. Gong, K.B. Letaief, "Space-frequency-time coded OFDM for broadband wireless communications," in *Proc. IEEE GLOBECOM'01*, pp. 519-523, Nov. 2001.

[166] Y. Gong, K.B. Letaief, "An efficient space-frequency coded wideband OFDM system for wireless communications," in *Proc. IEEE ICC'02*, pp. 5474-479, Jun. 2002.

[167] Y. Gong, K.B. Letaief, "An efficient space-frequency coded wideband OFDM system for wireless communications," *IEEE Trans. Commun.*, vol. 51, pp. 2019-2029, Nov. 2003.

[168] Q. Ma, C. Tepedelenlioglu, Z. Liu, "Full diversity block diagonal codes for differential space-time-frequency coded OFDM," in *Proc. IEEE GLOBECOM'03*, pp. 868-872, Dec. 2003.

[169] R.N. Akol, F. Takawira, "On performance of arithmetically coded differential space-time-frequency coding," submitted to *IEEE International Conference on Communications*, to be held in Glasgow, Scotland, United Kingdom, Jun. 2007.

[170] D. Rende, T.F. Wong, "Bit interleaved space-frequency coded modulation for OFDM systems," in *Proc. IEEE ICC'03*, pp. 2827-2831, Jun. 2003.

[171] D. Tujkovic, M. Juntti, M. Latva-aho, "Space-frequency-time turbo coded modulation," *IEEE Commun. Letters*, vol. 5, pp. 480-482, Dec. 2001.

[172] E. Biglieri, G. Caire, G. Taricco, J. Ventura, "Simple method for evaluating error probabilities," *Electronic Letters*, vol. 32, pp 191-192, Feb. 1996.

[173] J. Chen, T. Lv, H. Zheng, "Joint cross layer design for wireless QoS content delivery," *EURASIP Journal on Applied Signal Process.*, pp. 167-182, Feb. 2005.

[174] W. C. Jakes Jr., *Microwave Mobile Communication*, New York: Wiley, 1974.

[175] R. Janaswamy, *Radiowave Propagation and Smart Antennas for Wireless Communications*, Kluwer Academic Publishers, 2001.

[176] K. Yu, B. Ottersten, "Models for MIMO propagation channels, a review," *J. Wireless Commun. Mobile Comput.*, vol. 2, pp. 653-666, Nov. 2002.

[177] T.K Moon, W.C. Stirling, *Mathematical Methods and Algorithms for Signal Processing*, New Jersey: Prentice-Hall 2000.

[178] T. Poutanen, J. Kolu, "Correlation control in multichannel fading simulators," in *Proc. IEEE VTC'01, Spring*, pp. 318-322, May 2001.

[179] M. Abramovitz, I.A. Stegun, *Handbook of Mathematical Functions*, New York: Dover, 1972.